Spring 2018

Advancement in thermal energy storage using phase change materials

Rami Mohammad Reda Saeed

Department: Mining and Nuclear Engineering

ADVANCEMENT IN THERMAL ENERGY STORAGE USING PHASE CHANGE MATERIALS

by

RAMI MOHAMMAD REDA SAEED

A DISSERTATION

Presented to the Faculty of the Graduate School of the

MISSOURI UNIVERSITY OF SCIENCE AND TECHNOLOGY

In Partial Fulfillment of the Requirements for the Degree

DOCTOR OF PHILOSOPHY

in

NUCLEAR ENGINEERING

2018

Approved
Joshua P. Schlegel, Advisor
Carlos H. Castano
Ayodeji B. Alajo
Hyoung K. Lee
Fatih Dogan

ABSTRACT

The dissertation is intended to study the fundamental physical behavior of phase change materials (PCMs) and provide a comprehensive overview of the state of the art in their design and applications for thermal energy storage. Standard, predictive and thermodynamic models were presented to develop new PCM eutectic mixtures in a more scientific design approach. As new eutectic PCMs were developed, further research efforts were initiated to develop functionalized PCMs with enhanced thermal and physical properties to create the next generation of PCMs. Further efforts have been expanded to review several high-temperature PCM candidates with phase transition temperatures in the range of 70 ºC to 90 ºC for enhancing the passive safety and heat removal capabilities of the reactor containment during Loss of Coolant Accidents (LOCA). An optimum PCM candidate was selected and the temperature-dependent properties of the selected PCM were studied in detail. The study has also reviewed very high-temperature PCMs in the range of 300 ºC to 900 ºC which provide a unique opportunity to meet the variation in the power plant demand profiles. This review discussed various design and technical aspects on the concept of a coupled nuclear reactor thermal energy storage unit for several reactor types and identified numerous very high-temperature PCMs for potential improvements to Generation IV reactor designs and load shifting purposes. Finally, as a first step on experimentally studying a real PCM thermal energy storage system, a PCM heat exchanger in the form of parallel-plate heat exchanger was built and experimentally characterized for load shifting purposes.

ACKNOWLEDGMENTS

I would like to thank many people who have generously contributed to this work. First my wife, whose constant support and encouragement have been invaluable, and my family for all the sacrifices that they have made on my behalf in every imaginable level. My advisor Dr. Joshua Schlegel for holding me to high research standards, for giving me freedom to explore on my own, and for guiding me along the way. Dr. Carlos Castano, Dr. Ayodeji Alajo, Dr. Hyoung Lee and Dr. Fatih Dogan for serving on my advisory committee and for their insightful comments and advice. The R&D team and all employees at Phase Change Energy Solutions Inc. (PCES) - where part of this research was conducted - for the continuous encouragement. I am particularly appreciative to Dr. Sawafta, Chief Scientific Officer at PCES, not only for his time and constant support, but for his intellectual contributions to my career in general. I would like to extend my thanks to those who have had a strong influence early in my career, Dr. Elgohary, Dr. Kodah, Dr. Sabbarini, and Ms. Abunasser. Finally, my colleagues who have assisted along the journey of my PhD.

TABLE OF CONTENTS

Page

ABSTRACT iii

ACKNOWLEDGMENTS iv

LIST OF ILLUSTRATIONS ix

LIST OF TABLES xiii

SECTION

1. INTRODUCTION 1

1.1. OBJECTIVES AND SCOPE 1

1.2. AN INTRODUCTION TO PHASE CHANGE MATERIALS 5

1.2.1. Thermal Energy Storage. 5

1.2.2. Phase Change Materials. 7

1.2.3. Advanced Phase Change Analysis. 12

1.2.4. Advancement in Phase Change Eutectic Mixtures 22

1.3. APPLICATIONS OF PHASE CHANGE MATERIALS. 26

1.3.1. Nuclear Thermal Energy Storage Applications. 26

1.3.2. Space Applications. 26

1.3.3. Solar Power Systems. 27

1.3.4. Building Applications. 30

1.3.5. Solar Photovoltaic System 33

1.3.6. Electronics. 34

1.3.7. Other Applications. 35

2. EXPERIMENTAL METHODS 37

2.1. DIFFERENTIAL SCANNING CALORIMETRY (DSC). 37

2.2. GUARDED PARALLEL-PLATE HEAT FLOW METHOD..... 40

2.3. TRANSIENT HOT BRIDGE (THB) METHOD 46

2.4. OTHER METHODS AND INSTRUMENTS. 49

3. PREPARATION AND THERMAL PERFORMANCE OF METHYL PALMITATE AND LAURIC ACID EUTECTIC MIXTURE AS PHASE CHANGE MATERIAL (PCM)..... 51

3.1. DEVELOPMENT OF PCM EUTECTIC MIXTURES..... 52

3.2. MATERIALS AND METHODS..... 55

3.2.1. Theoretical Prediction of MP/LA Binary Mixture.. 56

3.2.2. Thermal Characterization. 57

3.3. RESULTS AND DISCUSSION 59

3.3.1. The MP/LA Eutectic Mixture..... 60

3.3.2. Specific Heat.. 63

3.3.3. Thermal Conductivity..... 64

3.3.4. Thermal Diffusivity. 66

3.3.5. Thermal Stability of MP/LA Eutectic Mixture. 68

3.4. FINDINGS AND FUTURE REMARKS 69

4. PREPARATION AND ENHANCED THERMAL PERFORMANCE OF NOVEL (SOLID TO GEL) FORM-STABLE EUTECTIC PCM MODIFIED BY NANO-GRAPHENE PLATELETS..... 71

4.1. DEVELOPMENT NEEDS 72

4.2. MATERIALS AND METHODS..... 76

4.2.1. Preparation of PCM.. 78

4.2.2. Thermal Characterization.. 79

4.2.3. Determination of Phase Transition Temperature of Bulk PCM. 81

4.3. RESULTS AND DISCUSSION 82

4.3.1. Thermal Performance of Form-Stable (Solid To Gel) Binary Eutectic PCM.. 83

4.3.2. Enhanced Thermal Performance of The Form-Stable PCM. 85

4.3.2.1. Effect of NGPs on phase transition. 85

4.3.2.2. Thermal conductivity enhancement. 87

4.3.2.3. Enthalpy curves and specific heat capacity. 89

4.3.2.4. Thermal diffusivity and density. 92

4.3.2.5. Optimum form-stable PCM mixture. 95

4.3.2.6. Enhanced supercooling of the thermal enhanced form-stable eutectic PCM 96

4.3.2.7. Melting and freezing phase transition temperature of bulk PCM. 99

4.3.2.8. Thermal reliability of the thermal modified form-stable eutectic PCM 102

4.4. PERFORMANCE REMARKS AND FUTURE DIRECTIONS 103

5. DEVELOPMENT OF HIGH-TEMPERATURE PCMs FOR ENHANCING PASSIVE SAFETY AND HEAT REMOVAL CAPABILITIES IN NUCLEAR REACTOR SYSTEM 105

5.1. PRELIMINARY SCREENING OF SUITABLE PCMs 107

5.2. OCTADECANOIC ACID AS A PROMISING PHASE CHANGE MATERIAL FOR ICE CONDENSORS 116

5.2.1. Background on Modulated DSCs and Direct Specific Heat Capacity Measurements in the Overlap and Phase Transition Region. 121

5.2.2. Temperature Dependent Phase Transition and Specific Heat Capacity.. 126

5.2.3. Temperature Dependent Thermal Conductivity.. 129

5.2.4. Temperature Dependent Density. 131

5.2.5. Temperature Dependent Thermal Diffusivity. 133

5.3. OUTCOMES AND DISCOVERIES 135

6. LOAD SHIFTING OF NUCLEAR POWER PLANTS USING THERMAL ENERGY STORAGE: A REVIEW 137

6.1. LOAD SHIFTING 137

6.2. DESIGN ASPECTS 139

7. DESIGN AND EXPERIMENTAL INVESTIGATION ON THE THERMAL PERFORMANCE OF PCM ENERGY STORAGE HEAT EXCHANGER 147

7.1. THERMAL ENERGY STORAGE FOR LOAD SHIFTING 147

7.2. EXPERIMENTAL FACILITY 157

7.3. EXPERIMENTAL PROCEDURE AND METHODS 163

7.4. ENERGY ANALYSIS 164

7.5. ANALYSIS OF THE PHASE CHANGE MATERIAL 166

7.6. EXPERIMENTAL ANALYSIS OF THE PCM HEAT EXCHANGER 170

7.6.1. Effect of Plate-Plate Spacing. 171

7.6.2. Thermal Energy Storage Performance. 173

7.6.3. Parametric Analysis. 180

7.7. FINDINGS AND PERFORMANCE REMARKS 183

8. CONCLUSION 185

REFERENCES 186

VITA 205

LIST OF ILLUSTRATIONS

Page

Figure 1.1. Thermal energy storage in PCMs 7

Figure 1.2. Comparison between thermal energy storage of Myristic Acid PCM and water..... 9

Figure 1.3. Classification of PCMs 10

Figure 1.4. Typical results from a differential Scanning Colorimetry (DSC) experiment..... 13

Figure 1.5. The enthalpy-temperate curve of phase change calculated from DSC results 14

Figure 1.6. Phase transition characteristics of PCMs using the enthalpy curve..... 15

Figure 1.7. Schematic for the cooling curve of PCM with supercooling (line a) and PCM with reduced supercooling (line b)..... 16

Figure 1.8. Hysteresis of PCMs: (a) the temperature rises again to the phase transition temperature, (b) the temperature does not rise to the phase transition, (c) real hysteresis caused by slow rate of crystallization of real difference between melting and freezing, (d) apparent hysteresis due to non-isothermal conditions during measurements [24]. 16

Figure 1.9. Sketch for thermal cycling stability of stable and unstable PCMs, i.e. Organic vs Inorganic..... 19

Figure 1.10. Sketch for the phase separation of inorganic or off-eutectic organic PCMs upon thermal cycling..... 20

Figure 1.11. Typical phase diagram for a binary eutectic PCM..... 22

Figure 1.12. Typical phase diagram of ternary eutectic mixture..... 24

Figure 1.13. Concentrated solar plant with carrier fluid for thermal energy storage [42] . 28

Figure 1.14. Utilization of thermal energy storage to match the supply with demand 28

Figure 1.15. Cylindrical storage tank with PCM storage [44] 30

Figure 1.16. PCMs storing heat (left) and releasing heat (right)..... 31

Figure 1.17. Ventilated ceiling with PCM for daily charging and discharging. 32

Figure 1.18. Reducing indoor temperature swing using PCMs [57]..... 32

Figure 2.1. Schematic diagram of a Tzero Discovery DSC cell [83] (left) and DSC instrument (right). 38

Figure 2.2. The guarded parallel-plate heat flow apparatus using Fox314 TA instrument [86]..... 42

Figure 2.3. Schematic for the guarded parallel-plate heat flow apparatus using Fox314 TA instrument [86] 43

Figure 2.4. The measured experimental and theoretical thermal conductivity of EPS specimen certified by NIST 46

Figure 2.5. The Transient Hot Bridge circuit [88] and experimental apparatus. 47

Figure 2.6. Accelerated thermal cycler used for thermal cycling of PCMs 49

Figure 3.1. The predicted phase diagram for the MP/LA binary mixture..... 57

Figure 3.2. DSC curves of methyl palmitate (MP) and lauric acid (LA). 59

Figure 3.3. DSC melting curves of the binary mixture series 61

Figure 3.4. DSC curves and total thermal energy storage for 60MP/40LA eutectic mixture. 62

Figure 3.5. DSC curves for the MP/LA binary mixture after thermal cycling..... 68

Figure 4.1. Schematic diagram for a stack of Nano Graphene Platelets (NGPs)..... 77

Figure 4.2. Digital photograph of (a)the eutectic PCM mixture (MP-LA), (b)form-stable gelled PCM (MP-LA/HPEC), and (c) the thermal modified form-stable eutectic PCM (MP-LA/HPEC/NGP10%). 78

Figure 4.3. The experimental setup using the Fox314 instrument. 81

Figure 4.4. DSC results for MP-LA eutectic PCM and form-stable gelled PCM (MP-LA/HPEC)..... 84

Figure 4.5. DSC results for gelled eutectic PCM modified by NGPs compared to MP-LA eutectic PCM and form-stable MP-LA/HPEC mixture..... 86

Figure 4.6. Thermal conductivity enhancement of PCMs with NGPs. 88

Figure 4.7. Enthalpy-temperature curve for the experimental PCM mixtures..... 90

Figure 4.8. Effect of HPEC and NGPs on the total thermal energy storage, latent heat contribution, and sensible heat contribution 92

Figure 4.9. The observed DSC freezing profile for various PCM mixtures 97

Figure 4.10. The temperature-time response during melting and freezing of PCMs..... 100

Figure 4.11. The DSC curves for the MP/LA/HPEC/NGP10% PCM mixture after 0, 1000, 5000, 10000, 15000, 20000, and 30000 thermal cycles..... 103

Figure 5.1. Sketch for ice condenser [158] 106

Figure 5.2. Preliminary screening of PCMs with suitable phase change temperature. 108

Figure 5.3. Experimental DSC spectrums for the polywax PCMs..... 110

Figure 5.4. Eutectic mixtures of polywax 756 and 655 (a) and ploywax 500 and 400(b). 112

Figure 5.5. Experimental phase transition spectrum for xylitol 113

Figure 5.6. DSC spectrum of hydrogenated castor oil (HCO). 115

Figure 5.7. Dependency of the DSC maximum heat flow signal on the measurement conditions [1]. 122

Figure 5.8. The measured experimental and theoretical specific heat capacity of Sapphire. 125

Figure 5.9. DSC results for phase transition of octadecanoic acid..... 126

Figure 5.10. Temperature-dependent specific heat capacity for the solid phase and liquid phase regions (figure a, white region) and the overlap phase transition region (figure b). 127

Figure 5.11. Temperature dependent thermal conductivity k(T) for solid and liquid phases. 130

Figure 5.12. Temperature dependent density ρ(T) for solid and liquid phases. 132

Figure 5.13. Temperature dependent thermal diffusivity α(T) for solid and liquid phases. 134

Figure 6.1. System block diagram for a nuclear reactor coupled with TES system 138

Figure 6.2. LW-SMR coupled with thermal energy storage [202]. 141

Figure 6.3. PB-FHR coupled with thermal energy storage [202]. 143

Figure 6.4. MHTGR coupled with thermal energy storage [202]. 144

Figure 7.1. A typical load profile of an industrial thermal system. 148

Figure 7.2. A typical commercial ice/water thermal storage system by CALMAC 149

Figure 7.3. A comparison between the proposed PCM energy storage system and ice energy storage system. 152

Figure 7.4. Image and schematic for the experimental storage heat exchanger unit 157

Figure 7.5. Picture and schematic for the heat exchange plates. 158

Figure 7.6. The experimental setup for optimization of various plate-plate spacing, 1 inch (25.4mm) left figures, and 2 in (50.8 mm) for right figures. 159

Figure 7.7. The measured thermal conductivities and R-values of the vessel insulation 160

Figure 7.8. Schematic of the experimental facility. 161

Figure 7.9. DSC results for the phase change transition of hexadecane ($C_{16}H_{34}$) 168

Figure 7.10. Outlet temperature profiles of different plate-plate spacing arrangement. .. 172

Figure 7.11. Thin film of PCM layer at the surface of plates during a discharge cycle... 172

Figure 7.12. A comparison of various outlet water temperature profiles with respect to time during the melting cycle at various flow rates and inlet water temperatures. 173

Figure 7.13. The cumulative energy storage profiles at various inlet conditions 174

Figure 7.14. Heat transfer coefficient of the PCM heat exchanger at various conditions. 175

Figure 7.15. Effectiveness of the PCM heat exchanger at various inlet conditions. 176

Figure 7.16. Outlet temperature as a function of PCM transition temperature and various inlet conditions. 178

Figure 7.17. Discharge profiles for various inlet condition. 179

Figure 7.18. The required number of heat exchanger units as a function of monthly thermal load at various operating/inlet conditions. 182

Figure 7.19. Immersion plates manufactured by Omega Thermo Products 184

LIST OF TABLES

Page

Table 1.1. Comparison between different families of PCMs [17-23] 11

Table 1.2. A comparison between the experimental values by Zhao et al. [38] and theoretical predicted values for a ternary eutectic mixture. 25

Table 2.1. Specification of the experimental DSC instruments 40

Table 2.2. Specification of the guarded parallel-plate heat flow apparatus using Fox314 TA instrument 45

Table 2.3. Specification of the transient hot bridge apparatus. 48

Table 3.1. Chemical data and theoretical thermal properties for the individual PCMs 55

Table 3.2. DSC results of Methyl Palmitate, Lauric Acid, and the binary mixture 60

Table 3.3. DSC results for three independent measurements of different samples of the 60MP/40LA eutectic mixture 63

Table 3.4. The specific heat capacity and total energy storage capacity values for PCMs..... 64

Table 3.5. Thermal conductivity test for liquid state PCMs using THB1 meter..... 65

Table 3.6. Thermal conductivity for solid state PCMs using Fox 314 heat flow meter..... 65

Table 3.7. The experimental density for the MP, LA, and MP/LA eutectic mixture..... 67

Table 3.8. The measured thermal diffusivity for MP, LA, and MP/LA eutectic mixture.. 67

Table 3.9. Thermophysical properties of the MP/LA binary mixture after thermal cycling..... 69

Table 4.1. The chemical and physical data of PCMs. 76

Table 4.2. The chemical data of the gelling agent..... 76

Table 4.3. Properties of the experimental Nano Graphene Platelets (NGPs)..... 77

Table 4.4. Optimizing the suitability and ratio of HPEC gelling agent. 83

Table 4.5. DSC data for gelled Eutectic PCM modified by NGPs. 85

Table 4.6. DSC data for gelled Eutectic PCM modified by NGPs compared to MP-LA eutectic PCM and form-stable MP-LA/HPEC mixture. 86

Table 4.7. Effect of NGPs on the thermal conductivity of gelled Eutectic PCM 88

Table 4.8. The measured specific heat capacity and thermal energy storage (TES) for the experimental PCMs..... 91

Table 4.9. Effect of the addition of NGPs on density 93

Table 4.10. Effect of the addition of NGPs on the thermal diffusivity 94

Table 4.11. A comparison on thermo-physical properties of different form-stable PCMs in other literature and the current study. 96

Table 4.12. The DSC results for melting and freezing temperature of PCM mixtures..... 97

Table 4.13. The DSC results for the MP-LA/HPEC/NGP10% PCM after thermal cycling..... 102

Table 5.1. List of high-temperature PCMs during the preliminary screening. 109

Table 6.1. Thermal characteristics for several types of nuclear reactors. 140

Table 6.2. High-temperature PCMs and their available thermo-physical properties..... 145

Table 7.1 A comparison between the PCM and ice energy storage system..... 152

Table 7.2. Potential applications of PCM energy storage heat exchanger system..... 153

Table 7.3. Specifications of the energy storage heat exchanger 157

Table 7.4. Inlet conditions for the experiments..... 164

Table 7.5. The chemical and physical data of the PCM..... 168

Table 7.6 Results for the thermal characteristics of hexadecane ($C_{16}H_{34}$)..... 169

Table 7.7. Results for the thermal conductivity of hexadecane ($C_{16}H_{34}$)..... 170

Table 7.8. Summary for thermal characteristics of the heat exchanger at various operating conditions..... 181

1. INTRODUCTION

1.1. OBJECTIVES AND SCOPE

Thermal Energy Storage (TES) has become one of the most pressing topics worldwide. The serious concern of public regarding greenhouse gases emissions, limited reserves of fossil fuel, and rapid growth of global energy have shed the light on the effective utilization of thermal energy. According to the U.S energy information administration [1], the global world energy use is estimated to increase from 1.7×10^{11} MWh in 2015 to $2.2x10^{11}$ MWh in 2040, an increase of 29%. Thermal energy storage provides a key method to reduce energy consumption and dependency on fossil fuels. Efficient utilization of energy can be achieved by matching the energy supply with demand by means of thermal energy storage systems. For instance, power plants can run at maximum power, and excess heat from production can be transferred to thermal storage systems where it is stored for later utilization during peak demand, increasing efficiency and reducing the mismatch between energy supply and demand. In this context, thermal energy storage using Phase Change Materials (PCMs) present a unique opportunity to reduce the need to fossil fuel and suppress greenhouse gases emission.

The ultimate objective of this research is to develop high-temperature phase change materials as potential candidates for passive safety mechanisms to improve the reliability and safety of nuclear reactors. The first step in that direction was developing methodologies and standards for thermal characterization of PCMs [2], and developing new eutectic PCMs for low temperature applications [3]. The results of that step have verified and improved key factors affecting the performance of PCMs and resulted in a more scientific design approach for developing eutectic PCMs. This approach was used in the next steps to study

the high-temperature PCMs for nuclear safety applications. The components of the overall research plan can be summarized as follows:

1. Uncertainty of Thermal Characterization of Phase Change Material by Differential Scanning Calorimetry Analysis [2].

   Scope: Advanced Methodologies and Standards for Thermal Characterization of PCMs.

2. Preparation and Thermal Performance of Methyl Palmitate and Lauric Acid Eutectic Mixture as Phase Change Material (PCM) [3].

   Scope: Developing New eutectic PCMs for low-medium temperature applications.

3. Preparation and Enhanced Thermal Performance of Novel (Solid to Gel) Form-stable Eutectic PCM Modified by Nano-Graphene Platelets [4].

   Scope: Enhancing heat transfer and functionality of the eutectic PCMs.

4. Development of High-Temperature PCMs for Enhancing Passive Safety and Heat Removal Capabilities in Nuclear Reactor Systems.

   Scope: Developing suitable PCMs for safety and performance enhancement of ice condenser system in the reactor containment.

5. Load Shifting of Nuclear Power Plants Using Thermal Energy Storage: A Review.

   Scope: Reviewing design concepts of several reactors and identifying high-temperature PCMs for potential improvements to Generation IV reactors and load shifting purposes.

6. Design and Experimental Investigation on the Thermal Performance of PCM Energy Storage Heat Exchanger.

   Scope: Parallel plate heat exchanger design utilizing PCMs as latent heat storage medium in the form of an energy storage vessel for load shifting purposes.

The research component of the first point was focused on developing thermal characterization methodologies and theoretical predictive capabilities using low temperature PCMs in the range of 20 ºC to 60 ºC. Further details of this effort can be found in the author's paper [2] and thesis [5]. This stage was a critical component for the development of the overall research plan. Developing standards and precise predictive capabilities have provided key understanding of the factors affecting PCM performance and resulted in a more advanced design approach for developing binary and ternary eutectic PCMs.

A comprehensive overview of the physical behavior of PCMs and state of the art in their design and applications for thermal energy storage are presented in Section 1.1. Section 2 provides a brief overview of the analysis and experimental methodologies.

Section 3 is focused on experimental investigations of developing new eutectic PCM mixtures. Naturally occurring organic PCMs such as fatty acid, methyl esters, and high-temperature sugar alcohols exhibit great thermal properties. Their applications, however, are limited due to the fixed phase transition temperature of the current existing PCMs. Hence, their individual melting temperatures are sometimes higher or lower than the required temperature for some applications. A theoretical thermodynamic model based on Schroeder-var equation was presented. The model provides a powerful tool to save time and money, initially predict the eutectic composition of eutectic PCMs, and to develop PCMs with phase transition temperatures that cannot be met with existing materials. A new binary PCM eutectic mixture was developed at the desired phase transition temperature with latent heat of fusion that is as much as 20% higher than other PCMs developed for applications in the same temperature range.

In Section 4, the research effort is focused on enhancing the thermal performance, functionality and crystallization process of eutectic PCMs. The major limitations of organic PCMs in general are the low thermal conductivity, leakage of its liquid phase, and supercooling. To address these issues, we presented characterization methods and developed a PCM characterized by an enhanced thermal performance, as well as novel (Solid to Gel) shape-stable eutectic PCM and reduced supercooling.

In Section 5, the objective was to characterize suitable PCMs for nuclear safety enhancement in the containment. PCMs with phase transition temperature in the range 70ºC to 90ºC and latent heat of around 200 kJ/kg or higher are proposed to solve many of the maintenance issues of the ice condenser system in Small Modular Reactors (SMRs).

Section 6 presents the concept of a coupled nuclear reactor thermal energy storage system utilizing high-temperature PCMs as a potential passive safety mechanism to improve the safety and reliability of SMRs, and for load shifting purposes. Developing PCMs with suitable phase transition behavior is the key. The technical and design aspects for several reactor types are discussed and wide range of binary and ternary mixtures of high-temperature eutectic PCMs are identified as potential candidates.

In Section 7, whereas the objective of the previous section was studying PCMs for energy storage and load shifting in nuclear reactors, this section presents experimental investigation of a parallel-plate heat exchanger design utilizing PCMs in the form of an energy storage vessel for load shifting purposes. A latent heat storage system was built to experimentally investigate the performance of PCMs for storage and release of thermal energy.

1.2. AN INTRODUCTION TO PHASE CHANGE MATERIALS

Thermal energy storage is a key technology for an effective utilization of energy. The applications of phase change materials for thermal energy storage have been the focus of extensive research in recent decades. Their use can reduce the size and cost of the system, offering higher thermal storage capacity and the ability to be used as a thermal management tool. The following sections present the fundamentals of phase change materials including the details of their physical behavior, design issues, and applications for thermal energy storage.

1.2.1. Thermal Energy Storage. There are three common ways to store thermal energy: sensible heat, latent heat and thermo-chemical energy. In sensible heat, energy is stored/released by raising/reducing the temperature of a storage material without changing the phase [6]. Besides the mass of storage material, the amount of sensible heat storage is limited by the temperature change of the system as seen in equation 1.

$$Q = m\int_{T1}^{T2} C_P.dT \tag{1}$$

Where Q is the sensible heat stored, m: is the mass of storage material, T_1 and T_2 are the temperature range which the process operates.

In latent heat storage systems, thermal energy is stored or released by the material while it experiences a phase transition from solid to liquid during a charging period, or liquid to solid during a discharging period. Phase change may also occur in form of liquid-gas phase transition characterized by even higher latent heat than solid-liquid. liquid-gas phase transition however is not commonly used for energy storage applications due to the

higher pressure and the impractical large volume involved. Unlike sensible heat, latent heat storage is attractive in that it stores larger amount of energy at constant temperature during phase transition. The storage capacity of a latent heat system is given by:

$$Q = m\left[\int_{T1}^{Tm} C_{P\_Solid}.dT + \Delta h + \int_{Tm}^{T2} C_{P\_Liquid}.dT\right] \quad (2)$$

Where Q is the latent heat stored in the system, m is the mass of storage material, T_m *is* melting temperature of storage material, Δh is the enthalpy or latent heat of storage material, T_1 and T_2 represent the temperature range and C_p is the specific heat capacity at constant pressure.

In thermo-chemical energy storage, heat is absorbed or released through a completely reversible chemical reaction when the molecular bonds are reformed and broken during an endothermic or exothermic reaction as given in equation 3. Due to the high cost of such systems, their applications are very limited [7]. The storage capacity of a thermo-chemical system is given by:

$$Q = ma_r\Delta h \quad (3)$$

Where Q is the thermo-chemical energy stored, m is the mass of storage material, a_r is the extent of conversion and Δh is the endothermic heat of the reaction.

1.2.2. Phase Change Materials. Phase Change Materials (PCMs) are latent heat energy storage materials that undergo solid-liquid phase transition at specific temperature known as the phase transition temperature [8-11]. As the PCM absorbs energy from the surrounding, the material changes its phase from solid to liquid while maintaining nearly constant temperature that corresponds to the phase transition temperature of the PCM. The absorbed energy is stored in the constituent atoms or molecules in the form of vibrational energy. When PCM absorbs its maximum energy storage capacity, the atomic bonds are loosened, and the PCM completes its transition from solid to liquid. This amount of energy absorbed during phase transition is known as the latent heat or enthalpy of fusion. Solidification, also known as freezing or crystallization, is the reverse of this process during which the energy is released, molecules are reordered, and the material transitions from liquid to solid at nearly constant temperature. This process can be seen in Figure 1.1.

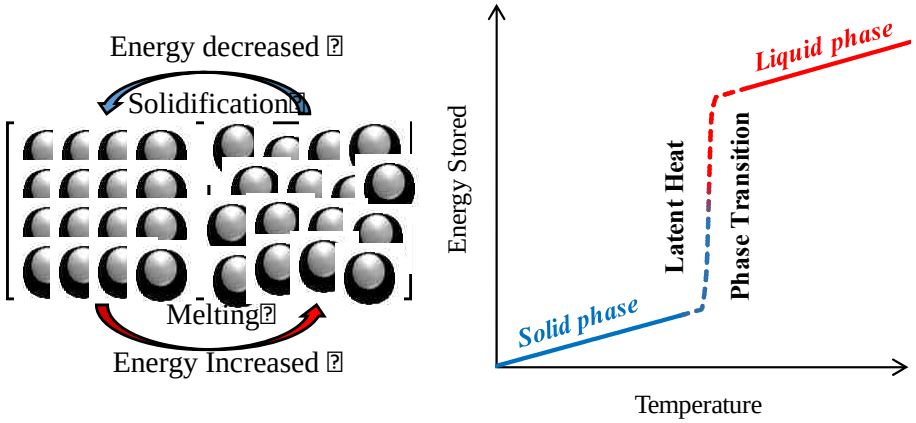

Figure 1.1. Thermal energy storage in PCMs

When choosing a PCM for a given application the main considerations are the phase transition temperature and the latent heat of fusion. The phase transition temperature needs to be within the operating range of the application, or within the temperature range at which the system needs to be maintained. The latent heat of fusion should be as high as possible. When compared to sensible heat storage materials, the main benefits of PCMs is the ability to maintain the system at nearly constant temperature during the phase transition in a passive way regardless of the applied heat flux. Therefore, efficient thermal management is only possible using PCMs, while sensible storage material can only store thermal energy over a temperature range. Moreover, PCMs have much higher energy storage density, reducing the volume of the system, and resulting in less material mass. PCMs, however, do not fully meet the requirements for all thermal energy storage systems. A wide range of technical solutions have been developed. For instance, current existing PCMs are only available at particular phase transition temperatures. Therefore, eutectic PCM mixtures can be developed to create new PCMs with improved properties and new phase transition temperatures. In addition, finding materials with very high latent heat as well as excellent heat transfer characteristics has been challenging. The low thermal conductivity and thermal diffusivity of PCMs prevent rapid system transients. Currently, the enhancement of heat transfer in PCMs is one of the most pressing topics.

A PCM based system can have a heat storage capacity that is 4-50 times larger than sensible heat storage materials [5]. For instance, water is a common storage medium for solar water heating systems in the range of 45°C to 60°C [7]. In Figure 1.2, the theoretical energy storage of a PCM tank -Myristic Acid with phase transition temperature of 54°C and latent heat of 220J/g - is compared to that of water.

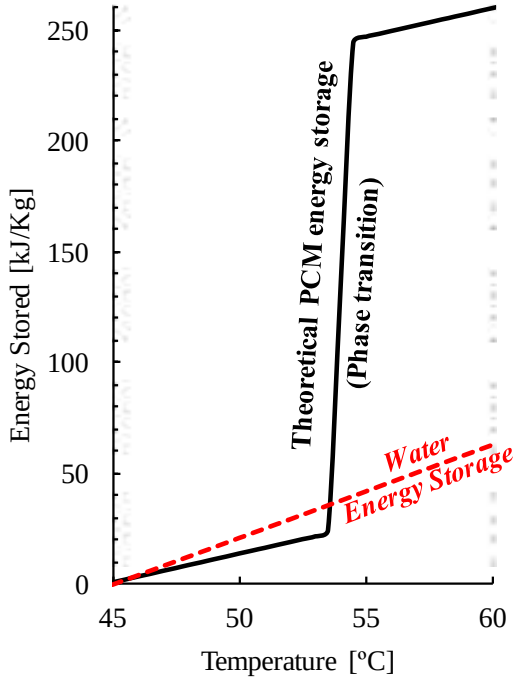

Figure 1.2. Comparison between thermal energy storage of Myristic Acid PCM and water

Theoretically, the PCM tank can store 260 Joules per 1 Kg of PCM compared to 63 Joules per 1 Kg of water, an increase of 313% in energy storage capacity over a temperature range of 15°C. For a storage temperature of 55°C and temperature range of 5°C, the energy storage of the PCM system is 11 times larger than a sensible heat storage system. In other words, a solar system with PCMs can be 4-11 times smaller than water systems and still able to store the same amount of thermal energy. Moreover, the PCM tank can store most of the energy at 54-55 °C, illustrating a higher useful quality for energy. The same concept can also be applied in larger solar energy power plants. PCMs can be integrated in the system to store the excess solar energy during periods of lower demand and utilize it later when the demand exceeds the supply.

PCMs are typically separated into three categories: organic, inorganic, and eutectics. A classification is given in Figure 1.3.

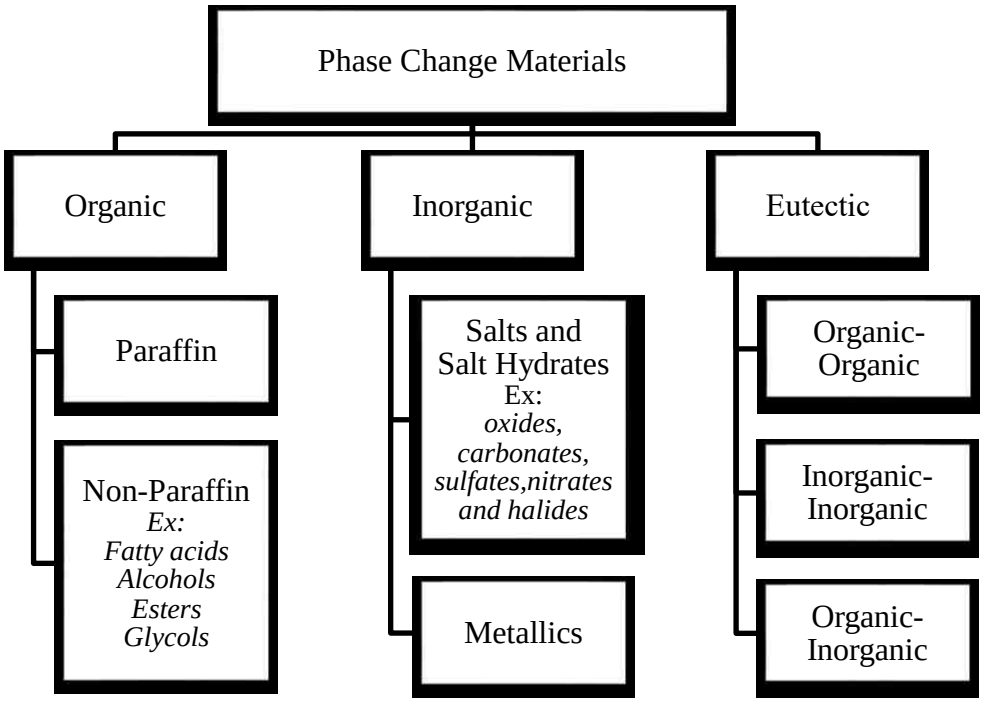

Figure 1.3. Classification of PCMs

In general, organic PCMs are the most popular type of PCMs, classified as Paraffin (C_nH_{2n+2}) and the non-paraffin such as fatty acids ($CH_3(CH_2)_{2n}COOH$) [12]. Depending on the hydrocarbon chain structure, each PCM has its particular phase transition temperature and latent heat of fusion. Most organic PCMs are characterized by excellent thermal stability, non-corrosiveness, non-toxicity, and little or no supercooling [13, 14]. Their major limitation is the very low thermal conductivity, relatively higher cost, and flammability [12]. Inorganic PCMs are classified as salts and metallic alloys. Salt hydrates

consist of a crystal matrix of water and salt solution [12, 15]. The high latent heat of some mixtures, low cost, ease of availability, high specific heat, and high thermal conductivity of salt hydrates are very attractive for practical application, however the supercooling and poor thermal stability upon cycling due to phase separation and dehydration are their main drawbacks [16]. Metallic alloys possess attractive thermo-physical properties such as high thermal conductivity and specific heat, however they are mostly available with very high phase transition temperatures, limiting their applications. Eutectic PCMs are two or more components that melt and freeze simultaneously. Details on eutectic PCMs are presented in Section 1.2.4 and Section 3. A comparison between different PCMs is given in Table 1.1.

Table 1.1. Comparison between different families of PCMs [17-23]

	Organics	Salts/Salt hydrates	Metallics
Latent heat	Fatty acids: 100–240 J/g Methyl esters: 200-250 J/g Sugar Alcohols: 200-300J/g Paraffins: 170-270 J/g	90 – 492 J/g	16-560 J/g
Cost	Moderate	Low	Low to high
Availability	Widely available	Widely available	varies
Conductivity	0.15 - 0.4 W/m.K	0.5-1.2 W/m.K	8-237 W/m.K
Specific heat	1.5 – 2.8 J/g.K	2.5 – 4.5 J/g.K	0.2-1.5 J/g.K
Density	0.7-0.96 kg/m^3	1.3-2.5 kg/m^3	1740-7030 kg/m^3
Supercooling	Minimal to Self-nucleating	High	Minimal
Melting	Very sharp	Wide-sharp	Very sharp
Phase separation	No phase separation	Separates	No separation
Thermal stability	Mostly stable	Mostly unstable	Stable
Flammability	Some are Flammable	Non-flammable	Non-flammable
Corrosiveness	Mostly Non-corrosive	Corrosive	Non-corrosive

1.2.3. Advanced Phase Change Analysis. Recent effort has been focused on the development of PCMs for wide range of applications, but a lot of the effort has been based on testing new materials rather than targeting limitations of PCMs in general through understanding of the underlying causes. A wide range of energy storage applications have been proposed using PCMs, from small electrical devices to large scale space applications. In order to develop technical solutions and overcome the limitations of current PCMs, the physics of phase change needs to be fully understood. This section is intended to provide a compressive overview of the fundamental physical behavior of PCMs, limitations and methods to enhance it.

For practical application, a variety of PCMs can be found with a desirable operating temperature range, and high latent heat of fusion. However, there are a number of key factors that must be also considered. The most detailed information about the phase change transition can be obtained from the differential scanning calorimetry (DSC) experiments. Details on the DSC experiments can be found in Section 2. From such experiments, the heat flow during the solid-liquid phase transition can be extracted at a resolution of better than 0.01°C for some advanced DSCs, which provide the most comprehensive information about the phase change process. Information that can be obtained from the DSC experiments includes but not limited to: phase change latent heat of fusion, phase transition temperature, phase separation, phase change temperature range, sensible heat component, crystallization, decomposition, supercooling and thermal stability. In order to characterize the physical behavior of PCMs during the phase change process, the DSC spectra and results should be fully understood. Figure 1.4 shows a typical result from a DSC

experiment for PCMs. In short, the DSC measures the amount of heat absorbed or released by the PCM sample as a function of temperature.

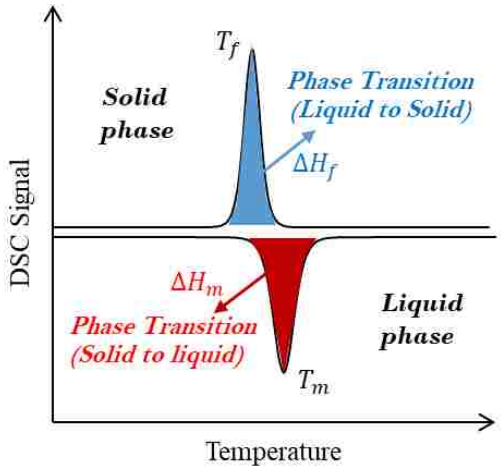

Figure 1.4. Typical results from a differential Scanning Colorimetry (DSC) experiment

The red shaded area represents the enthalpy of fusion for the solid to liquid phase transition (ΔH_m), similarly, the blue shaded area (ΔH_f) refers to liquid to solid phase transition. The peak temperature for the solid to liquid phase transition peak is the melting temperature (T_m), and the peak temperature for the liquid to solid phase transition peak is the freezing temperature (T_f), also known as the solidification temperature.

In order to obtain comprehensive and detailed information about the phase change process, the DSC spectrum should be further analyzed. Thus, the enthalpy-temperature curve is calculated from the DSC spectrum using thermodynamic calculations as presented in detail in Section 3.3.2. With the enthalpy-temperature curves, as seen in Figure 1.5, in

addition to the latent heat of fusion (ΔH) and phase transition temperatures, it becomes possible to measure the direct specific heat capacity (C_p), total energy storage or enthalpy sum and the phase transition temperature range (τ).

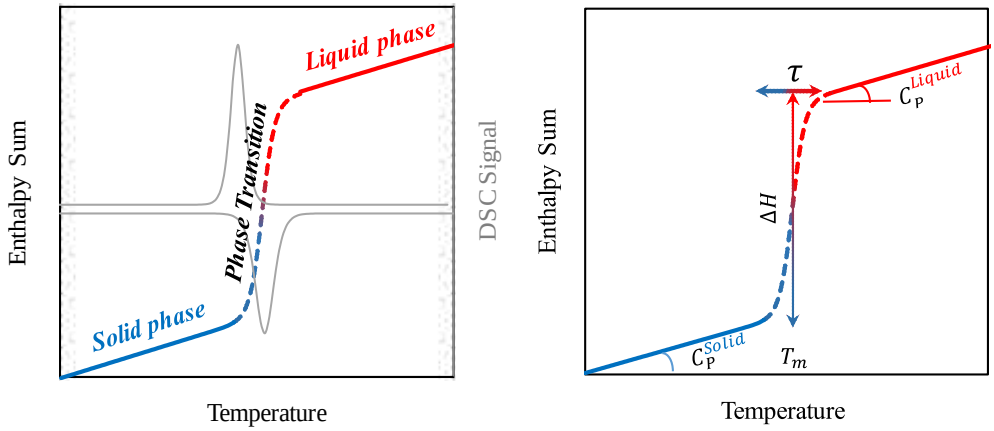

Figure 1.5. The enthalpy-temperate curve of phase change calculated from DSC results

One of the benefits to using the enthalpy curve when describing phase transition of PCMs is that the temperature control, specific heat, latent heat and state of phase for different PCMs can be easily compared. Some examples for the phase transition characteristics for an ideal PCM and common PCM are given in Figure 1.6. Additionally, the enthalpy-temperature curve is used as an input for the modelling and simulation of transient behavior of PCMs in many software packages such as EnergyPlus and Modelica.

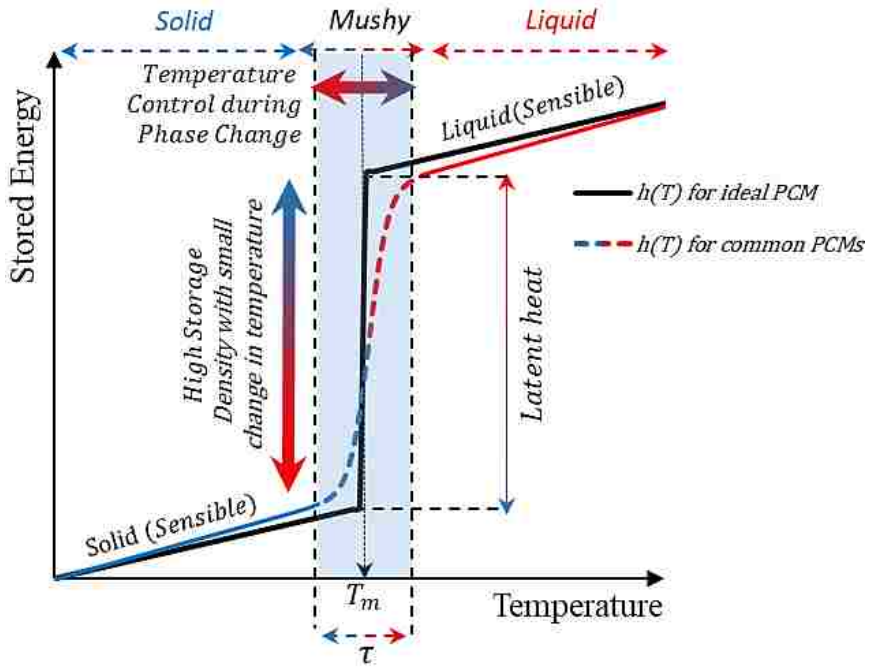

Figure 1.6. Phase transition characteristics of PCMs using the enthalpy curve

In the case of ideal PCM, it is assumed that the enthalpy-temperature curve is the same for the solid-to-liquid phase transition during melting and liquid-to-solid phase transition during freezing. However other phenomena such as hysteresis and supercooling can influence this reversible balance. Supercooling occurs when the PCM during liquid to solid phase transition has to reach temperatures well below the phase transition temperature to start crystallization and to release the latent heat of solidification. Figure 1.7 shows an example for a PCM with significant supercooling (line a) and another with reduced supercooling (line b).

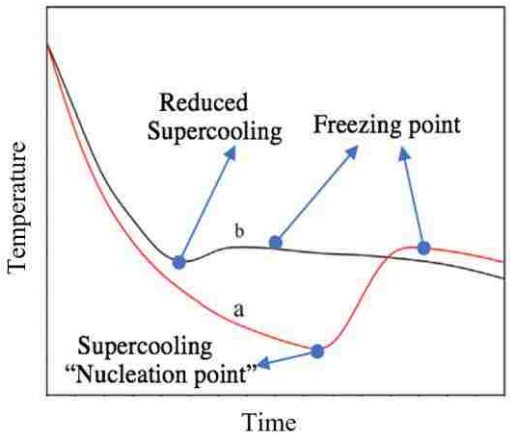

Figure 1.7. Schematic for the cooling curve of PCM with supercooling (line a) and PCM with reduced supercooling (line b)

Soares et al [24] presented different cases that can lead to hysteresis as given in Figure 1.8.

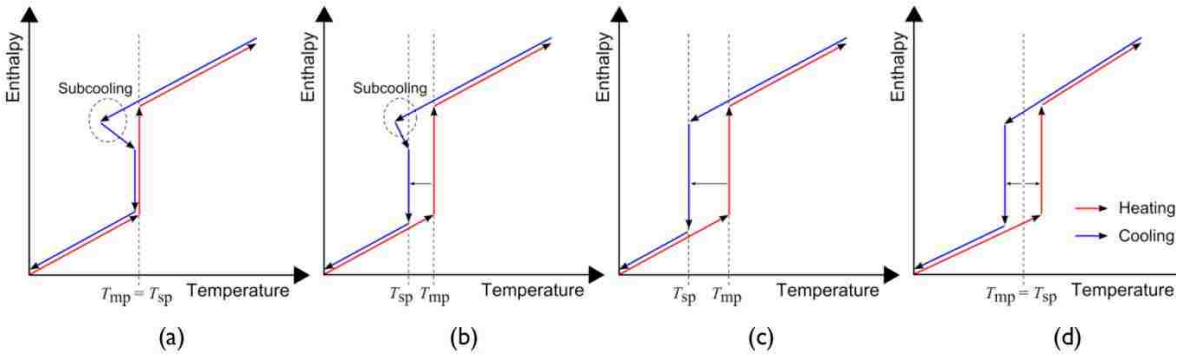

Figure 1.8. Hysteresis of PCMs: (a) the temperature rises again to the phase transition temperature, (b) the temperature does not rise to the phase transition, (c) real hysteresis caused by slow rate of crystallization of real difference between melting and freezing, (d) apparent hysteresis due to non-isothermal conditions during measurements [24].

The effect of hysteresis and supercooling of PCMs, and methods to reduce it, are discussed in detail in Section 4.3. “Fake” hysteresis can be measured in some cases due to non-isothermal conditions, particularly, during DSC calorimetric measurements. In this case, it is called apparent hysteresis as described by Mehling and Cebeza [25]. Hence, the actual crystallization temperature can be measured using other methods such as the T-history method as shown in Section 4.4.2.7.

Nowadays, the DSC method is the most reliable method to characterize the phase transition characteristics of PCMs [26-29]. However, calorimetric measurements for PCMs require extra precautions. For example, determination of specific heat and enthalpy-temperature curve using conventional DSCs is time consuming and require several steps. in some cases, it can provide inaccurate or misrepresentative data for PCMs due to several uncertainty sources. A study on the uncertainties sources of calorimetric measurements on PCMs and methodologies to produce reliable data can be found in the author’s paper [2]. Advanced techniques such as baseline measurements, higher resolution, and modulated heat flow signal are required to eliminate uncertainty sources. For that reason, the new advanced modulated-DSCs (M-DSC) are preferred due to their sufficient precision, increased resolution, flat baseline, and ability to measure direct specific heat by separating several thermal events [24]. In short, the main limitations of the DSC method are: (a) Some transient thermal events are omitted such as convection, non-uniformity and heating rate imbalance; The new modulated-DSCs however have shown promising abilities to account for these thermal events particularly for PCM composite mixtures. (b) Only few milligrams of PCM are tested in a DSC experiment which may not represent the actual behavior of bulk PCM. (c) The required steps for advanced methodologies and standards of accurate

measurements are time consuming and complex. (d) The advanced modulated DSCs are very expensive compared to the conventional dynamic DSCs.

Now that the fundamental of phase change and analysis of PCMs are discussed, the question becomes what kinematic and physical behavior of PCMs are of interest. First and foremost, the phase transition temperature and latent heat of fusion are the primary parameters when choosing a PCM. The latent heat of fusion. must be as high as possible to minimize the system size and maximize the storage capacity. The phase transition temperatures must be within the operation temperature of the system, with melting temperature that is as high as reasonably possible in order to maximize the effective transient thermal storage/management time, and freezing temperature that is as close as possible to melting and higher than the temperature during normal operating conditions or off-peak conditions. Finally, a narrow phase transition range (τ) is desirable.

Another important parameter is the thermal and chemical stability. Some PCMs tend to separate upon several cycles of melting and freezing. For organic PCMs where the material is consisting of single or blends of PCMs, they tend to show excellent thermal reliability in literature [3, 9, 20, 30]. Eutectic mixtures of organic PCMs however require a very careful consideration. Because of the nature of eutectic mixtures, an off-eutectic composition could lead to a phase transition separation of the individual components upon thermal cycling. Most salt hydrates have also been known by their poor thermal stability in many cases [18, 24, 25, 31]. In Figure 1.9, the effect of thermal cycles on the thermal performance of stable PCM (i.e. Organic PCMs) is compared to that of a non-stable PCM (i.e. Inorganic Salt hydrates).

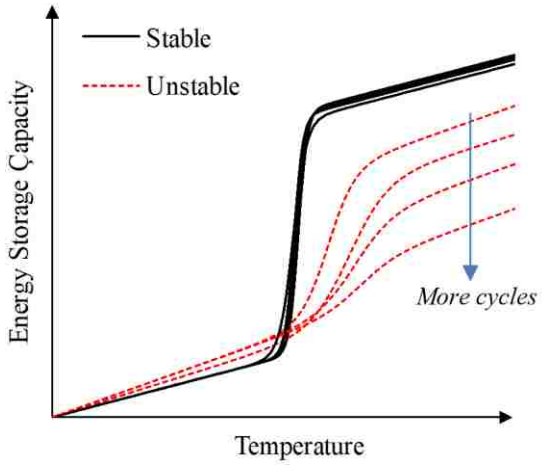

Figure 1.9. Sketch for thermal cycling stability of stable and unstable PCMs, i.e. Organic vs Inorganic

In the case of unstable PCMs, and salt hydrate PCMs in particular, the short life cycle and inconsistent performance is the major concern. Salt hydrates are salt and water in a crystal matrix at discrete ratios (Salt.$n$$H_2O$). Upon cycling, due to the higher density of salt in the PCM solution, salt tends to settle down and separates. This phenomenon is called phase separation. As a result, the eutectic composition between salt and water molecules no longer exists, and salt becomes unavailable for recombination with water during the subsequent liquid to solid transition, causing a phase separation and forming sharp crystals with higher phase transition temperatures [25]. This also results in a decreased storage capacity after several thermal cycles and wider/higher phase transition temperatures. An example on the phase separation of PCMs is shown in Figure 1.10.

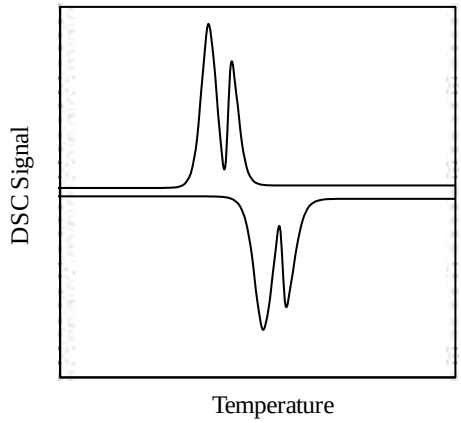

Figure 1.10. Sketch for the phase separation of inorganic or off-eutectic organic PCMs upon thermal cycling.

The simple phase separation shown in Figure 1.10 is closer to the phase separation for an off-eutectic composition of organic PCMs. However, the phase separation for salt hydrates (salt.$n$$H_2O$) is more complex. Strictly speaking, for salt hydrates, even a eutectic composition would still show phase separation upon cycling in some cases. An example of salt hydrate PCM is calcium chloride hexahydrate ($CaCl_2.6H_2O$ salt hydrate). The $CaCl_2.6H_2O$ has 50 wt% of $CaCl_2$ and 50 wt% of water, and phase transition temperature of around 29 °C [32]. When salt starts to segregate due to its higher density, part of the mixture will possess higher water content than the eutectic $CaCl_2.6H_2O$ composition. This can produce a new localized PCM composition with different phase diagram and melting behavior. In other words, forming a (Salt.$n$$H_2O$) composition with lower (n), i.e. $CaCl_2.4H_2O$ with a phase transition temperature of 45.3°C.

Numerous attempts were made to enhance thermal stability and prevent phase separation of salt hydrates. One way is to reduce the distance that material compositions

can separate by packaging in small shallow containers, however, this method was found to be insufficient for long-term stability [25]. The distance that the phases can separate has to be reduced to a microscopic scale rather than few millimeters. This can be achieved by forming a gel matrix to crosslink the different compositions of the PCM mixture. For example, Qian et al. [33] found that fumed silica can be used as a gelling agent for pristine PEG PCM. Ryu et al [32] investigated Borax as a thickening agent for stabilization of inorganic salt hydrate PCMs. Lane [34] gives several examples of thickeners for several PCMs.

Sustainability is one of the key factors when choosing a PCM. Organic PCMs possess more favorable characteristics over all other types in terms of sustainability. When compared to salt hydrates, organic PCMs (i.e. fatty acids) are derived from agricultural by-products, made from food grade, non-toxic, vegetable oil and plant-based ingredients that are sustainable, renewable, biodegradable, and environmentally friendly. Myristic acid, for example, is a common PCM used for thermal energy storage in solar applications that can be found in palm kernel oil, coconut oil and animal fats [35]. In the contradictory, while salt hydrates are readily available, they are not however sustainable or biodegradable.

Various limitations and drawbacks of current existing PCMs and methods to reduce them are discussed in Section 3 and Section 4. These limitations include for example the unavailability of reliable PCMs at some temperatures, leakage problem of the liquid phase PCM, supercooling, and the low thermal conductivity of PCMs. Section 4 discusses in detail how nanomaterials are utilized to modulate the thermo-physical properties of phase change materials such as thermal conductivity, thermal diffusivity, specific heat, viscosity/shape stability, density and thermal energy storage capacity.

1.2.4. Advancement in Phase Change Eutectic Mixtures. Figure 1.11 shows a typical phase diagram for a binary eutectic PCM. Component A melts at T^A and component B melts at T^B. The addition of component A to component B leads to a decrease in the melting temperature along the red line. Similarly, the addition of A to B leads to the same trend. Point E corresponds to the eutectic point of the mixture. At this point both components melt together. Some PCM mixtures do not form a eutectic system, and some of them may form mixtures with a very low latent heat. S^A and S^B represent the solid state of components A and B. L^A and L^B represent the liquid state of components A and B. L represents a partial liquid state of the eutectic system. The mixture at the eutectic point has stable performance and both components crystallize or melt simultaneously. Away from the eutectic molar ratio multiple phase change events may occur at different temperatures and phase separation usually exists.

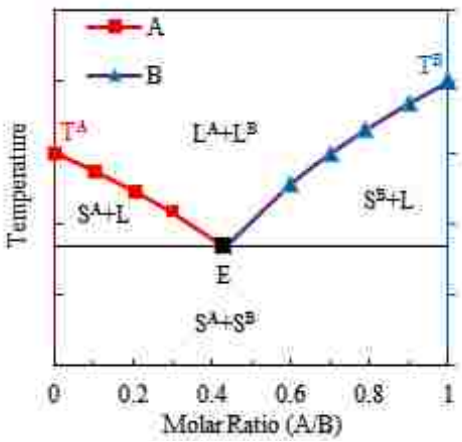

Figure 1.11. Typical phase diagram for a binary eutectic PCM.

The eutectic composition and phase change temperature for a binary mixture PCM can be theoretically predicted by thermodynamic calculations using equation (4) [36]. The latent heat of fusion for the eutectic mixture can be calculated using equation (5) [37] .

$$T_m = \frac{H_i}{\frac{H_i}{T_i} - R\, ln\, X_i} \quad , i = A, B \tag{4}$$

$$H_m = T_m \sum_{i=0}^{n} \left[\frac{X_i\, H_i}{T_i} + X_i \left(C_{P,i}^{Liq} - C_{P,i}^{Sol} \right) ln \frac{T_m}{T_i} \right] \quad , i = A, B \tag{5}$$

Where H_i is the latent heat of fusion for components A and B in units of J/mole, and T_i is the melting temperature of the individual PCM components A and B in Kelvin. T_m is the predicted melting temperature of the eutectic mixture in Kelvin, X_i is the molar ratio of components A and B, R is the universal gas constant, H_m is the latent heat of fusion for the binary mixture in J/mole, $C_{P,i}^{Liq}$ and $C_{P,i}^{Sol}$ are the specific heats at constant pressure of the component "*i*" for both the solid and liquid phase in J/mol·K,.

When a mixture of three PCMs is prepared, the phase diagram of ternary eutectic system is more complex and can be expressed by an equilateral triangle as shown in Figure 1.12. The ternary mixture consists of A, B, and C as the pure PCM components. The line AB, AC, and CB represents binary mixtures of the corresponding components, and the numbers on each line represent the molar or mass ratio of the corresponding binary mixture. Whereas, the intersection of the three lines inside the triangle represent the ternary mixture. For example, the point E is an example for a possible ternary eutectic composition consist of 50% of component C, 20% of B and 30% of C.

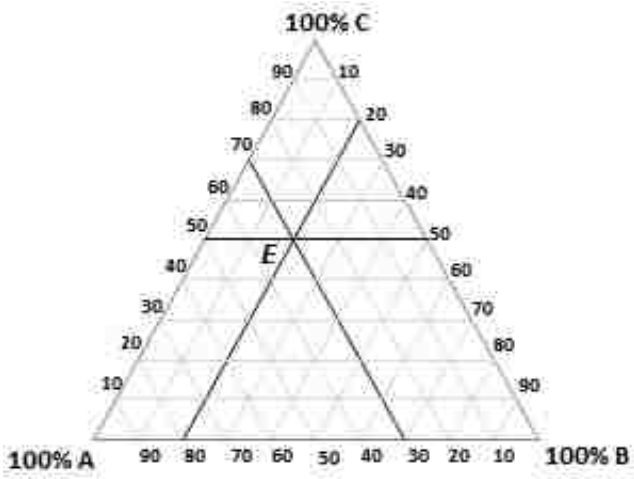

Figure 1.12. Typical phase diagram of ternary eutectic mixture.

On the basis of full understanding of the binary mixture phase diagram, we are proposing a ternary eutectic system consisting of three different components based on a pseudo-binary mixture thermodynamic model. First, two components are tested to form a binary eutectic mixture. Taking A with B for example, If the selected two components A/B lead to an ideal binary mixture, the resulted binary mixture A/B is considered as single component (A/B) and mixed with another component, C for example, to form a pseudo-binary mixture from the three components as (A/B) is the first one, and C as the second component. The final ternary mixture would be (A/B)/C in the form of pseudo-binary mixture. Therefore, the same theoretical prediction thermodynamic model used for binary mixtures can be used to create a new ternary eutectic PCM and determine the composition, molar ratios, melting temperature and the heat of fusion of the pseudo-binary mixture.

In order to test this model, the predicted results from the thermodynamic model is compared with the experimental values for ternary and pseudo-binary mixtures in a study by Zhao et al. [38]. The study prepared a ternary mixture of lauric acid-myristic acid-stearic acid (LA-MA-SA). The experimental melting temperature and latent heat of fusion for the resulted ternary mixture were 29.35°C and 186.5 J/g, respectively. The corresponding molar ratios were (60:30:10) for the experiential ternary mixture. The proposed theoretical prediction model for (LA-MA)/SA as a pseudo-binary mixture determined the melting temperature and the corresponding molar ratios within a relative error of 0.44% and 1.32%, respectively, as given in Table 1.2. The corresponding theoretical molar ratios were (60:31.6:8.4). The authors also experimentally compared a pseudo-binary mixture and the ternary mixture and reported a negligible difference between the two mixtures. These comparisons and results provide a theoretical and experimental support for the approach of pseudo-binary mixture as a successful and viable method.

Table 1.2. A comparison between the experimental values by Zhao et al. [38] and theoretical predicted values for a ternary eutectic mixture.

Mixture	Eutectic Composition (%)	T_m [°C]
Literature Ternary: LA:MA:SA	60 : 30 : 10	29.3 °C
Theoretical Pseudo binary: LA:(MA/SA)	60 : (34.5/65.5)	31.1 °C
Theoretical ternary: LA:MA:SA	60 : 31.6 : 8.4	31.1 °C
Error	1.32%	0.44%

1.3. APPLICATIONS OF PHASE CHANGE MATERIALS

Phase Change Materials are being used for wide range of applications, from small size electronics to the large-scale concentrated solar plant applications; very low temperature space applications at -40°C to very high temperature power plant applications at 700°C. This section is intended to provide an overview on few selected popular applications of PCMs.

1.3.1. Nuclear Thermal Energy Storage Applications. A comprehensive overview and proposed designs for the applications of PCMs in nuclear reactor power plants are given in details in Section 5 and Section 6.

1.3.2. Space Applications. The applications of PCM for space systems can be traced back to 1970s when NASA developed thermal capacitors and implemented PCMs in moon vehicles, diver's suites, and Skylabs. PCMs were integrated in the diver's suit as a thermal control system to regulate the rate of heat exchange between the skin and composite, and as a thermal storage block to generate heat. U.S Pat. No 4,855,410 describes details of different designs utilizing PCMs as a thermal capacitor for moon vehicles and diver's vests [39].

Very recently, phase change materials were used as a critical component in the design of the Neutron Star Interior Composition Explorer (NICER) - a NASA explorers program mission to the study of the extraordinary electromagnetic and nuclear physics environments embodied by neutron stars from aboard the International Space Station (ISS) [40]. On June 3, 2017, NICER was launched successfully and transported to the ISS. During the actual trip, the transport vehicle provided power to the NICER payload. One of the biggest challenges for the thermal control system was to maintain the electronic

components above their survival temperature limit (-30°C) during the transfer of NICER from the transport vehicle to the installation cite on the ISS. During installation, NICER must survive without any heating power for as long as 6 hours until being re-powered. This was achieved by utilizing a developed PCMs with phase transition temperature of -10 °C and latent heat of 217 J/g between the heat spreader and instruments optical bench. Only 4.32 kg of PCM was used, which successfully released up to 937 kJ of thermal energy during the 6 hours without power during installation.

1.3.3. Solar Power Systems. PCMs have applications in both large solar power plants and smaller domestic solar energy systems. For solar power systems, the major drawback has always been the limited effectiveness to periods when radiant solar energy is high. While the demand is not limited to daylight hours, it becomes an issue for commercial solar power plants. Thermal energy storage using phase change materials is a unique solution for a viable economical design of large-scale solar plants.

An extensive review of different types of concentrating solar power plants can be found in Barlev et al., [41]. In these plants, large-size concentrated mirrors are used to reflect the sunlight and heat a carrier fluid. The heated fluid is then directed to an evaporator creating steam to run a steam turbine. In some cases, the gain from solar energy is greater than the capacity or demand on the steam turbine. This excess energy has to be released as loss or stored in inefficient sensible heat water storage tanks. This changed dramatically with the development of PCMs. The excess thermal energy can be stored in thermal storage tanks utilizing PCMs at a temperature close to the steam lines temperature. The stored energy can be released later at high-temperature during times of decreased supply,

enhancing the efficiency and economical aspects. This process is shown in Figures 1.13 and 1.14.

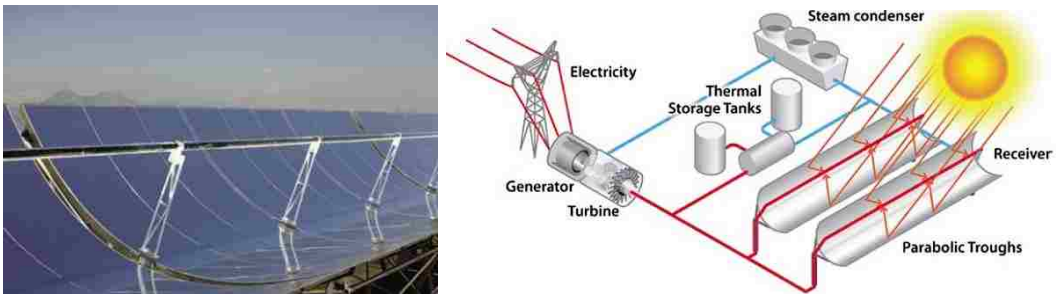

Figure 1.13. Concentrated solar plant with carrier fluid for thermal energy storage [42] .

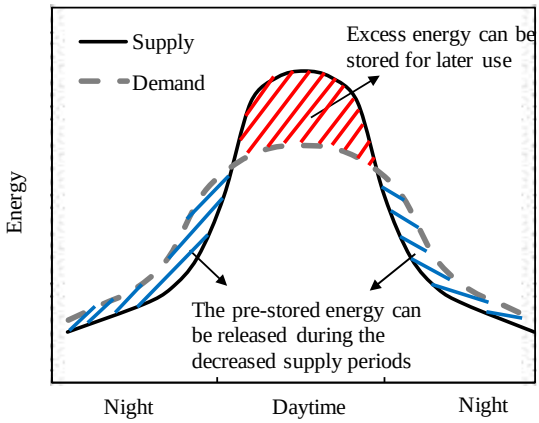

Figure 1.14. Utilization of thermal energy storage to match the supply with demand

Thermal energy storage systems give the ability to increase the capacity of the solar power plants, thus, reducing the need for combining the plants with conventional fossil fuel systems to supply the grid during off-peak solar periods. In a conventional solar plant, it is

common to design the plant at a capacity that is lower than the normal peak demand and operate a fossil-fuel system at part load to match the supply with demand. However, using PCMs for thermal energy storage, the plant can be designed at higher capacity. Excess energy during the daytime can be stored in the PCM by transferring heat to an insulated storage tank. During the decreased supply periods when the solar gain is less (i.e night time or a cloudy day), the carrier fluid runs through the storage tank where the PCM releases its energy at elevated temperature that corresponds to its phase transition temperature. While these PCM systems have an extremely efficient thermal design, their major drawback is the high cost and high corrosiveness of the current existing molten salt PCMs at elevated temperature [43].

Smaller scale solar systems also have potential for thermal energy storage by integrating PCM to improve efficiency for hot water production and heating systems. The conventional systems consist of flat plate solar collector in the form of an enclosure with a glass cover and tubes from inside. The heat transfer fluid after passing through the solar collector tubes is stored in an insulated tank to supply domestic hot water or support a small electrical or gas boiler. The effectiveness of conventional solar plate collectors is limited to daylight hours and storage of limited hot water in tanks. The solar system can be designed to store extra heat in a PCM vessel for use during the evening or early morning hours, reducing the dependency on electrical or gas heating. The PCM can also be integrated inside the water storage tank. For instance, Ghoneim [44] studied a solar system containing encapsulated PCMs in tubes in a cylindrical water storage tank shown in Figure 1.15. Several designs of PCM energy storage in combination with solar heating systems are studied in literature [44-48].

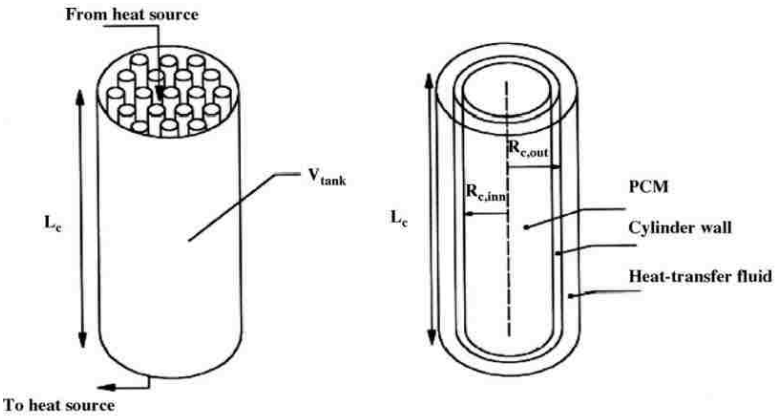

Figure 1.15. Cylindrical storage tank with PCM storage [44]

1.3.4. Building Applications. The concept of thermal energy storage in buildings using PCMs is one of the most enduring topics. For the last 40 years, thousands of studies have found that PCMs in buildings have a significant impact on the thermal management and energy savings due to its ability to store and release heat at nearly constant temperature around comfort room temperature [49-55]. PCMs are incorporated into the building through wallboards, ceiling, floor, air-conditioning systems, or by incorporating them directly through gypsum mixture, cement paste, and mortar [5-7]. PCMs with phase transition temperature in the range of 23-27 °C are usually used for reducing indoor temperature swing and reducing energy consumption by shifting temperature peak hours.

During hot weather conditions, incident heat or energy is absorbed by the PCMs in the form of latent heat while maintaining constant temperatures that correspond to the phase transition temperature as shown in Figure 1.16. In other words, although more energy is still being added to the building structure, this excess energy will not lead to an increase in temperature because PCMs will store this energy as latent heat. Solidification or freezing

is the reverse of this process, during which the PCM transfers the stored energy to the surroundings at constant temperature when surrounding is relatively cold. During cold weather conditions, PCMs help in capturing and storing the heat that would have leaked out of the building if no PCMs were installed, therefore, When the temperature decreases below the phase transition temperature, the PCMs will release that stored energy to the building in the form of latent heat and maintain the temperature of the buildings within comfort levels; thus, preventing the indoor temperature from getting excessively cold.

Figure 1.16. PCMs storing heat (left) and releasing heat (right).

PCMs in buildings are more efficient in places where the temperature swing during day and night is high, to charge and discharge the PCM daily. However, PCMs above the ceiling tiles coupled with a ventilation system that works at night to discharge the PCM help to increase its efficiency when temperature swing is smaller. Figure 1.17 shows an example for such systems [56].

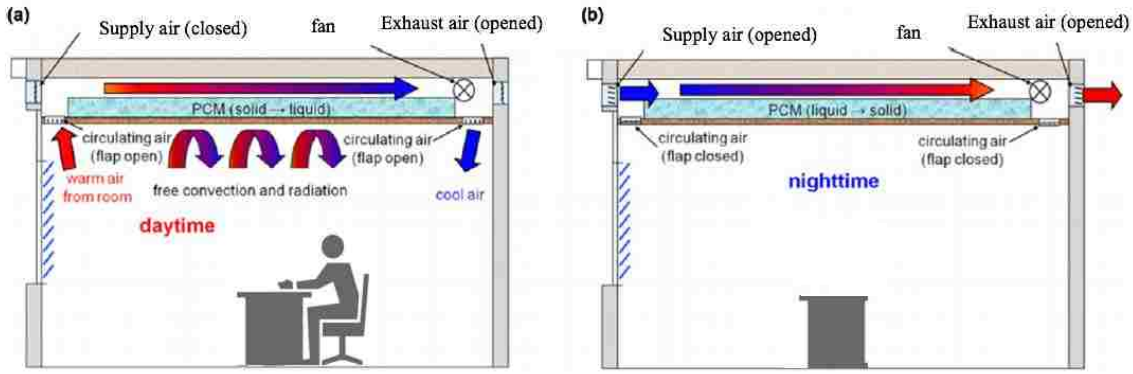

Figure 1.17. Ventilated ceiling with PCM for daily charging and discharging.

Figure 1.18 shows an example for increasing the thermal mass using PCM-gypsum mixtures to reduce the indoor temperature swing by 56% [57]

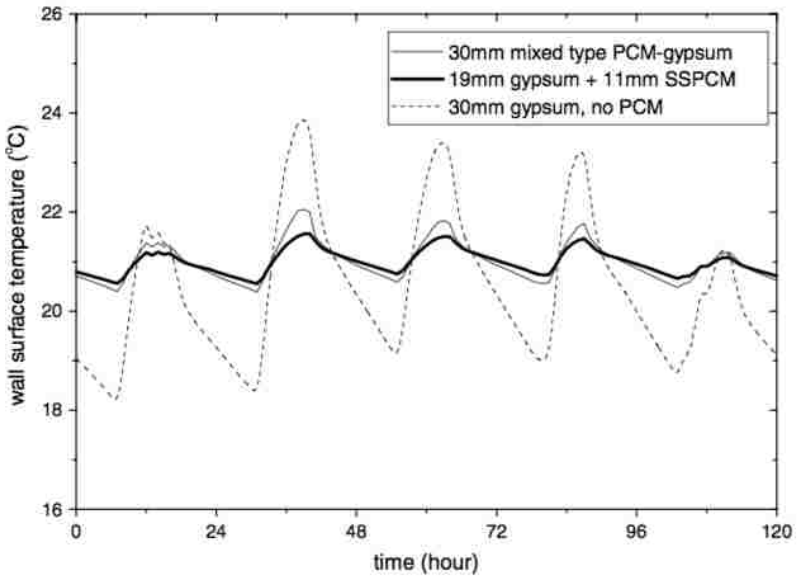

Figure 1.18. Reducing indoor temperature swing using PCMs [57]

1.3.5. Solar Photovoltaic System. The energy generated from Photovoltaic (PV) panels depends on the intensity of the solar radiation, the quality of the panels in use and the surface temperature of the panels [58]. The efficiency of generating energy from PV panels decreases with temperature. Only 10-20% of the incident solar radiation is converted into electric energy in PV panels; the rest is either reflected or causes overheating of the system [59]. The temperature rise of PV modules is known to cause a decrease in power efficiency by 0.5% per kelvin above the standard test conditions (STC) of 25 °C. [60-62]. During the day, the temperature of a typical the PV panels may rise to 80°C or higher, which accounts for about a 28% loss in solar to electrical conversion efficiency with respect to the STC.

Several studies have been devoted to the use of mechanical fans, water circulation, pumps, or other types of equipment that consume energy to enhance the free cooling and efficiency of PV panels. Integrating PCMs in PV panels provides a novel passive solution to prevent overheating and remove heat from PV systems. Such PV-PCM systems can operate for a longer time at the desirable temperatures where higher efficiency is achieved. Even when compared to natural ventilation methods, PCMs have a greater potential to enhance the efficiency of PV systems because they are not affected by the speed or direction of wind. Moreover, the excess and stored heat in a PCM can be utilized to provide heat to buildings or any other system when it solidifies. Hasan et al. [63] developed a PV-PCM system to reduce PV temperature dependent power loss and to increase the conversion coefficient. The PV peak temperature was kept below 45 °C at a solar intensity of 950 W/m^2. This peak temperature value is over 20°C lower than that of the PV system without PCM. In another study, Atkin and Farid [64] developed a novel design of PV-PCM

consisting of a PCM infused graphite with external fins to improve heat sink at the rear side of the module. It was shown that the overall efficiency can be increased by 13% using this thermal regulation system. Ma et al. [65] noted that the PV–PCM system can be extremely feasible from the economical side if integrated with a solar thermal system that can absorb the excess heat from the PV-PCM panels and discharge the stored heat in PCMs to provide building heat services.

1.3.6. Electronics. Thermal management using PCM based cooling systems provide a unique solution for electrical devices and ships that do not operate for long continues periods. Such PCM based cooling systems can maintain the temperature of electronics and prevent overheating [66, 67].

Kandasamy et al. [66] studied the performance of a PCM thermal management system for cooling portable electronic devices. A PCM package was designed to meet the heat dissipation and size requirements of the device. Yin et al. [68] analyzed the thermal management and performance of composite PCM in a passive electronic cooling system. The system insured a greater reliability against the thermal shock of high heat flux. The heat transfer coefficient in this system was found to be 3 times greater than those cooling systems without PCM. In another work, Tan et al. [69] studied a PCM based heat storage unit for the cooling of mobile electronic devices. The PCM-based system maintained the temperature of chips within a moderate temperature range for 2 hours of transient operation. The configurations allowed the electronics to operate at a high-power dissipation for a longer period time.

1.3.7. Other Applications. Phase change materials are found to have large number of applications and variety of possible technical solutions. For example, special bandages and textiles equipped with PCMs for heating/cooling medical therapy [70]. Lv et al. [71] presented a thermal protection system during cryosurgery. A micro-encapsulated PCMs delivered to the tissue by injection were used to protect the healthy tissues near the cancerous tumor from thermal injury. Wang et al. [72] developed a bio-sensing technique using thermal probes of RNA aptamer-functionalized nanoparticles of PCMs to detect thrombin with high sensitivity. The PCM thermal probe absorbs heat and results in a sharp thermal signal during the temperature scan to determine the existence and amount of thrombin based on the position and area of the peaks.

Phase change materials are also proposed for textile and thermal cooling vest used by athletes to reduce the risk of dehydration and fatigues by controlling the body temperature [73]. PCMs were filled in a special glass windows [74]. The PCM-filled windows are more thermally effective than air filled windows and capable of absorbing the heat for thermal radiation. PCMs have also been used to avoid the overheating of Lithium-ion batteries to extend the lifespan [75]. PCMs have also applications to enhance the efficiency of electric and combustion engines [76]. PCES were used in vehicles for thermal comfort by companies like BMW [77].

Phase change materials with a phase transition temperature of 2°C to 8°C are suitable for storage and transport of medical and temperature sensitive products such as drugs and food. The encapsulated PCM is pre-conditioned under their solidification temperature, and then products are loaded around the PCM in a container so that PCM undergoes a solid to liquid phase transition through the trip, maintaining the temperature

for the product low enough. Similarly, Gin et al. [78] studied low temperature PCMs in a freezer during loss of electrical power or door openings. It was found that the use of PCMs reduces the temperature rise significantly and results in lower energy consumption. Ahmed et al. [79] used PCMs in transportation trucks where the heat transfer through the walls was reduced by 29.1% causing a massive energy saving, and allowing the us of a smaller refrigeration system. Low temperature PCMs were also used to transport of temperature sensitive food in special containers [18].

2. EXPERIMENTAL METHODS

This section will detail the experimental background which describes the methods and instruments used for thermal characterization of PCMs. Section 2.1 will describe the differential scanning calorimetry (DSC) method. Then Section 2.2 will discuss the guarded parallel-plate heat flow method which provides a measuring tool for the thermal conductivity, R-value, T-history, and specific heat of liquid and solid PCMs. Section 2.3 will describe the transient hot bridge method for thermal conductivity measurements. Finally, Section 2.4 will summarize the specifications of other instruments used in this research such as the thermal cycler and analytical microbalance.

2.1. DIFFERENTIAL SCANNING CALORIMETRY (DSC)

Differential scanning calorimetry (DSC) is a widely used method to characterize the thermal properties of PCMs [9, 11, 29, 80, 81] among other methods like the differential thermal analysis (DTA) and T-history method [82]. The DSC is used to measure the thermophysical properties of PCMs during phase change such as melting temperature, melting enthalpy and specific heat.

In DSC experiments, the amount of heat required to increase the temperature of a material sample (sample pan) is measured and compared to that of an empty pan (reference pan) in identical conditions. A schematic diagram for the key component of the DSC chamber is shown in Figure 2.1.

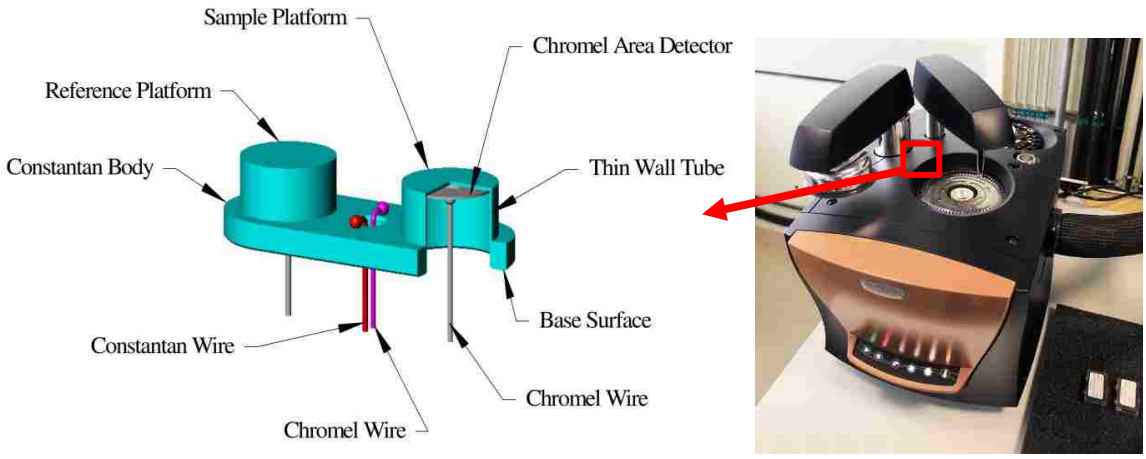

Figure 2.1. Schematic diagram of a Tzero Discovery DSC cell [83] (left) and DSC instrument (right).

The constantan disk, also called DSC cell, consists of two identical calorimetry platforms approximately 6 mm in diameter. The materials are loaded in special DSC pans approximately 5 mm in diameter and 1 mm in height and positioned above the calorimeter platforms. The typical PCM sample mass is in the range of 5 to 10 mg. An electrical resistance heater is used to provide a constant heating rate. For cooling cycle, a constant cooling rate is provided using a refrigerated cooling system that fits around the DSC cell via a cooling ring. The refrigerated cooling system can be a compressor-based system or liquid nitrogen-based system.

The typical range for heating and cooling rate is 1 ˚C per minute to 5 ˚C per minute. The heat applied by the DSC flows radially though the electrical constantan disk toward the reference and sample pan. During thermal events such as phase transition, the system transfers more heat to the sample pan to maintain the given heating rate and the same

temperature of the sample and reference. The heat flow into the sample pan is measured as a function of temperature and the difference in heater voltage between the sample and reference pan is proportional to the thermal response of the PCM sample. The result of DSC measurements is a heat flow curve versus temperature.

The new advanced modulated DSCs (M-DSC) provide great benefits for measurements of special composites and materials such as non-uniform PCM mixtures, samples with high percentages of impurities, and PCM with solid-solid or solid-gel phase transition. The M-DSCs can apply a modulated sinusoidal temperature variation rather than monotonically increasing variation. This can help to retrieve data not obtained by conventional DSCs by separating the specific heat capacity component (reversing heat flow) from the kinetic component (non-reversing heat flow) such as thermal curing reactions or decomposition. The advanced M-DSCs also accounts for the resistance and capacitance through the sample, as well as heating rate imbalance. Further details on the M-DSC significance for specific heat measurements in the overlap and phase transient regions can be found in Section 5.3.1 and Section 5.3.2.

The specification of the DSCs used in this study are given in Table 2.1. Further details on the thermodynamic models used for the enthalpy measurements, baseline correction, heating and cooling rates, specific heat capacity measurements, and type of DSC pans are found in the methods sections of each section as they varied from one study to another.

Table 2.1. Specification of the experimental DSC instruments

	Seiko DSC6200	Discovery M-DSC
Manufacturer	SEIKO Instruments	TA Instruments
Type	Heat Flux DSC	Modulated DSC
Temperature sensors	Chromel-alumel Thermocouple	Diffusion-bonded sensor
Temperature range	-15°C to 500°C	-90°C to 750°C
Temperature accuracy	±0.1°C	±0.025 °C
Temperature precision	NA	±0.005 °C
calorimetric precision	1%	±0.04%
Baseline noise	0.5 μW	<0.08 μW
Baseline	Varies, non-flat	flat "zero" baseline
Refrigeration system	Compressor based	TA-RSC90
Direct C_p accuracy	NA (only with muli-steps artifact calculations and baseline subtraction)	>97%

2.2. GUARDED PARALLEL-PLATE HEAT FLOW METHOD

The guarded parallel-plate heat flow method provides an alternative approach to characterize some of the thermo-physical of PCMs. Most of thermal analysis techniques such as the DSC method are designed to test small, pure and homogeneous samples. The problem has been discussed in our previous work [2]; where we determined the uncertainty sources and developed methodologies and standards for thermal characterization of PCMs using the DSC method. In summary, due to the low thermal conductivity and thermal diffusivity of PCMs, the non-equilibrium thermal gradients in the DSC pan becomes significant and measured data are often shifted to higher or lower values. In addition, the DSC method is not capable to measure the thermal conductivity and thermal diffusivity. Despite that some complex mathematical methods were developed for thermal

conductivity measurements using the advanced modulated DSCs (M-DSC), the measurement uncertainty of such models can be as high as 10-20% [84, 85]. Specific heat measurements using the DSC required several steps that are very time consuming and the uncertainty sources of such experiments can be significant. The advanced M-DSCs which has a flat "zero" baseline for direct specific heat measurements are very expensive and limited advanced options are available. In Section 4, we also found that the DSC method is not accurate enough to measure the actual enhancement in the degree of supercooling.

In order to completely characterize the thermal behavior of PCMs in an accurate and detailed manner, a combination of DSC and other methods is required. First, the enthalpy, detailed phase transition behavior, melting/freezing temperatures, and specific heat if possible are determined using the DSC method. Second, a guarded parallel-plate heat flow apparatus can be used to measure thermal conductivity, temperature-time history (T-history), and real supercooling of a bulk PCM samples.

In the current study, the guarded parallel-plate heat flow method was applied using the Fox314 TA instrument shown in Figure 2.2, and an additional thermocouples and data acquisition unit. The instrument chamber provides an isothermal and temperature-controlled boundary condition using 12-inch x 12-inch upper and lower temperature-controlled plates and a well-insulated side walls. The experimental sample is placed in between the top and bottom plates, and the position of the plates is automatically adjusted using four optical sensors to establish a full contact with the surface of the measured sample. For measurements of solid phase, PCM samples are usually heated above their phase transient temperature and molded to form a rectangular thin brick with a flat surface before being position between the plates. Liquid samples are usually encapsulated and

vacuumed in a very thin polymeric film to form a pouch, and then the instrument optical encoders are expected to automatically adjust the upper and lower plates to compress and establish full contact with the sample.

Figure 2.2. The guarded parallel-plate heat flow apparatus using Fox314 TA instrument [86]

Using this apparatus, the thermal conductivity of samples can be measured in accordance to ASTM C518 and ISO 8301[86]. The heat flux transducer is less than 1 mm in thickness to preclude heat flow distortion. Type-E thermocouples are positioned within 0.1 mm of the plates surface in the center of each heat flux transducer and are used for plate temperature control. An additional optional thermocouple kit is attached at the surface of the samples and is used to enhance measurement accuracy, allow for wider thermal conductivity measurement range, and to eliminate the impact of interface resistance. The heating and cooling power is provided by a solid state thermoelectric system consists of two arrays of solid-state peltier elements and ThermoCube 400 recirculating chiller designed by Solid State Cooling Systems. The solid state thermoelectric system works as

a thermoelectric generator when heat is needed and as a thermoelectric cooler when cooling is needed. A multistage PID algorithm ensures that the temperature of the plates is within the set-point and adjust the power of the thermoelectric cooler every 0.5 seconds. A schematic of the setup is shown in Figure 2.3. The upper and lower plates were initially configured and calibrated by TA Instruments for extended temperatures from -20 ℃ to 95℃. The complete apparatus is calibrated using fiberglass reference materials (NIST 1450b and 1450d) certified by the National Institute of Standards and Technology (NIST) at various temperatures.

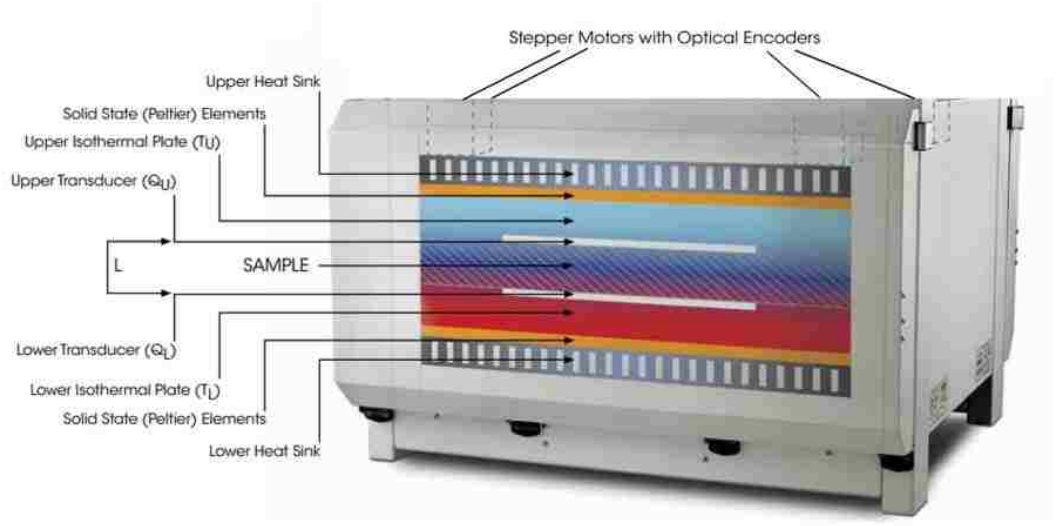

Figure 2.3. Schematic for the guarded parallel-plate heat flow apparatus using Fox314 TA instrument [86]

During thermal conductivity experiments, the apparatus establishes a steady state one-dimensional heat flux through the test sample between the two plates. The plates are set a at constant but different temperatures to establish a thermal gradient through the

sample. The temperature difference between the top and bottom plates is a user defined value to perform measurements at various averaged temperatures. The bottom plate is usually the cold plate (lower temperature setpoint) while the top plate is set at higher temperature. The measured thermal conductivity, thermal diffusivity or thermal resistance can be calculated using Fourier's law of heat conduction. The thermal conductivity of the teste sample is given by:

$$k = (S_1.E_1 + S_2.E_2)/2 \ * (L/\Delta T) \quad (6)$$

Where *k* is the thermal conductivity (W/m.K), *S* is the calibration factor for the heat flux transducer, *E* is the heat flux transducer output (V), the subscripts *1* and *2* refer to the first and second heat flux transducer. *L* is the separation between the top and bottom plate, ΔT is the temperature difference across the specimen (K).

During T-History measurements, two identical samples of the same thickness are placed in between the top and bottom plates. Additional sensors are positioned at the center in between the two samples. The bottom and top plate are set at the same temperature (T_i) until thermal equilibrium is obtained throughout the sample. The plates temperature is increased to (T_f). The transient thermal response, such as phase transition, of the material from T_i to T_f can be obtained by recording the temperature at the center in between the two samples as function of time.

Specific heat measurements can also be obtained using this apparatus in accordance to ASTM C1784 - 13 (Standard Test Method for Using a Heat Flow Meter Apparatus for Measuring Thermal Storage Properties of Phase Change Materials and Products). However, in this study direct specific heat measurements were conducted using a

modulated DSC (M-DSC) and in some cases using thermodynamic baseline calculations using conventional DSC.

The specifications of the guarded parallel-plate heat flow apparatus are given in Table 2.2. The exact algorithm and measurement conditions of each experiment can be found in the methods section of each section as they vary from one study to another.

Table 2.2. Specification of the guarded parallel-plate heat flow apparatus using Fox314 TA instrument

Property	Value
Temperature range	-20 to 95 ℃
Temperature accuracy	±0.1°C
Temperature resolution	±0.01°C
Thermal conductivity range	0.001 to 2.5 W/m.K
Thermal conductivity accuracy	±2%
Thermal conductivity reproducibility	±0.5%
Heating/cooling system	Solid state thermoelectic system
Additional/optional accessories	External thermocouple kit and external Daq unit
Comply with	ASTM C518, ISO 8301, ASTM 1784-18, EN 12664, and JIS A 1412 Standards.

Figure 2.4 shows the experimental measured thermal conductivity of 300 mm x 300 mm expanded polystyrene (EPS) specimen (#15081133) certified by the National Institute of Standards and Technology (NIST) [87]. The NIST standard specimen was tested to verify the accuracy and calibration of the instrument apparatus. The instrument accuracy

and reproducibility for thermal conductivity is within 2% and 0.5%, respectively, as per the manufactured. These values are found to be within the measured experimental error varied from -0.3% minimum to 1.6% maximum with a mean absolute percentage error of ±0.9%.

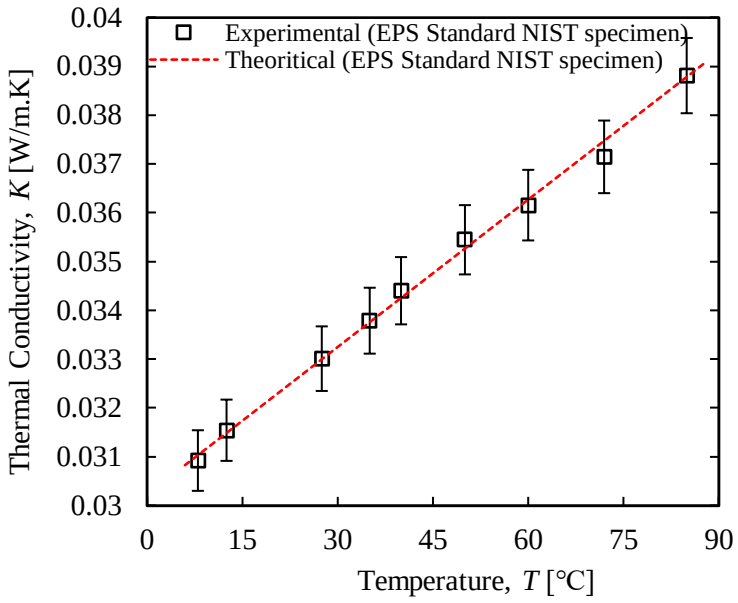

Figure 2.4. The measured experimental and theoretical thermal conductivity of EPS specimen certified by NIST

2.3. TRANSIENT HOT BRIDGE (THB) METHOD

The transient hot bridge (THB) method is an alternative approach to measure thermal conductivity and thermal diffusivity of samples. The THB apparatus is particularly suitable for liquid samples as it requires only few steps for sample preparation. The THB apparatus is a modified measuring method of the Hot Wire and the Transient Hot Strip

method. The THB apparatus using the thermal conductivity measuring instrument (THB1, Linseis Inc., USA [88]) is shown in Figure 2.5.

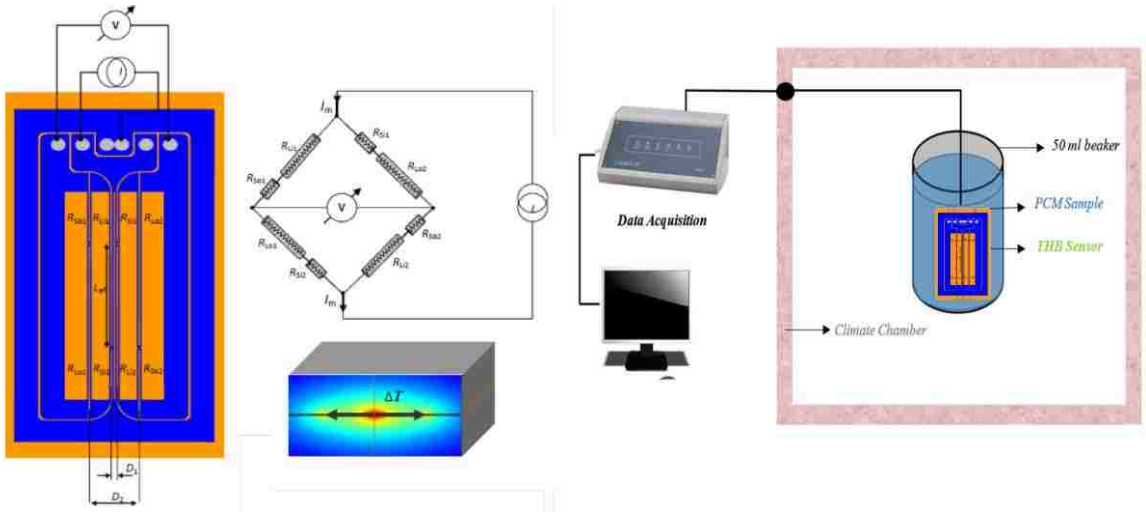

Figure 2.5. The Transient Hot Bridge circuit [88] and experimental apparatus.

The transient temperature response of samples is measured using a calibrated semi-infinite medium model. A constant heat flux is emitted by the THB sensor consists of strip shaped conductor that is directly inserted into the sample. This causes a slight increase in temperature. The voltage as a function of time is recorded. The model assumes that the temperature rise over time is proportional to the thermal transport properties of the tested material.

$$k = \frac{\alpha . R_{eff}^2 . \ln(g)}{4\pi . L_{eff} . d(Us)_{max}} . \left(\frac{I_m}{2}\right)^3 . \left[\left(\frac{D_1}{D_2}\right)^{\frac{2.D_1^2}{D_2^2 - D_1^2}} - \left(\frac{D_1}{D_2}\right)^{\frac{2.D_2^2}{D_2^2 - D_1^2}}\right] \quad (7)$$

Where k is the thermal conductivity, the signal d(Us) is the measured voltage increment over a certain period of time ln(t) where the signal slope is maximum, R_{eff} is the effective electrical resistance, L_{eff} is the effective length, α is the thermal coefficient of the nickel foil resistor used in the sensors, I_m is the applied current, D_1 is the distance between the two inner strips of the sensor, D_1 is the distance between the two outer strips of the sensor

The temperature of measurement was controlled using a climate chamber (UN260, Memmert GmbH, Germany) with an accuracy of 0.1°C. The chamber was equipped with special penetrations for the THB wires and sensor. The exact algorithm and measurement conditions of each experiment can be found in the methods section of each section as they vary from one study to another. Table 2.3 gives the specification of the transient hot bridge apparatus.

Table 2.3. Specification of the transient hot bridge apparatus.

Property	Value
Temperature range	-150 to 200 ºC
Temperature accuracy	±0.5°C
Thermal conductivity range	0.01 to 1 W/m.K
Thermal conductivity accuracy	±2%
Heating/cooling system	External Chambers
Additional/optional accessories	Kapton insulated sensor
Comply with	Modified method of the Hot Wire and the Transient Hot Strip method (DIN EN 993-14, DIN EN 993-15)

2.4. OTHER METHODS AND INSTRUMENTS

Thermal cycling of PCMs was performed using an accelerated thermal cycler that can go through many cycles in the shortest possible testing time. The samples were thermally cycled by allowing it to go through multiple phase transitions in sealed 1 Liter bottles or 50 ml tubes following a user defined temperature protocol that fluctuates above and below the PCM transition temperature. The thermal cycler is a custom designed environmental chamber (CT-64-6-SCT/AC, Cincinnati Sub-Zero) shown in Figure 2.6. The exact temperature protocol and hold time of each experiment can be found in the methods section of each section as they vary from one study to another.

Figure 2.6. Accelerated thermal cycler used for thermal cycling of PCMs

A common cause for systematic errors of DSC measurements for enthalpy and specific heat is improper selection of the laboratory scale used for weighing DSC samples. Therefore, extreme accuracy and precision for measuring sample pass are required. The

experimental DSC samples were controlled using a micro analytical balance (Mettler MX5, METTLER TOLEDO, Switzerland) at a precision of 0.01 mg.

Thermal diffusivity can be measured using the Fox314 apparatus or THB meter. However, the uncertainty of thermal diffusivity using these two methods can be as high as 5% [86, 88]. Therefore, for maximum accuracy the thermal diffusivity was calculated using equation 8 where the specific heat capacity (C_p), thermal conductivity (k) and density (ρ) are calculated using the most accurate available method for each parameter. Using this approach, the uncertainty for thermal diffusivity is expected not to exceed 3.2%.

$$\alpha = \frac{k}{\rho \times C_p} \tag{8}$$

3. PREPARATION AND THERMAL PERFORMANCE OF METHYL PALMITATE AND LAURIC ACID EUTECTIC MIXTURE AS PHASE CHANGE MATERIAL (PCM)

The content of this section has been published in "Saeed, et al. (2017). Preparation and thermal performance of methyl palmitate and lauric acid eutectic mixture as phase change material (PCM). Journal of Energy Storage, 13, 418-424" [3]. Some information may have been omitted, shortened, or reformatted for purposes normal to dissertation writing.

A series of binary mixtures of Methyl Palmitate (MP) and Lauric Acid (LA) were prepared and investigated, aiming for potential phase change material (PCM) for thermal energy storage systems. The thermal analysis of the PCM binary mixtures was investigated by means of Differential Scanning Calorimetry (DSC). A theoretical and experimental determination of the eutectic mixture was established. The results indicated that the eutectic binary mixture of 60%MP and 40%LA has desirable properties of phase transition temperatures within the comfort temperature range (T_m= 25.6 ºC, T_f= 20.2 ºC) and high latent heat capacity (ΔH_m= 205.4 J/g, ΔH_f=205.8 J/g). The paper experimentally studied the other important thermo-physical properties required for modelling and stimulating the PCM in any storage systems such as thermal conductivity, enthalpy curve, phase diagram, specific heat, thermal diffusivity, and density. The thermal stability test indicated that the eutectic mixture had reliable thermal performance upon thermal cycling. Based on all these results, the MP-LA eutectic mixture is a promising material for thermal energy storage.

3.1. DEVELOPMENT OF PCM EUTECTIC MIXTURES

The limited reserves of fossil fuel, rapid growth of global energy consumption, and the increased environmental concerns of greenhouse gas emissions have shed the light on the importance of having an effective utilization of energy. According to the U.S. Energy Information Administration (EIA), The total energy consumption by the residential and commercial building sectors was estimated to be 41% of the total U.S energy consumption in 2015 [89]. Heating and cooling of buildings alone account for 58% of the total energy consumption in the residential and building sectors [90], and therefore account for over 20% of U.S. energy consumption. Reducing this energy consumption through gains in efficiency is a key method for reducing dependency on fossil fuels. Phase change materials (PCMs) have potential for reducing residential energy requirements and reducing energy demand [60, 91]. PCMs are unique in that they store and release large amounts of energy at nearly constant temperature during phase transitions. They have been used in buildings for thermal regulation, reducing energy consumption, and reducing indoor temperature swing. To achieve these objectives, PCMs in buildings are usually incorporated into the building through wallboards, ceiling, and floor by enclosing the PCM in microscopic polymer films that form a sort of panel that can be installed on top of the ceiling, behind the wallboards, or under the floor [91]. Another common technique is incorporating the PCM through gypsum, cement paste, and mortar by impregnating the PCM directly through the construction material to form a matrix and therefore increasing the thermal mass of the building [92-94].

Developing a suitable eutectic PCM for room-temperature applications in buildings is very challenging. The American Society of Heating, Refrigerating and Air-Conditioning

Engineers (ASHRAE) standard 55-2013 [95] reported that the average comfort temperature ranges from 19°C to 27°C. Paraffins with suitable melting temperature have been studied by many researchers [96-98]. However, their major drawback of high cost has limited their potential use for energy savings in buildings [99]. Salt hydrate PCMs are limited because of the supercooling and phase separation upon cycling [100, 101]. In contrasts, fatty acids feature a long-term stability upon cycling, economic feasibilities, little or no supercooling, smaller volume change during phase transition, and non-toxicity [13, 14, 18]. Methyl esters have the benefits of high latent heat, lower cost, chemical stability, no corrosiveness to buildings materials, and less flammability [102, 103]. However, the major limitations of fatty acids and methyl esters are the low thermal conductivity, and that their individual melting temperatures are higher than the comfort temperature for buildings. Therefore, eutectic mixtures can be prepared to adjust the melting temperature of the individual PCMs to the comfort range.

Several studies have found that eutectic mixtures of fatty acids possess desirable characteristics for building applications. For example, Sari et al. [104] investigated a eutectic mixture of Capric acid and Stearic acid with suitable melting temperature of 26.04°C and melting latent heat 176.6 J/g. Wen et. al [105] prepared a eutectic mixture of Capric acid and Lauric acid with melting temperature of 19.09°C and melting latent heat 141.5 J/g. Khawaji et. al [106] studied a eutectic mixture of decanoic acid and tetradecanoic acid with melting temperature of 20.5°C and melting latent heat of 153 J/g. moreover, the study was one of a few studies to investigate the other thermo-physical properties of the eutectic mixture such as specific heat capacity, thermal conductivity, and

thermal diffusivity. An extensive review of suitable PCMs for buildings can be found in references [98, 107].

It can be concluded that previous studies concerning eutectic mixtures usually lack experimental determination of the thermal stability upon cycling. Because of the nature of the eutectic mixture, the precise determination of the eutectic composition ratio is very crucial for consistent performance and long-term stability. Therefore, the eutectic composition for the mixture must be determined in fine steps around the theoretical eutectic point, and experimentally tested over several thermal cycles, otherwise, an off-eutectic composition will lead to a phase transition separation of the individual components upon thermal cycling. Furthermore, the important thermo-physical properties such as the specific heat capacity, thermal conductivity, and thermal diffusivity, for both liquid and solid phase, were not reported for eutectic mixtures in most of previous studies. Only a few existing studies examined these additional thermo-physical properties in a detailed manner. Such information is required for modeling the optimum amount, effectiveness, and position of PCMs before being integrated into a thermal system.

The current organic based eutectic mixtures with a suitable phase transition temperature for thermal comfort in buildings typically have lower latent heats than other PCMs, reducing their effectiveness. Moreover, most previous research has been focused on mixtures of fatty acids with fatty acids, paraffin with paraffin, methyl esters with methyl esters or salt hydrates with salt hydrates [37, 107-110]. Reports on mixture of fatty acid with methyl ester to form PCM eutectic mixtures are very few so far. Because of the high latent heat of methyl esters, and the other advantages of fatty acids mentioned above, eutectic mixtures consisting of fatty acids and methyl esters are very promising and are

expected to have excellent thermal performance – comparable to that of individual PCMs – but within the comfort temperature range. In this study a eutectic mixture of a methyl ester with a fatty acid, namely a methyl palmitate and lauric acid binary system, is studied as phase change energy storage material for thermal regulation in buildings. The aim was to develop a PCM with suitable phase transition temperature and with high energy storage capacity compared to current PCMs, then to provide detailed information on thermo-physical data such as thermal conductivity, enthalpy curves, phase diagrams, thermal cycling effects, specific heat, thermal diffusivity, and density. These data are very important to simulate the actual behavior of PCM in any thermal energy storage application.

3.2. MATERIALS AND METHODS

Methyl Palmitate (MP, 99% purity) and Lauric Acid (LA, 99% purity) were supplied by Sigma Aldrich and used as components in preparation of MP/LA binary eutectic mixture. The chemical data and theoretical thermal properties for the individual PCMs are listed in Table 3.1. The components of MP/LA mixture were heated up to 50°C and mixed homogeneously by stirring for 30 minutes.

Table 3.1. Chemical data and theoretical thermal properties for the individual PCMs

Name	Scientific Name	Molecular Formula	CAS Number	Melting point [°C]	Latent heat [J/g]	specific heat [J/g.K] @ 25°C	Density g/ml @ 25°C
Methyl Palmitate (MP)	Methyl hexadecanoate	$C_{17}H_{34}O_2$	112-39-0	29.0	229.5	1.75	0.852
Lauic Acid (LA)	Dodecanoic acid	$C_{12}H_{24}O_2$	143-07-7	44.0	188.7	2.01	0.883

3.2.1. Theoretical Prediction of MP/LA Binary Mixture. The phase change temperature, binary mixture, and the optimum mixing ratio for a binary mixture PCM can be theoretically predicted by thermodynamic calculations using the, equation 9 [36]. The latent heat of fusion for the binary eutectic mixture can be calculated using the model proposed by Zhang et al. [37] as given in equation 10.

$$T_m = \frac{H_i}{\frac{H_i}{T_i} - R \ln X_i} \quad , i = A, B \tag{9}$$

$$H_m = T_m \sum_{i=0}^{n} \left[\frac{X_i H_i}{T_i} + X_i \left(C_{P,i}^{Liq} - C_{P,i}^{Sol} \right) ln \frac{T_m}{T_i} \right] \quad , i = A, B \tag{10}$$

Where ΔH_i is the latent heat of fusion for components A and B in units of J/mole, and T_i is the melting temperature of the individual PCM components A and B in Kelvin. T_m is the predicted melting temperature of the eutectic mixture in Kelvin, X_i is the molar ratio of components A and B, R is the universal gas constant, H_m is the latent heat of fusion for the binary mixture in J/mole, $C_{P,i}^{Liq}$ and $C_{P,i}^{Sol}$ are the specific heats at constant pressure of the component "*i*" for both the solid and liquid phase in J/mol·K,.

The predicted phase diagram using equatin 8 and 9 and the theoretical data is shown on Figure 3.1. The theoretical eutectic point for the MP/LA binary mixture was found at 60/40 molar ratio, with melting temperature of 24.0°C and latent heat capacity of 206.6 J/g for melting.

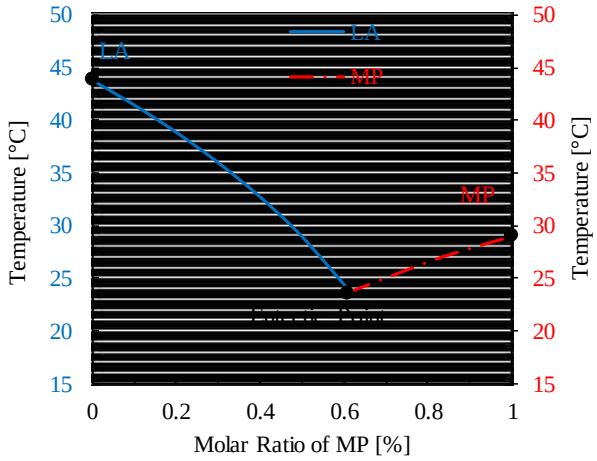

Figure 3.1. The predicted phase diagram for the MP/LA binary mixture

3.2.2. Thermal Characterization. The investigation of MP/LA eutectic mixture included several experiments around the theoretical eutectic point until an ideal PCM mixture at a certain mass percentage is found with a single desirable sharp melting peak and high latent heat. The melting onset temperature (T_{om}), melting temperature (T_m), The freezing onset temperature (T_{of}), Freezing temperature (T_f), and latent heat of fusion (ΔH) were measured using a Seiko DSC6200 colorimeter (Seiko Instruments) and DSC2010 (TA instruments). The DSC measurements were performed using aluminum sample pans and lids (TA pans #900786.901, and TA Lids #900779.901). The temperature and enthalpy calibration were performed using a standard mercury, indium, tin, and zinc samples over a temperature range of -38°C to 419°C with nitrogen purge gas at 20 mL/min and heating rate of 3°C/min.

The temperature repeatability, calorimetric sensitivity, and calorimetric precision for the calorimeter is ±0.1°C, 1µW and ±1%, respectively. The samples of each material were first heated until fully melted before they were prepared in a DSC sample pan.

In order to accurately determine the enthalpy-temperature curve and the specific heat capacity of the PCMs, a DSC baseline measurement using two empty pans was performed. The baseline measurement is a DSC run using an empty sample and reference pans over the entire temperature range using the same heating rate that will be used for the subsequent measurements. The resulting signal is the DSC baseline that has to be subtracted from the heat flow signal of the subsequent PCM measurements. By following this methodology, the heat capacity contribution of only the PCM material in the DSC pan is measured.

The enthalpy as function of temperature –also known as the total thermal energy storage- is determined from the DSC thermogram results by integrating the heat stored in a given temperature (DSC signal) using equation 11 [111].

$$H(T_i) = \int_{T_i}^{T_{i+1}} C_p(T).dT = \int_{T_i}^{T_{i+1}} \frac{\delta Q/dt}{dT/dt}.dT = \int_{T_i}^{T_{i+1}} \frac{\delta Q}{dT}.dT \qquad (11)$$

Where $H(T_i)$ is the enthalpy or energy storage at a single temperature increment between T_i and T_{i+1}, $\frac{\delta Q}{dt}$ is the heat flow in units of *W/g*, and dT/dt is the DSC heating rate in units of *℃/sec*.

The study of the thermal conductivity for the liquid state of PCMs was done using the Transient Hot-Bridge technique using a thermal conductivity measuring instrument (THB1, Linseis Inc., USA) for liquid samples following the steps described in Section 2.3. The thermal conductivities for the solid state eutectic PCM were measured using the heat flow meter (FOX 314, TA instruments, USA) following the steps described in Section 2.2.

As the heat capacity of samples for the solid and liquid state is experimentally measured using the DSC, thermal diffusivity can be calculated as previously given in Section 2.4 using equation 8.

3.3. RESULTS AND DISCUSSION

The DSC thermograms and the thermal analysis results of individual PCMs, MP and LA, are given in Figure 3.2. A scanning rate of 3 ºC/min and sample mass of 7.5 mg was chosen as an appropriate measuring conditions for PCMs [2]. As shown in Figure 3.2, for MP, the melting and freeing temperature is 29.6ºC and 24.0ºC, respectively. The latent heat of melting is 227.6J/g, and the latent heat of freezing is 224.7J/g. For LA, the melting and freeing temperature is 44.1ºC and 39.9ºC, respectively. The latent heat of melting is 185.5J/g, and the latent heat of freezing is 181.4J/g.

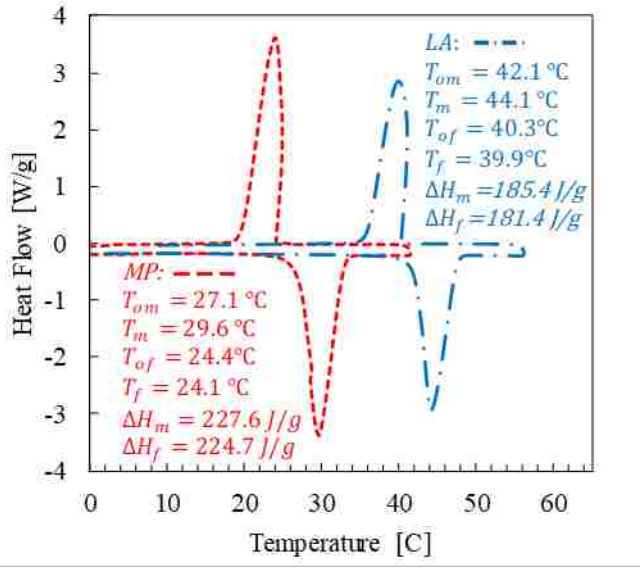

Figure 3.2. DSC curves of Methyl Palmitate (MP) and Lauric Acid (LA).

3.3.1. The MP/LA Eutectic Mixture. The investigation of eutectic mixtures is usually performed by a series of experiments until an ideal PCM mixture with a certain mass percentage is found at a certain melting temperature with a single desirable "sharp" peak and high enthalpy.

A series of binary mixtures were prepared and summarize in Table 3.2. The DSC melting curves of the binary mixture series are shown in Figure 3.3. As can be seen in Table 3.2 and Figure 3.3, the binary mixtures with the MP/LA molar ratios of 60/40, 62.5/38.5, 65/45, 70/30, and 80/20, show one melting peak. The other ratios with higher Lauric Acid content show an incongruent melting by forming a mixture with a second peak at slightly higher temperature.

Table 3.2. DSC results of Methyl Palmitate, Lauric Acid, and the binary mixture

MP/LA	T_{om} [°C]	T_m [°C]	T_{of} [°C]	T_f [°C]	ΔH_m [J/g]	ΔH_f [J/g]
MP	27.1	29.6	24.4	24.1	227.6	224.7
80/20	22.8	26.4	19.6	19.0	198.7	197.2
70/30	21.7	25.6	19.4	18.5	195.3	195.1
65/45	21.9	26.1	19.2	18.1	198.6	196.9
62.5/38.5	22.4	25.8	21.5	20.2	203.7	201.9
60/40	22.5	25.7	21.9	20.4	205.6	205.5
57.5/42.5	22.1	25.3, 29.5	22.1, 22.8	20.2, 22.5	192.6	191.3
40/60	22.1, 31.3	25.0, 34.1	21.2, 29.8	20.1, 29.1	137.5, 56.3	126.5, 75.3
20/80	22.5, 35.1	24.6, 39.2	20.2, 33.0	19.6, 33.1	48.5, 125.1	45.2, 123.1
LA	42.1	39.9	40.3	44.1	185.5	181.4

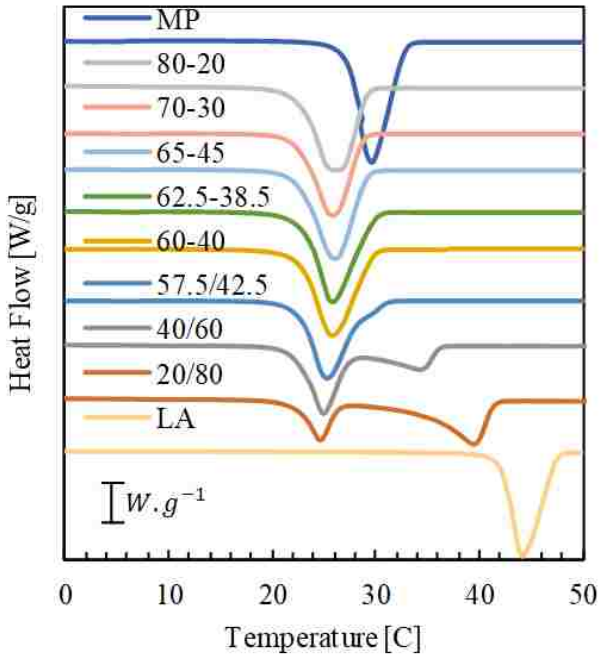

Figure 3.3. DSC melting curves of the binary mixture series

By comparing the binary mixtures of MP/LA molar ratios with single phase change peak: 60/40, 62.5/38.5, 65/45, 70/30, and 80/20, it can be seen that the binary mixture of MP/LA ratio 60/40 has the most desirable phase change behavior for the following reasons: 1. Higher latent heat of fusion; 2. Lower supercooling (difference between melting and freezing temperatures); 3. Suitable phase change temperature that helps to prevent overheating by start absorbing its latent heat capacity of melting during hot conditions when the temperature exceeds the melting temperature (T_m=25.7 °C), and prevent temperature drops by start releasing its latent heat capacity of freezing during cold conditions when the temperature drops below the freezing temperature (T_f =20.4 °C). Therefore, maintaining the indoor conditions within the comfort temperature range (18-26 °C) as determined by (ASHRAE) standard 55-2013 [95].

The DSC curve and enthalpy as function of temperature for MP/LA eutectic mixture (60/40) are shown in Figure 3.4. The thermal analysis results for MP/LA eutectic mixture is also summarized in Figure 3.4. The pre-calculated theoretical results provide evidence that the Schroeder-Van Laar equation [37] is valid for binary mixtures of fatty acids with methyl esters, with uncertainty in melting temperature of 0.56% and precise prediction for the molar ratio of the binary mixture. In order to check the reproducibility of the 60MP/40LA measurements, three samples of MP/LA at 60/40 ratio were prepared separately and measured using the DSC. Table 3.3 shows the DSC results for the three different samples of the 60MP/40LA eutectic mixture.

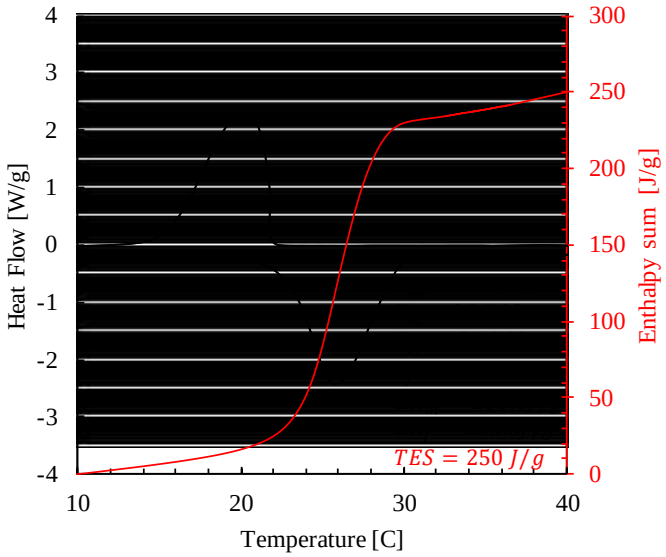

Figure 3.4. DSC curves and total thermal energy storage for 60MP/40LA eutectic mixture.

Table 3.3. DSC results for three independent measurements of different samples of the 60MP/40LA eutectic mixture

Sample	T_{om} [°C]	T_m [°C]	T_{of} [°C]	T_f [°C]	ΔH_m [J/g]	ΔH_f [J/g]
1	22.5	25.7	205.6	21.9	20.4	205.5
2	25.4	25.5	203.7	21.8	20.0	203.8
3	25.5	25.7	206.9	21.8	20.2	208.2
Average	25.6	25.6	205.4	21.9	20.2	205.8

The average data for the thermo-physical properties listed in Table 3.3 show an experimentation consistency by featuring a relatively small variation in the measured data from one experiment to another. The standard deviation for the phase change temperatures is only within ±0.1ºC and ±0.2ºC for melting and freezing, respectively, whereas as the standard deviation for latent heat is within ±1.6 J/g and ±2.2 J/g for melting and freezing, respectively.

3.3.2. Specific Heat. The specific heat capacity is a key parameter in describing the thermal energy storage during sensible heat processes (before and after phase transitions). The specific heat capacity of PCMs was determined using the enthalpy-sum curve, as the slope of the sensible heat part before the phase transition region for the solid phase, and after the phase transition region for the liquid phase.

The experimental results for the specific heat capacity (C_p) and the total energy storage (TES) or the enthalpy-sum of PCMs through a temperature range of 15°C around the melting temperature are shown in Table 3.4.

Table 3.4. The specific heat capacity and total energy storage capacity values for PCMs

PCM		C_P^{Sol} J/g.K	C_P^{Liq} J/g.K	TES J/g.K
MP		1.610	2.248	309
LA		2.040	2.093	248
MP/LA	Sample 1	1.507	2.011	251
MP/LA	Sample 2	1.485	1.875	246
MP/LA	Sample 3	1.549	1.971	255
MP/LA	**Average**	**1.513 ±0.032**	**1.952 ±0.069**	**250 ±4**

The average specific heat capacity was found to be (C_p^{sol}= 1.513 ± 0.032 J/g.K, C_p^{liq}= 1.952 ± 0.069 J/g.K), which corresponds to 2.15% and 3.58% uncertainty for the specific heat capacity of solid and liquid, respectively. The measured values of specific heat capacity for the eutectic mixture are lower than that of the individual components.

3.3.3. Thermal Conductivity. In order to assure precision and repeatability, the reported values for thermal conductivity of liquid samples were the average of at least 10 measurements for each sample, or until an uncertainty of 0.003 W/m.K or lower for thermal conductivity is achieved. A delay time of 5 times the measuring time was set between the single measurements to allow the sample to cool down and back to steady state before the next measurement run when the THB1 meter used.

Table 3.5 shows the results for thermal conductivity of the liquid state for MP, LA, and MP/LA eutectic mixture using the THB1 meter. The thermal conductivity of the MP/LA mixture was found to be 0.1729 W/m.K for liquid state PCM.

Table 3.5. Thermal conductivity test for liquid state PCMs using THB1 meter

Test	MP K [W/m.K] @ 35°C	LA K [W/m.K] @ 35°C	60MP/40L K [W/m.K] @ 35°C
1	outlier	outlier	0.1727
2	0.1795	outlier	outlier
3	0.1793	outlier	0.1731
4	0.1782	0.1633	0.1730
5	0.1762	0.1632	0.1729
6	outlier	0.1638	Outlier
7	outlier	0.1636	0.1729
8	0.1783	0.1639	0.1727
9	0.1789	0.1637	0.1727
10	0.1788	0.1630	0.1728
Average	0.1785	0.1635	0.1729
±*Std*	±0.0010	±0.0003	±0.0001

Table 3.6 shows the results for the thermal conductivity for the solid state of MP, LA, and MP/LA eutectic mixture using the heat flow meter FOX 314. The thermal conductivity of the MP/LA mixture is 0.1802 W/m.K for solid state PCM.

Table 3.6. Thermal conductivity for solid state PCMs using Fox 314 heat flow meter

PCM	Average thermal conductivity [W/m.K] @ 12°C	±Std
MP	0.1923	0.0005
LA	0.1754	0.0003
MP/LA	0.1802	0.0003

The thermal conductivities for the eutectic mixtures and individual PCMs are relatively low for an ideal PCM. In general, this is expected for organic PCMs. The thermal conductivity can be improved by adding metallic fillers or nanomaterials as proposed by several studies [112-114]. The thermal conductivity for the solid state was found to be slightly higher than the thermal conductivity of liquid state. This difference is justified because of the nature of heat transfer through solid where the degree of crystallinity is higher compared to liquid state where the molecules are disordered [115]

3.3.4. Thermal Diffusivity. The thermal diffusivity is a principal factor for describing the performance of PCMs in energy storage systems as it governs the diffusion during heat transfer. Therefore, the investigation of thermal conductivity, latent heat, and heat capacity alone is insufficient for predicting the overall heat transfer enhancement of PCMs or to model and stimulate the acual behavior of PCM in any system. Only a few existing studies examined all of these additional thermo-physical properties in a detailed manner.

The thermal diffusivity for MP/LA eutectic mixture and individual components was calculated as previously decribed in Section 2.4 using equation 8. The measured specific heat capacity, density, and thermal conductivity for both solid and liquid state were used to calculate the thermal diffusivities for the solid and liquid phases of the eutectic mixture. Table 3.7 shows the measured densities for the solid and liquid state which were used to calculate the thermal diffusivity for the MP, LA and MP/LA eutectic mixture shown in Table 3.8.

Table 3.7. The experimental density for the MP, LA, and MP/LA eutectic mixture

PCM	ρ_{Sol} g/ml @ 12°C	ρ_{Liq} g/ml @ 35°C
MP	0.8621	0.8238
LA	0.8885	0.8562
MP/LA	0.8877	0.8406

Table 3.8. The measured thermal diffusivity for MP, LA, and MP/LA eutectic mixture

PCM	α_{Sol} mm^2/s @ 12°C	α_{Liq} mm^2/s @ 35°C
MP	0.139	0.096
LA	0.097	0.091
MP/LA	0.134	0.105

It was noted that the MP/LA eutectic mixture has a small decrease in its density when it melts. Therefore, the volume expansion during phase transformation from solid to liquid is minimal (5.3%) and not expected to cause any problems when the materials are encapsulated in panels or containers for any applications. The thermal diffusivity of the MP/LA eutectic binary mixture was found to be 0.134 mm^2/s for the solid phase and 0.105 mm^2/s for the liquid phase. These values are within the normal range for other organic based PCMs as reported in other studies [100, 106].

3.3.5. Thermal Stability of MP/LA Eutectic Mixture. The thermal performance stability of the eutectic mixture was tested using the DSC by measuring the effect of thermal cycles on the melting temperature, freezing temperature, latent heat of melting, and latent heat of freezing. The sample was heated up to 25 °C above its melting point and then was cooled down to 25 °C bellow its melting to go through a complete thermal cycle. Table 3.9 and Figure 3.5 show the DSC tests of MP/LA at 0, 50, 100, 150, 200, 250, 300, and 350 thermal cycles. The changes in the thermal performance of the MP/LA binary mixture are at an acceptable level for PCMs. The freezing peak has become narrower with a slight decrease in the freezing temperature. The melting peak shows no significant changes in shape or magnitude. It can be observed from Table 3.9 that the change in latent heat values was not obvious with increasing number of thermal cycles. The small changes in melting phase change temperature are in acceptable level for PCMs and also within the uncertainty of the DSC method.

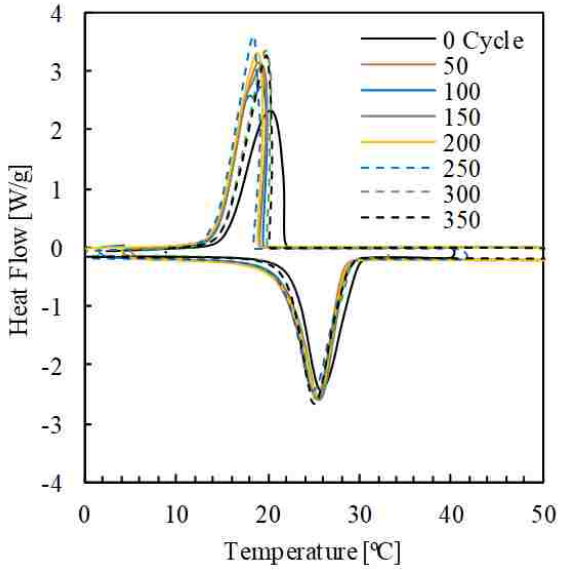

Figure 3.5. DSC curves for the MP/LA binary mixture after thermal cycling

Table 3.9. Thermophysical properties of the MP/LA binary mixture after thermal cycling

Cycle	T_{om} [°C]	T_m [°C]	ΔH_m [J/g]	T_{of} [°C]	T_f [°C]	ΔH_f [J/g]
0	22.5	25.7	205.6	21.9	20.4	205.5
50	22.0	25.3	203.5	19.8	19.0	205.5
100	22.1	25.6	203.7	19.8	19.3	205.3
150	22.3	26.1	204.4	20.0	19.4	205.4
200	22.4	25.8	205.0	19.3	19.0	204.9
250	22.1	25.4	203.9	18.9	18.5	205.2
300	22.3	25.4	205.5	19.8	19.8	205.5
350	22.4	25.1	204.2	20.1	19.9	205.2
Average	22.3	25.6	204.5	20.0	19.4	205.3
±Std	*±0.2*	±0.3	±0.8	±0.9	±0.6	±0.2

3.4. FINDINGS AND FUTURE REMARKS

The study characterized a eutectic mixture of MP and LA as a potential PCM for thermal energy storage applications. It was found that binary mixture consisting of 60%MP and 40%LA molar ratio is the optimum PCM and suitable for thermal energy storage and room temperature thermal regulation, particularly due to the following reasons: 1) Relatively high latent heat capacity (ΔH_m= 205.4±1.6 J/g, ΔH_f= 205.8±2.2 J/g). 2) Suitable phase transition temperatures that fall within the human comfort temperature range (T_m=25.6 ºC, $T_{f=}$20.4 °C). 3) The eutectic mixture was stable over 350 thermal cycles and showed less than ±0.2 ºC and ±0.6 ºC change in melting and freezing temperature, respectively, and less than ±0.8 J/g and ±0.2 J/g change in latent heat capacity of melting and freezing, respectively. 4) The individual PCMs used to prepare the eutectic mixture (MP and LA) are organic based PCMs and therefore they are nontoxic and available with

economical feasibilities for energy storage applications in buildings. 5) Suitable for encapsulation in panels due it its small volume change during phase transition.

The measured thermo-physical properties such as thermal conductivity, specific heat capacity, enthalpy curve, and thermal diffusivity provided a useful database for modelling and stimulating the prepared PCM in buildings to recommend the optimum loading and distribution of PCMs based on different climate regions. Although the thermal analysis of the eutectic mixture showed a desirable overall thermal performance, additional tests are required to verify the compatibility of this PCM with the construction materials in case of direct incorporating through gypsum, cement and mortars. Moreover, it is difficult to maintain the PCM in the construction material matrix when the PCM is in melted or liquid state and therefore leakage can occur. For that reason, enclosing the PCM in microscopic polymer films is an advisable option in this case. The study of this eutectic mixture with combatable gelling agents is another option to prevent leakage and maintain the PCM in the matrix. The measured thermal conductivity is relatively lower than ideal PCM (0.1785 W/m.K for liquid, 0.1802 W/m.K for solid) which can limit the heat transfer rates during phase transitions, therefore, additional tests by adding metallic fillers or nanomaterials can be studied to overcome this drawback.

4. PREPARATION AND ENHANCED THERMAL PERFORMANCE OF NOVEL (SOLID TO GEL) FORM-STABLE EUTECTIC PCM MODIFIED BY NANO-GRAPHENE PLATELETS

The content of this section has been published in "Saeed, et al. (2018). Preparation and enhanced thermal performance of novel (solid to gel) form-stable eutectic PCM modified by nano-graphene platelets. Journal of Energy Storage, 15, 91-102." [4]. Some information may have been omitted, shortened, or reformatted for purposes normal to dissertation writing.

This study presents the development of form-stable eutectic mixtures, modified with nanoscale structures for enhanced thermal performance. These additives may result in the next generation of phase change materials (PCMs) for thermal energy storage systems. An appropriate gelling or thickening agent (2-hydroxypropyl ether cellulose) is introduced so that the PCM will lose its fluidity, become form-stable, and the liquid leakage problem will be overcome. Nano-graphene platelets (NGPs) are added in order to enhance the thermal properties and overall heat transfer. The principle of the T-history method was applied using a parallel plate heating/cooling guarded plate apparatus to determine the true phase transition temperatures of bulk PCM. The supercooling of the enhanced shape stable mixture was reduced to be less than 0.1ºC. The accelerated thermal reliability test indicated that the enhanced form-stable eutectic mixture has reliable thermal performance over a postulated lifetime of 80 years. As a result, the developed form stable PCM eutectic mixture is a promising material for thermal energy storage.

4.1. DEVELOPMENT NEEDS

The demand for providing effective utilization of thermal energy for thermal comfort in buildings is increasing rapidly. Phase change materials (PCMs) have been proposed for improving residential heating and cooling systems, a field which comprises as much as 24% of the energy consumed in the United States each year [89, 116]. The use of PCMs can reduce energy consumption in this area by as much as 30% to 50% [50, 91, 117]. In general, PCMs store/release thermal energy from/to the surrounding medium while remaining constant temperature corresponding to its phase transition temperature [22].

In order for a PCM to provide energy saving benefits, the material should offer a high thermal storage capacity and an ability to store and release heat at nearly constant temperature around comfort room temperature [31]. The average comfort temperature ranges from 19°C to 27°C as reported by the American Society of Heating, Refrigerating and Air-Conditioning Engineers (ASHRAE) standard 55-2013 [95]. PCMs have been used in buildings by incorporating them through wallboards, ceiling tiles, floor, Air-conditioning systems, and even by incorporating them directly through gypsum mixture, cement paste, and mortar [93, 94, 118]. However, the challenge has been developing PCMs with suitable melting temperatures and high latent heats, along with a thermal conductivity and heat capacity high enough to be useful. Moreover the liquid phase of PCMs creates design challenges, such as possible leakage, which reduces their effectiveness. The current pure PCMs do not exhibit all the desirable physical and thermal properties.

Thermal conductivity and specific heat capacity are key factors to assist the absorption and release of energy in the PCM storage system. If the thermal conductivity and heat capacity are low, the heat flux cannot effectively diffuse and stored into the mass

of PCM, and only the layer of PCM closest to the heat source melts [22]. Enhancement of heat transfer in PCMs can lead to an improved performance and a larger reduction in energy consumption – reducing energy costs and greenhouse gas emissions. Most organic PCMs have an undesirably low thermal conductivity, in the region of 0.15 W/m.K [5]. These materials may act as thermal insulators instead of thermal storage media. Therefore heat transfer enhancement is required for practical application [119]. With thermal conductivities as low as 0.15 W/m.K for organic based PCMs, they may act as a thermal insulator instead of a thermal storage medium. Enhancement in heat capacity increases the amount of energy that can be stored as sensible heat. This is very important particularly when the PCMs works beyond its phase transition period, such as during harsh weather conditions, especially when the discharge in the previous cycle was not enough to reach the phase transition range (latent heat region).

Another drawback of current PCMs is the possibility of leaking due to fluidity of the liquid phase. The liquid phase creates design challenges focused on the integration and containment of liquid phase PCM without affecting the system reliability and performance. In addition to the problem of PCM leakage, many studies [30, 118, 120, 121] also reported that the use of liquid PCMs in cement paste, mortar, and gypsum mixture significantly decrease the compressive strength and structural strength of the structure. Li et al. [122] reported that previous studies have mainly been focused on the preparation of PCM building composites, but did not consider the expected PCM leakage when the material melts. Their results showed that the leakage of PCM from cement mixtures was significant when the PCM was incorporated with the cement paste composite without the use of modifier or gelling agent. The PCM leakage ratio from the PCM/Cement composite when

PCM melted was 57.3%, which is considered to be very high and causes a large decrease in the thermal energy storage capacity of the PCM composite. Moreover, incorporating pure PCMs was found to have a significant effect on the composite structural strength. Therefore, it's very important to provide a semi form-stable or shape-stabilized PCM composite.

The current methods to integrate PCMs in a system include the direct immersion method, melt blending method, graft copolymerization method, intercalation method, microencapsulation, and the sintering method. Deep details on these methods can be found in the references [18-27]. In summary, direct immersion cannot prevent PCM leakage and can lead to reduced structural strength [123, 124]. Melt blending causes phase separation [125]. Graft copolymerization is known to significantly decrease the latent heat of fusion and reduce stability [126-128]. Intercalation increases the system costs [129, 130]. Microencapsulation can deteriorate the heat transfer rate due to the increased thermal resistivity [129, 131]. Sintering is a long and complex process with narrow applications [132]. In previous work [3], we presented a new binary eutectic PCM using methyl ester and fatty acid PCMs, specifically, methyl palmitate and lauric acid. The resulting PCM had a phase transition temperature within the comfort temperature range (T_m =25.6ºC, T_f =20.2ºC) and high latent heat capacity (ΔH_m =205.4J/g, ΔH_f =205.8J/g). These properties remained stable through over several freeze/melt cycles. However, the thermal conductivity of this PCM is low, resulting in large thermal gradients that limit the ability of PCM to maintain the internal environment at constant temperature. The problem of liquid leakage also remains.

This paper presents the development of form-stable eutectic mixtures, modified with nanoscale structures for enhanced thermal performance. These additives may result in the next generation of PCMs. An appropriate gelling or thickening agent, in this case 2-hydroxypropyl ether cellulose (HPEC) is introduced so that the PCM will lose its fluidity, become form-stable, and the liquid leakage problem will be overcome. Nano-graphene platelets are added in order to enhance heat transfer.

In addition to form-stabilizing, the gelling agent is expected to improve the stability over multiple freeze/melt cycles. This is accomplished by preventing phase separation in eutectic mixtures. Moreover the gel can work as a crosslinked medium and prevent nanostructures from migrating, maintaining the homogeneity of the mixture and preventing phase separation or segregation [22]. Further desirable effects can be achieved with a gelling agent, such as an increased heat capacity due to the enhanced crystallinity. [133-135]. Although this method has the benefits of simplicity and low cost, the compatibility of a certain gelling/thickening agent with a certain PCM is not always guaranteed. A certain gelling agent may successfully gel/thicken only a certain group of PCMs. When a eutectic mixture is prepared from two PCM groups, the suitability of the gelling agent has to be proven with experiments. The addition of nano-graphene platelets to the PCM will not only enhance heat transfer, but improve fire retardancy [136]. The final formulation of this enhanced PCM has better advantages and more desirable properties. It will be an attractive energy storage option for use in wallboards, ceiling tiles, floors, building structures, and air conditioning units to reduce temperature variations and energy consumption.

4.2. MATERIALS AND METHODS

Methyl Palmitate (MP) and Lauric Acid (LA) were supplied by Sigma Aldrich and used to prepare the MP/LA binary eutectic mixture. The chemical and physical data for the PCMs are listed in Table 4.1.

Table 4.1. The chemical and physical data of PCMs.

PCM Name	Scientific Name	Purity	Molecular weight [g/mol]	CAS Number	Molecular Formula
Methyl Palmitate (MP)	Methyl-hexadecanoate	99%	270.4507	112-39-0	$C_{17}H_{34}O_2$
Lauic Acid (LA)	Dodecanoic acid	99%	200.3178	143-07-7	$C_{12}H_{24}O_2$

The thickening and gelling agent used is 2-hydroxypropyl ether cellulose (HPEC). The material was supplied by Ashland. The chemical data are listed in Table 4.2.

Table 4.2. The chemical data of the gelling agent.

Scientific Name (CA index name)	Supplier / product name	Physical from	CAS number
2-hydroxypropyl ether cellulose (HPEC)	Ashland / Klucel-G	Powder	9004-64-2

Nano graphene platelets (NGPs) have been selected as a nanostructure candidate for the proposed MP-LA PCM. NGPs have extremely high thermal conductivity. Their unique morphology is comprised of a short stack of platelets in planar form as shown in Figure 4.1. Besides a high thermal conductivity, NGPs have a unique characteristic of increasing flame retardancy [136], which may be important in applications such as

residential houses and buildings. Moreover, the unqiue structure of NGPs as nano-layers form an efficient heat conduction link compared to many types of nanoparticles or CNTs.

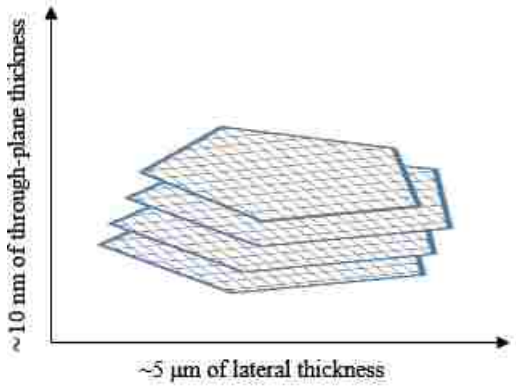

Figure 4.1. Schematic diagram for a stack of Nano Graphene Platelets (NGPs)

The selected NGPs have an average through plane thickness of 10 nanometers, a lateral thickness of ≤5 micrometers, and a specific surface area of 15 m^2/g. The characteristics of NGPs supplied by the manufacturer (Angstron) are shown in Table 4.3.

Table 4.3. Properties of the experimental Nano Graphene Platelets (NGPs)

Product Name	Visual	Density	Surface Area	Through Plane Thick	Lateral Thickness
Nano Graphene platelets (NGPs)	Fluffy, light powder	≤ 2.2 g/cm^3	≥15m^2/g	10 nm	≤5 μm

4.2.1. Preparation of PCM. The binary eutectic mixture (MP-LA) at molar ratio of 60/40 was prepared via physical blending at 50 °C and confirmed by experimental and thermal characterization reported in our previous work [3]. In the current study the HPEC gelling agent was added to the MP-LA mixture at a by-mass ratio of 10% and stirred for 30 minutes at 50 ºC. The MP-LA/HPEC was then heated to 70 ºC to allow the gel to soften before adding the NGP at by-mass ratios of 1%, 3%, 5%, or 10% and stirred for 30 minutes.

Figure 2 shows a digital photograph of (a) the eutectic PCM mixture (MP-LA), (b) form-stable gelled PCM (MP-LA/HPEC), and (c) the nanostructure-enhanced form-stable eutectic PCM (MP-LA/HPEC/NGP10%).

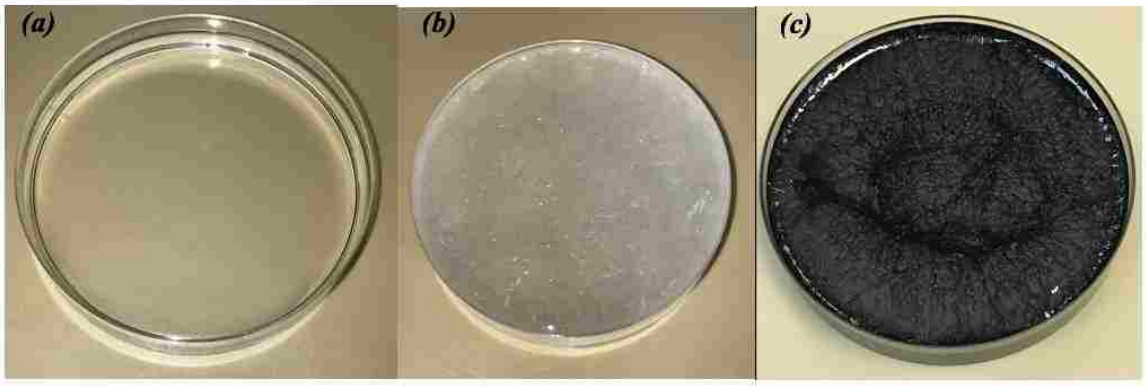

Figure 4.2. Digital photograph of (a) the eutectic PCM mixture (MP-LA), (b) form-stable gelled PCM (MP-LA/HPEC), and (c) the thermal modified form-stable eutectic PCM (MP-LA/HPEC/NGP10%).

4.2.2. Thermal Characterization. Differential scanning calorimetry (DSC) was carried out using the Seiko DSC6200 colorimeter (Seiko Instruments) and Discovery M-DSC (TA instruments). The DSC samples were tested using aluminum sample pans and lids (TA pans #900786.901, and TA Lids #900779.901). DSC measurements were performed using 7-8 mg sample mass. The heating/cooling rate was 3°C/min per recommendations for high accuracy [2, 137]. Three measurements performed for each PCM and the averages are reported here. The thermo-physical properties measured by the DSC include the melting temperature (T_m), freezing temperature (T_f), latent heat for melting (ΔH_m), and latent heat for freezing (ΔH_f). The TA Discovery Modulated DSC (M-DSC) was specifically chosen for enthalpy measurements of gelled PCM samples. The instrument uses a modulated, sinusoidal temperature variation rather than monotonically increasing variation, and thus can retrieve data not obtained by conventional DSCs. This allows the M-DSC to separate the specific heat capacity component (reversing heat flow) from the kinetic component (non-reversing heat flow) such as thermal curing reactions or decomposition. Such advanced M-DSCs provide great benefits for measurements of special materials (form-stable PCMs in this case). Form-stable materials will not form a thin film layer in the DSC pan as in the case of liquids, and require special consideration for crystallization, resistance, and capacitance through the sample.

The specific heat of the PCMs was determined from the enthalpy-temperature thermodynamic calculations. In order to accurately measure the specific heat using this method, a special methodology was used. First, a DSC baseline measurement was performed using two empty sample and reference pans at the same heating rate for the subsequent experimental measurement. Second, the same pan used for the baseline

measurement was used to test the PCM sample. Third, the resulting baseline signal in the first step was subtracted from the heat flow signal of the PCM sample. Therefore, the measured heat capacity is only for the PCM material, as the specific heat of the pans and DSC baseline is subtracted. Fourth, the DSC heat flow signal is used to measure the enthalpy as function of temperature by integration the heat stored over a given temperature increment using equation 12 [111]. The specific heat capacity of PCMs was then measured as the slope of the sensible heat section in the enthalpy-temperature curve before the phase transition region for the solid state, and the slope of the sensible heat section after the phase transition region for the liquid phase, using equation 13.

$$H(T_i) = \int_{T_i}^{T_{i+1}} C_p(T).dT = \int_{T_i}^{T_{i+1}} \frac{\delta Q/dt}{dT/dt}.dT = \int_{T_i}^{T_{i+1}} \frac{\delta Q}{dT}.dT \quad (12)$$

$$C_p(T) = \frac{dH(T)}{dT} \quad (13)$$

Where $H(T_i)$ is the enthalpy or energy storage between the temperature increments T_i and T_{i+1} in units of J/g, $\frac{\delta Q}{dt}$ is the DSC heat flow signal in units of *W/g*, dT/dt is the DSC heating rate in units of *℃/sec*, and $C_p(T)$ is the specific heat capacity in units of J/g.K.

The thermal conductivity was measured using the transient hot bridge conductivity instrument (THB1, Linseis Inc., USA) for PCMs in liquid state following the steps described in Section 2.3. The thermal conductivity for the PCMs in solid state were measured using a heat flow meter (FOX 314, TA instruments, USA) as described in Section 2.2. Similarly, the thermal diffusivity and density were measured following the steps in Section 2.4 equation 8.

4.2.3. Determination of Phase Transition Temperature of Bulk PCM. The measured phase transition temperatures using the DSC method are often systematically shifted to lower or higher values depending on the measurement conditions, such as scanning rate. Moreover, the influence of non-equilibrium thermal gradients in the DSC sample pan is very significant, particularly for PCMs where the thermal conductivity is relatively low. The effect of these uncertainty sources can be reduced by using an appropriate heating/cooling rate, sample mass, calibration method, and advanced DSCs. The T-history method has also been applied to more accurately measure phase transition temperatures using a parallel, guarded plate apparatus to determine the response of bulk PCM, and to measure the actual supercooling of PCM mixtures.

The experiments were performed using the Fox314 instrument as a parallel heating/cooling guarded plates apparatus to create an isothermal and temperature-controlled environment. A schematic of the experimental setup and instrument is shown in Figure 4.3.

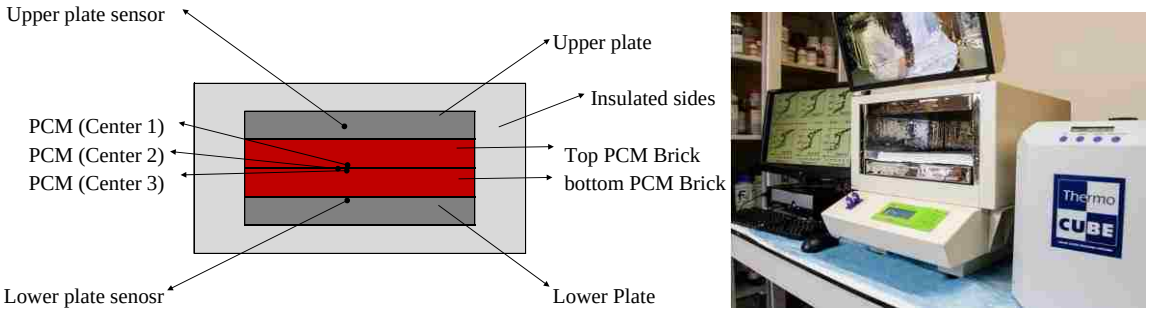

Figure 4.3. The experimental setup using the Fox314 instrument.

The upper and lower plates can be heated or cooled, and the instrument plates control temperature to within ±0.01°C. The PCM mixtures were encapsulated in a 6-mil LLDPE white thin-film, forming an 11.5x11.5 in PCM pouch/brick. Vacuum was applied to ensure that no air exists in the encapsulated PCMs. The mass of PCM mixture in the PCM brick/pouch was 1.4 kg. The encapsulated PCM bricks were inserted, one atop another, with the exterior walls/boundary of the instrument well insulated. The temperature sensors were embedded in and between the two PCM bricks at the following locations: Surface of the top plate, at the center between the two PCM bricks, and surface of the bottom plate. The instrument has four optical encoders which automatically adjust the bottom/upper plates position to compress and establish a full contact with the sample.

For the determination of melting phase transition of PCMs, the top and bottom plates were initially set to a 10°C fixed temperature to discharge/freeze the PCM. Once equilibrium was obtained the plates' temperature was raised to 45°C to provide a "step" driving force, and the temperature-time response of the PCM at the center was recorded. For the determination of freezing phase transition of PCM equilibrium was initially achieved at 45°C, and the temperature-time response during freezing was recorded after temperature of the plates were set to 10°C.

4.3. RESULTS AND DISCUSSION

In Section 3 and our previous work [3], a new binary eutectic PCM using methyl ester and fatty acid PCMs, specifically, methyl palmitate and lauric acid was developed and characterized. This section presented the development of a modified form-stable PCM of that eutectic mixtures with enhanced thermal performance using nanoscale structures,

reduced supercooling, and enhanced shape stability through a solid to gel phase transition to prevent leakage and enhance crystallization.

4.3.1. Thermal Performance of Form-Stable (Solid To Gel) Binary Eutectic PCM. In general, the addition of gelling agent will decrease the amount of active PCM in the mixture and therefore decrease the energy storage capacity of the PCM mixture. For that reason, the objective was to determine the optimum and minimum amount of HPEC gelling agent required to prevent leakage and provide a form-stable PCM composite.

Table 4.4 shows the observed results of various mixtures including HPEC. After initial preparation of PCM mixtures, the gelled PCM samples were allowed to cool in a chamber at 30ºC for 24 hr. The leakage ratio was calculated as the mass fraction of the leaked material to the total mixture.

Table 4.4. Optimizing the suitability and ratio of HPEC gelling agent.

MP-LA %	HPEC%	Texture of mixture	Leakage ratio of PCM
100	0	Liquid	100%
97.5	2.5	Very thin gel	45.4%
95	5	Thin gel	18.8%
92.5	7.5	Gel	0%
90	10	Thick gel	0%
87.5	12.5	Thick gel	0%
85	15	Thick gel	0%

As indicated by the resulting leakage ratios in Table 4.4, at percentage of 5% or less of HPEC gelling agent, the liquid PCM separated from the supporting gelled mixture,

and then leakage of liquid PCM occurred. All samples with percentages of 7.5% or higher for HPEC were completely gelled with a form-stable texture and showed 0% of the liquid (PCM) leaching out of the mixture. The ratio of 10% HPEC as a gelling agent was considered the optimum ratio as no further benefits in the texture and leakage prevention were achieved at higher ratios. The 10% ratio for HPEC was considered for further thermal analysis throughout the study.

The prepared form-stable PCM was studied using the DSC to test for any disturbance in the phase transition process of the PCM, and results were compared to the original MP-LA mixture prior to adding the gelled PCM. The DSC thermogram is shown in Figure 4.5.= and the DSC results for phase transition are summarized in Table 4.5

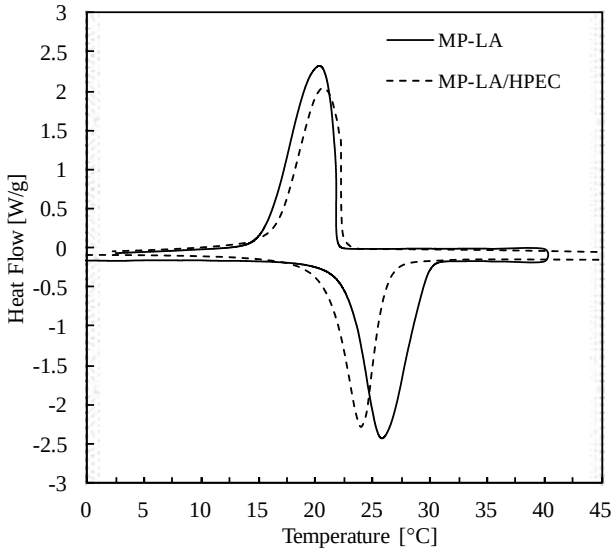

Figure 4.4. DSC results for MP-LA eutectic PCM and form-stable gelled PCM (MP-LA/HPEC).

Table 4.5. DSC data for gelled Eutectic PCM modified by NGPs.

PCM Name	T_m °C	T_f °C	ΔH_m J/g	ΔH_f J/g
MP-LA	25.60	20.20	205.4	205.8
MP-LA/HPEC	24.06	20.80	177.9	176.4

The DSC thermal analysis shows that the addition of HPEC gelling agent did not cause any phase separation or incongruent melting. The prepared form stable PCM shows a single narrow melting phase change peak melting temperature at 24.06°C and a latent heat of 177.9 J/g. This suggested that the addition of 10 wt% of (HPEC) gelling agent slightly decreased the melting temperature and latent heat of the eutectic PCM by 5.6% and 13.3%, respectively. The addition of HPEC gelling agent showed a relatively narrow melting peak compared to the melting peak of MP/LA, which is a desirable behavior since the latent heat of fusion can be stored in a smaller temperature range.

4.3.2. Enhanced Thermal Performance of The Form-Stable PCM. The solid to gel nature of the developed PCM can provide a continuous network surrounding the mixture and work as a cross-linking medium for thermal modulation additives such as the NGPs in the current study. The NGPs were added to the mixture to enhance the thermal conductivity and the overall heat transfer process.

4.3.2.1. Effect of NGPs on phase transition. The NGPs were added to the PCM at various mass fractions (1%, 3%, 5%, and 10%). The effect of NGPs on the melting phase transition was evaluated in order to evaluate the optimum NGP concentration before any phase separation or incongruent melting can occur. Figure 4.5 displays the DSC curves of the form-stable PCM with the addition of NGPs (MP-LA/MHE-C/NGP) at various

concentrations and compares them to pure (MP-LA) and to the gelled (MP-LA/MHE-C) PCMs. The DSC results, weight fraction of PCMs, and full width at half maximum (*FWHM*) for the melting peaks are listed in Table 4.6.

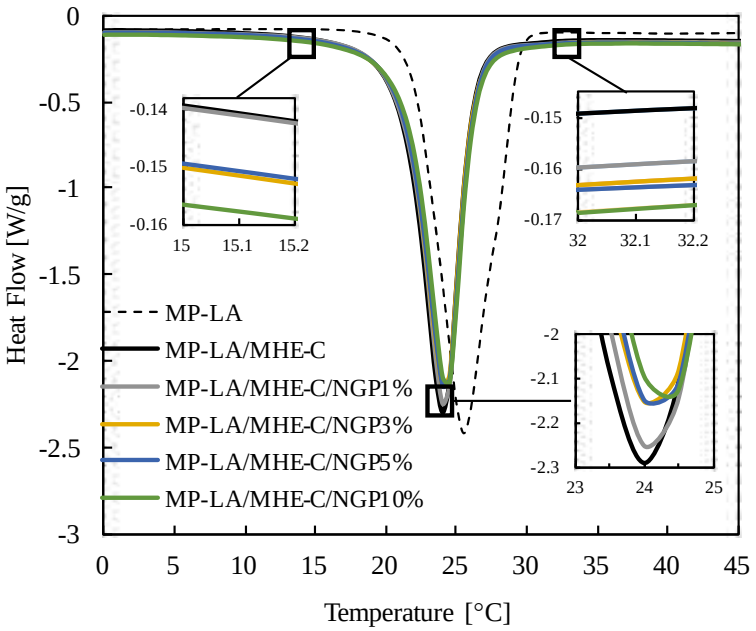

Figure 4.5. DSC results for gelled eutectic PCM modified by NGPs compared to MP-LA eutectic PCM and form-stable MP-LA/HPEC mixture.

Table 4.6. DSC data for gelled Eutectic PCM modified by NGPs compared to MP-LA eutectic PCM and form-stable MP-LA/HPEC mixture.

PCM Name	PCM wt%	T_m °C	ΔH_m J/g	*FWH* °C
MP-LA	100%	25.60	205.4	4.25
LA-LA/HPEC	90.0%	24.06	177.9	2.91
MP-LA/HPEC /NGP1%	89.1%	24.13	174.1	2.87
MP-LA/HPEC/NGP3%	87.3%	24.16	171.5	2.86
MP-LA/HPEC/NGP5%	85.7%	24.21	170.1	2.88
MP-LA/HPEC/NGP10%	81.8%	24.29	165.6	2.79

The DSC thermal analysis shows that the addition of NGPs did not cause any phase separation or incongruent melting. All the mixtures with NGPs showed a single narrow phase change melting peak. The addition of NGPs at ratio of 10% showed the narrowest *FWHM* of 2.79°C, which is a desirable behavior since it can completely store its latent heat of fusion in a smaller temperature range. A slight increase in the melting temperature was observed with the addition of NGPs to the gelled PCM. The melting temperature increased by only 0.23°C when NGPs at a mass fraction of 10% were added. This increase in measured melting temperature is very close to the accuracy of DSC thermocouples (±0.05°C). Therefore, it can be concluded that no major effect was observed on the melting temperature due to the addition of NGPs. Many previous studies [8, 108, 138-141] have reported a change in melting temperature of PCMs with addition of different additives for thermal conductivity enhancement. The slight increase in the measured melting temperature can be explained by the increase in thermal conductivity and thermal diffusivity of PCM samples with the increase of the NGP mass fraction. Supported by observations in a previous work [2], increasing the thermal conductivity of samples decreases the internal thermal gradient inside the PCM samples. Decreasing the internal thermal gradients also decreases the thermal lag between the DSC thermocouples and the bulk of the sample, and the instrument response increases.

4.3.2.2. Thermal conductivity enhancement. Table 4.7 and Figure 4.6 show the results of thermal conductivity measurements for the thermally enhanced form-stable PCM at various ratios of NGPs and compares them to pure and gelled PCMs. The relative increase in thermal conductivity (Change in *K*%) with the addition of NGP is compared to that of the PCM prior to the addition of NGPs. The listed values are the average of 10

measurements for each sample with uncertainty of 0.003 W/m·K. A time delay of 5 times the experiment time was set between the single measurements to allow for thermal relaxation of PCMs and return to steady-state before the next measurement performed. The measurements for liquid and solid states were performed at 35°C and 12°C, respectively.

Table 4.7. Effect of NGPs on the thermal conductivity of gelled Eutectic PCM

PCM Name	PCM wt%	K^{Solid} W/m.K	$Change\ in\ K$ %	K^{melted} W/m.K	$Change\ in\ K$ %
MP-LA	100%	0.1802	x	0.1729	x
LA-LA/HPEC	90.0%	0.1715	0%	0.1656	0%
MP-LA/HPEC /NGP1%	89.1%	0.2265	32.1%	0.2183	31.9%
MP-LA/HPEC/NGP3%	87.3%	0.2486	44.9%	0.2354	42.2%
MP-LA/HPEC/NGP5%	85.7%	0.2847	66.0%	0.2639	59.4%
MP-LA/HPEC/NGP10%	81.8%	0.3468	102.2%	0.3273	97.7%

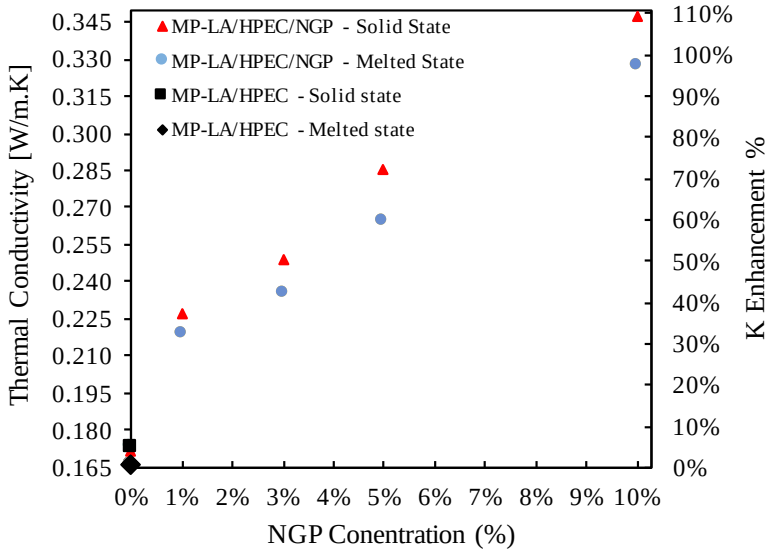

Figure 4.6. Thermal conductivity enhancement of PCMs with NGPs.

The thermal conductivity of the liquid MP-LA eutectic mixture decreased from 0.1729 W/m·K to 0.1656 W/m·K when HPEC was added as a gelling agent. This can be explained by the low thermal conductivity of HPEC. However, the thermal conductivity was significantly increased by adding NGPs. The thermal conductivity for the solid state PCM with NGP mass fractions of 1, 3, 5, and 10% increased by 32.1%, 44.9%, 66.0%, and 102.2%, respectively, when compared to the form stable PCM. Similarly, the liquid thermal conductivity increased by 31.9%, 42.2%, 59.4%, and 97.7% with the addition of NGPs. The largest influence of NGPs on thermal conductivity was reported at the highest mass fraction of NGP.

4.3.2.3. Enthalpy curves and specific heat capacity. The enthalpy-temperature curve is a key factor in describing the total thermal energy storage capacity of PCMs. The enthalpy-temperature curve provides information on the combined effect of latent heat and sensible heat. The study of enthalpy (total energy storage) is very crucial when thermal modulators or additives are used to enhance the thermal performance. In general, the addition of additives - NGPs in this case - will decrease the measured latent heat per unit mass due to the decrease of the active PCM in the overall mixture, as can be seen in Table 4.6. However total energy storage of PCMs is a combination of latent heat and sensible heat. Therefore an increase in specific heat capacity can partially compensate for the reduction in latent heat. The increase in specific heat capacity with the addition of NGPs leads to an increase in the fraction of the total thermal energy storage (TES) caused by the sensible heat contribution. The increase in the sensible heat contribution toward the total TES is very important especially when the PCM works within wide temperature ranges.

Figure 4.7 shows the experimental enthalpy-temperature curve calculated directly from the DSC signal using the method described in Section 4.3.2. The specific heat for the solid state is calculated as the slope of the enthalpy-temperature curve before the phase transition region (sensible heat of solid state). Similarly, the specific heat capacity for the liquid state is calculated as the slope after the phase transition region (sensible heat of melted state).

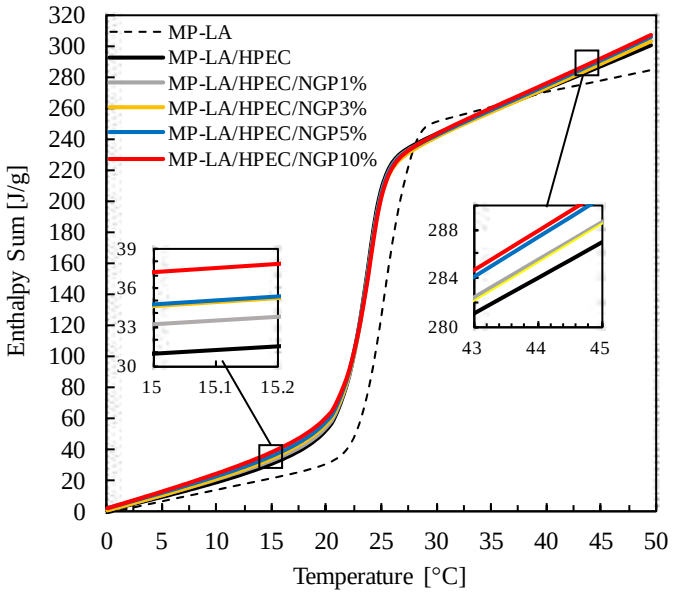

Figure 4.7. Enthalpy-temperature curve for the experimental PCM mixtures.

Table 4.8 shows the experimental values for the specific heat capacity (C_p) of the solid and melted state, and the total energy storage (TES) over a temperature range of 20°C around the melting temperature, for various enhanced PCM mixtures. It can be observed

that a significant increase in specific heat capacity was observed for the form-stable PCM (47.5% for melted state, and 24.7% for solid state) even before adding the NGPs. Several studies showed that the heat capacity of a material can be enhanced by enhancing its crystallinity [133, 135]. For instance, Shin et al, [135] showed an enhancement of up to 54% in the specific heat capacity by dispersing an additive of silica (SiO_2) as gelling agent in a molten salt PCM. Therefore, the significant increase in the specific heat capacity when the HPEC gelling agent was added is not only related to the specific heat capacity of these additives but is also attributed to the enhanced crystallinity of the prepared PCM eutectic mixture. The increase in specific heat capacity through addition of NGPs was also very significant: 52.2% and 64.8% for the solid and melted state PCM in the case of 10% NGPs.

Table 4.8. The measured specific heat capacity and thermal energy storage (TES) for the experimental PCMs

PCM Name	C_p^{solid} [J/g.K]	$Change\ in\ C_p^{solid}$ (%)	C_p^{melted} [J/g.K]	$Change\ in\ C_p^{melted}$ (%)	TES [J/g]	$Change\ in\ TES$ (%)
MP-LA	1.513	-	1.952	-	285.0	-
LA-LA/HPEC	1.887	+24.7%	2.879	+47.5%	286.1	0.4%
MP-LA/HPEC /NGP1%	2.051	+35.6%	3.055	+56.5%	386.9	0.7%
MP-LA/HPEC/NGP3%	2.126	+40.5%	3.121	+59.9%	288.4	1.2%
MP-LA/HPEC/NGP5%	2.135	+41.1%	3.222	+65.1%	288.5	1.2%
MP-LA/HPEC/NGP10%	2.302	+52.2%	3.216	+64.8%	289.4	1.5%

The main goal of adding NGPs was to enhance the poor thermal conductivity for the prepared MP/LA eutectic mixture. Figure 4.8, which shows the total energy storage, latent heat storage and sensible heat storage capacity for the PCM mixtures, indicates that although addition of NGPs decreases the latent heat storage the total thermal energy storage remains similar.

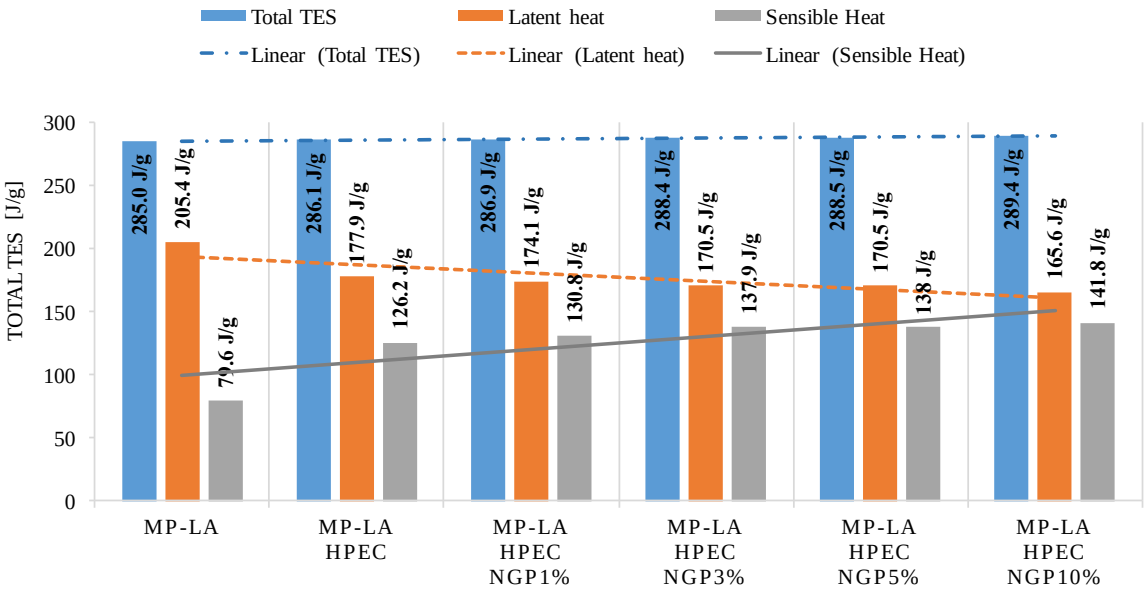

Figure 4.8. Effect of HPEC and NGPs on the total thermal energy storage, latent heat contribution, and sensible heat contribution.

4.3.2.4. Thermal diffusivity and density. Prior to measuring the thermal diffusivity, the physical density for the solid state PCM was determined. Table 4.9 shows the density for the prepared PCM mixtures. The density for the form-stable PCM and enhanced PCM is compared to the density for the pure PCM.

Table 4.9. Effect of the addition of NGPs on density

PCM Name	ρ^{solid} [g/ml]	$Change\ in\ \rho^{solid}$ (%)	ρ^{melted} [g/ml]	$Change\ in\ \rho^{melted}$ (%)	$Volume\ Expansion$ (%) $(\rho^{solid} - \rho^{melted})/\ \rho^{solid}$
MP-LA	0.8877	x	0.8406	x	5.31%
LA-LA/HPEC	0.8930	0%	0.8470	0%	5.15%
MP-LA/HPEC /NGP1%	0.9042	1.25%	0.8583	1.33%	5.08%
MP-LA/HPEC/NGP3%	0.9254	3.62%	0.8861	4.62%	4.25%
MP-LA/HPEC/NGP5%	0.9522	6.63%	0.9125	7.73%	4.17%
MP-LA/HPEC/NGP10%	1.0051	12.55%	0.9714	14.69%	3.35%

When compared to the HPEC gelling agent, the addition of NGPs was found to increase the density of PCM. This is attributed to the higher density of NGPs, about 2.2 g/cm^3. The density was increased by 13.31% and 14.62% for the melted and solid state PCM, respectively, when 10% of NGPs added. The increase in density is very desirable, as more energy can be stored per unit volume. It's also noted that the enhanced form-stable PCMs maintained a smaller volume expansion during phase transformation than pure or form-stable mixtures.

Additional thermo-physical properties such as thermal diffusivity have been rarely studied in a detailed manner for PCMs. The thermal diffusivity is a key parameter in describing the diffusion of heat in practical applications. The latent heat capacity and phase transition temperature alone are not enough to simulate the actual behavior of PCMs or to predict the overall heat transfer enhancement in a thermal energy storage application. The effect of NGPs on the thermal diffusivities of the PCM mixtures are listed in table 4.10.

Table 4.10. Effect of the addition of NGPs on the thermal diffusivity

PCM Name	α_{Solid} [mm^2/s]	$Change\ in\ \alpha_{Solid}$ (%)	α_{melted} [mm^2/s]	$Change\ in\ \alpha_{melted}$ (%)
MP-LA	0.134	x	0.105	x
LA-LA/HPEC	0.102	0%	0.068	0%
MP-LA/HPEC /NGP1%	0.122	20.00%	0.083	22.71%
MP-LA/HPEC/NGP3%	0.126	24.16%	0.085	25.65%
MP-LA/HPEC/NGP5%	0.140	37.60%	0.090	32.84%
MP-LA/HPEC/NGP10%	0.150	47.27%	0.105	54.28%

It was noted that the addition of gelling agent decreased the thermal diffusivity of the PCM by 24% for the solid state and 35.2% for the melted state. The reduction in thermal diffusivity with the addition of HPEC is attributed to the fact that the gelling agent enhanced the ability of PCM material to store energy (specific heat capacity) rather than diffusing it (thermal conductivity). The observed results for heat capacity enhancement (Table 4.8) and thermal conductivity reduction (Table 4.7) with the addition of HPEC gelling agent clearly support this observation. However, thermal diffusivity of the enhanced form-stable PCM increased with the addition of NGPs. When compared to the thermal diffusivity of the form-stable PCM, the addition of NGPs at mass fractions of 1%, 3%, 5%, and 10% increased the thermal diffusivity by 20.00%, 24.16%, 37.60%, and 47.27% for the solid state, and by 22.71, 25.65%, 32.84%, and 54.28% for the liquid state. With 10% NGPs, the thermal diffusivity of the form-stable enhanced PCM was found to be similar to that of the pure PCM. The addition of NGP at mass fraction of 10% enhanced

both the ability to store heat (specific heat capacity) and the diffusion of heat (thermal conductivity and thermal diffusivity).

4.3.2.5. Optimum form-stable PCM mixture. It can be noted from the detailed analysis for the thermo-physical properties for the modified PCMs that the enhanced form-stable PCM mixture with mass fraction of 10% NGPs (MP-LA/HPEC/NGP10%) can be considered as the optimum mixture for the following reasons:

1. The narrowest *FWHM* of 2.79°C, which is a desirable behavior since it can completely store its latent heat of fusion in a smaller temperature range,
2. No significant changes on the original melting phase change temperature,
3. Acceptable latent heat value,
4. The PCM is form-stable,
5. Highest specific heat capacity,
6. Highest density, therefore, more energy stored per unit volume,
7. Smallest volume expansion during phase transition,
8. Highest thermal diffusivity.

In summary, the enhanced form-stable PCM with 10% NGP maintains a balance between the normal decrease in latent heat with additives and the enhancement of the overall heat transfer and thermo-physical properties. Table 4.11 compares the DSC results of the current form-stable PCM (MP-LA/HPEC) and the thermal enhanced form-stable PCM (MP-LA/HPEC/NGP10%) to the reported results of other form-stable PCMs in the literature.

Table 4.11. A comparison on thermo-physical properties of different form-stable PCMs in other literature and the current study.

Form-stable PCMs	T_m °C	ΔH_m J/g	T_f °C	ΔH_f J/g	Ref
Capric-Myristic-Palmitic acid /expanded graphite	18.6	128.2	16.6	124.5	[142]
Palmitic-Capric acid / Diatomie	28.7	104.0	19.7	96.1	[143]
Capric-Lauric acid / Diatomite	20.1	66.8	-	-	[144]
Stearic-Capric acid / activated-attapulgite	21.8	72.6	20.3	71.3	[145]
Capric-Myristic acid / Expanded perlite	21.7	85.4	20.7	89.8	[146]
Capric-Palmitic acid / Vermiculite	23.5	72.0	21.4	67.2	[105]
Capric-Stearic acid / Vermiculite	25.6	71.5	24.9	69.6	[105]
Capric-Palmitic acid /Polyamide-6/Expanded graphite	27.4	134.4	20.0	132	[147]
Capric-Stearic acid / Polyamide-6	28.6	116.9	19.4	113.7	[147]
Capric-Lauric-Palmitic acid / SiO2 nanofibers	21.7	100.9	6.4	96.5	[148]
Capric-Palmitic acid / SiO2 nanofibers	28.1	108.6	18.7	102.2	[148]
Capric-Myristic-Stearic acid/Cellulose acetate SiO2	22.0	99.8	6.4	96.7	[149]
Methyl Palmitate-Lauric acid / HPEC	**24.1**	**177.9**	**20.5**	**176.4**	**Present**
Methyl Palmitate-Lauric acid / HPEC / NGP10%	**24.2**	**165.6**	**24.2**	**164.1**	**Present**

It was observed that the new form-stable PCM possess a higher latent heat of fusion than the other form-stable PCMs studied with suitable melting temperature for thermal comfort in buildings. For that reason, the next two sections will further focus on the supercooling, or difference between melting and freezing temperatures, as well as the thermal reliability of the optimum PCM mixture (MP-LA/HPEC/NGP10%) over 30,000 of thermal cycles.

4.3.2.6. Enhanced supercooling of the thermal enhanced form-stable eutectic PCM. The degree of supercooling is the difference between the melting and freezing temperature, ($\boldsymbol{T_m - T_f}$). The degree of supercooling should be as small as possible for

optimum. The degree of supercooling should be as small as possible for optimum energy storage outcomes [20]. In general, the degree of supercooling is relatively high in PCMs due to the poor rate of crystal growth. Several reports showed that supercooling can be reduced by the use of suspended particles or impurities such as nanoparticles [149-153]. These additives can work as a nucleating sites and therefore increase the rate of crystal growth. Table 4.12 and Figure 4.9 show the effect of NGPs on the freezing temperature.

Table 4.12. The DSC results for melting and freezing temperature of PCM mixtures

PCMs Name	T_m °C	T_f °C	$T_{m-}T_f$ °C
MP-LA	25.6	20.2	5.4
MP-LA / HPEC	24.1	20.5	3.6
MP-LA / HPEC / NGP10%	24.2	24.2; 21.5	0; 2.7

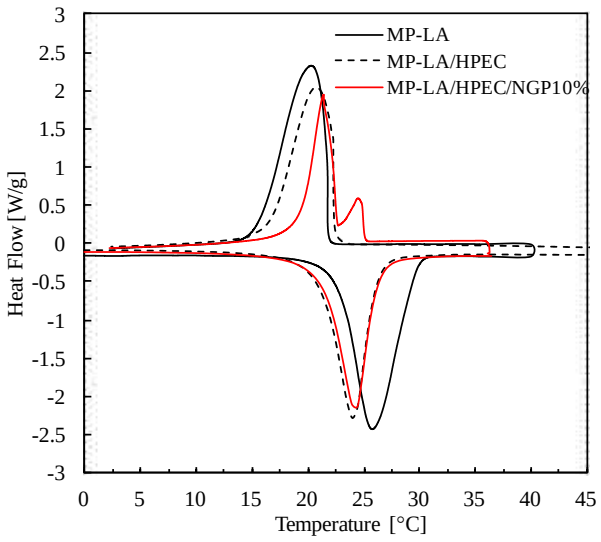

Figure 4.9. The observed DSC freezing profile for various PCM mixtures.

The enhanced form-stable PCM showed a much faster crystal growth. A freezing peak was detected at 24.2ºC. In other words, energy can start to be discharged at higher temperatures compared to pure PCM and form-stable PCM mixtures. This is attributed to the formation of small cold regions known as “cold-fingers” [19] that serve as a nucleating cites due the presence of NGPs. It is worth to mention that the double freezing peak should not be explained as a phase separation, for the following reasons: 1. The phase separation, if any, would also separate the melting phase transition peak, however the melting peak did not show a separation but appeared as a single narrow peak; 2. A phase separation peak, if any, would separate the original freezing peak and appear at a temperature lower than that of the original freezing peak. 3. The second freezing peak was detected at temperature equal to that of the melting peak. Therefore, the second freezing peak is attributed to a reduced supercooling and enhanced crystallization rate.

In addition to NGPs, the HPEC thickening agent was also able to reduce the degree of supercooling. Various thickening agents have been found useful to overcome the supercooling of PCM in some literature. For instance, Qian et al. [33] fownd that silica gel can reduce the degree of supercooling of pristine PEG PCM by 22.3%. Ryu et al [32] investigated the performance of Borax which is mainly a thickening/gelling agent. Their results showed that Borax can reduce the supercooling of salt-hydrate PCMs from 15°C to 3-4°C. It is suggested that some thickening agents provide a surface where the crystal formation can grow faster, which in terns can greatly reduce the degree of supercooling. Another hypothesis is that some thickening/gelling agents behaves like impurities that can trigger the nucleation and crystallization process, especially when added to pure liquid mixtures. Mehling et al. [25] described that as a heterogeneous nucleation, means that

nucleation can be started by impurities in PCM or even cracks at the wall of the vessel than contain the PCM. In the current research, it was found that the addition of NGPs, which act as impurities in the PCM, were able to completely eliminate supercooling. There is still no reliable theoretical approach to the nucleation process in PCM, however Lane [154] provides detailed investigation of PCM nucleation, crystallization, and nucleators.

4.3.2.7. Melting and freezing phase transition temperature of bulk PCM. Further effort was devoted to eliminating any uncertainties or potential measurement errors that may arise using the DSC method for determination of true melting and freezing phase transition temperatures. The non-equilibrium thermal gradient and applied scanning rate using the DSC, particularly for PCMs where thermal conductivity is low, can be strong enough to deviate the measured transition temperatures from true values. Despite the use of an advanced modulated-DSC (TA Discovery M-DSC) -with improved resolution and ability to account of the scanning rate imbalance-, the small PCM samples during a DSC cooling scan may not have enough time to start crystallization, therefore, affecting the measured degree of supercooling.

The principle of the T-history method was applied using the TA Fox314 instrument as a parallel, guarded plate heating/cooling apparatus to determine the phase transition temperature response of bulk PCM, and to measure the actual supercooling of PCM mixtures. The individual experiments for PCM bricks of MP-LA, MP-LA/HPEC, and MP-LA/HPEC/NGP10% were performed using the method described in Section 4.3.3. The temperature-time curve for melting and freezing of PCMs is shown in Figure 4.10.

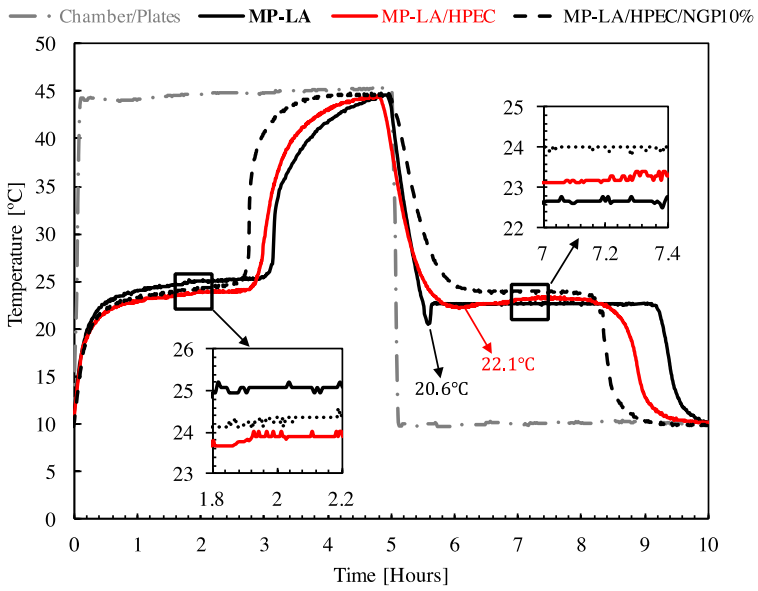

Figure 4.10. The temperature-time response during melting and freezing of PCMs.

The slopes of the temperature during the solid to liquid (melting) cycle decline for the first 30 min, and then become almost flat at around $t \in (1.8hr\ to\ 2.2hr)$. During this period, the solid to liquid (melting) phase transitions take place at 25.0°C, 23.8°C, and 24.2°C respectively, for the MP-LA, MP-LA/HPEC, and MP-LA/HPEC/NGP10% PCMs. These experimental values are in good agreement with the DSC melting values of 25.6°C, 24.1°C, and 24.2°C.

The temperature during liquid to solid (freezing) phase transition became almost constant for all the PCMs at around $t \in (7.0hr\ to\ 7.4hr)$. For MP-LA, it can be seen that the temperature of the MP-LA mixtures continued to decrease with steep slope until the temperature reached 20.6°C before triggering the solidification phase transition at measured temperature of 22.7°C. Similarly, the temperature of the MP-LA/HPEC mixture reached 21.1°C before the solidification process is triggered at measured temperature of

23.1°C. In other words, crystallization starts only after the temperature decreases well below the phase change temperature. This indicated that MP-LA exhibited supercooling at 20.6°C, and the MP-LA/HPEC also exhibited supercooling at around 21.1°C. On the contrary, MP-LA/HPEC/NGP10% showed no supercooling and the liquid to solid (freezing) phase transition took place at 24.1°C.

It can be concluded that the DSC was able to predict only the initial/lower freezing temperature (supercooling temperature) for the MP-LA and MP-LA/HPEC. The measured freezing temperature for MP-LA and MP-LA/HPEC using the DSC method was 20.2°C and 20.5°C, respectively; These values were found to be slightly lower than the values of 20.6°C and 22.1°C obtained using the T-history method, as shown in Figure 4.10. Moreover, the triggered solidification lines (freezing) in Figure 4.10, at slightly higher temperatures after the supercooling temperature was reached, were not detected using the DSC method. Therefore, the T-history method is essential for the determination of the true degree of supercooling. In conclusion, the MP-LA/HPEC/NGP10% was found to have excellent freezing behavior using both the DSC and the experimental apparatus, with less than 0.1°C different between melting and freezing temperature.

When comparing the melting and freezing behavior of PCMs, it was obvious that the melting and freezing for MP-LA/HPEC/NGP10% took relatively less time to complete when compared to that of MP-LA and MP-LA/HPEC. Despite the higher specific heat capacity and overall TES which are theoretically expected to increase melting/freezing time, the reduced melting/freezing time is attributed to higher overall heat transfer rate due to the increased thermal conductivity. In other words, the thermally enhanced shape stable PCM can store/release heat more rapidly in practical energy storage applications.

4.3.2.8. Thermal reliability of the thermal modified form-stable eutectic PCM.

The thermal reliability of the enhanced form stable PCM was experimentally evaluated for over 30000 thermal cycles. For use in building heating and cooling applications, this represents over 80 years of daily cycling. The thermal reliability test is important to test the long-term stability of the PCM mixture. Prior to the DSC measurements the prepared samples were subjected to thermal cycles using an accelerated thermal cycler system (Cincinnati Sub-Zero, Model#:CT-64-6-SCT/AC). The samples were heated up to 60ºC and then cooled down to 4ºC to go through a complete thermal cycle, and the cycler was programed to hold the temperature for 15 minutes before each step to guarantee that the PCM samples will go through a complete phase transition. Table 4.13 and Figure 4.11 show the impact of thermal cycles on the melting temperature, freezing temperature, and latent heat capacity of melting and freezing.

Table 4.13. The DSC results for the MP-LA/HPEC/NGP10% PCM after thermal cycling.

Cycle	T_m [°C]	ΔH_m [J/g]	T_f [°C]	ΔH_f [J/g]
0	24.2	165.6	24.2; 21.5	164.1
1000	24.0	165.9	24.0; 21.2	165.0
5000	24.1	164.8	24.0; 21.2	163.3
10000	24.0	164.0	24.0; 21.3	162.9
15000	23.8	163.5	23.8; 20.8	162.1
20000	23.5	162.4	23.5; 20.6	161.5
30000	23.2	160.9	23.0; 20.5	160.0

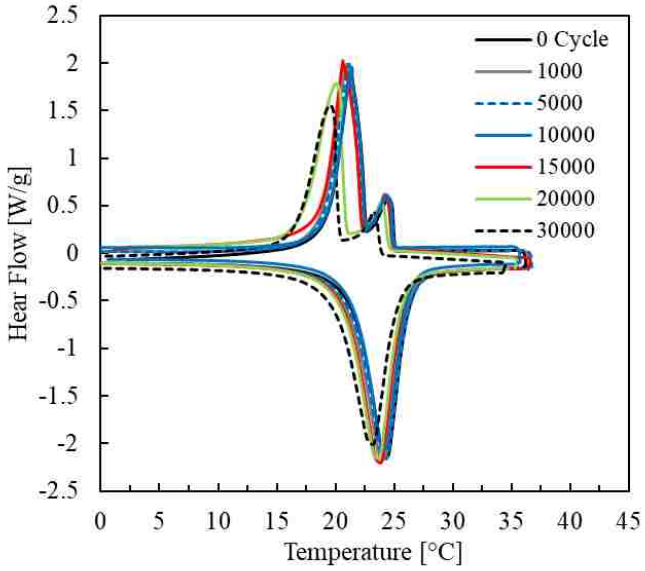

Figure 4.11. The DSC curves for the MP/LA/HPEC/NGP10% PCM mixture after 0, 1000, 5000, 10000, 15000, 20000, and 30000 thermal cycles.

The changes in the measured values are acceptable for PCMs. The melting and freezing peaks showed no significant changes in shape or magnitude. It can be concluded that the effect of thermal cycles on the latent heat values was not significant. After 30000 cycles, the changes in melting temperature, freezing temperature, latent heat for melting, and latent heat for freezing are within 4.3%, 4.7%, 2.9%, and 2.6% over a postulated lifetime of 80 years.

4.4. PERFORMANCE REMARKS AND FUTURE DIRECTIONS

The study presented a form-stable eutectic PCM, modified with nanoscale structures for enhanced thermal performance. The PCM eutectic mixture consists of methyl ester and fatty acid PCMs, specifically, methyl palmitate (MP) and lauric acid (LA). A

gelling agent consists 2-hydroxypropyl ether cellulose (HPEC) was introduced so that the PCM lost its fluidity, became form-stable, and the liquid leakage problem was overcome. Nano-graphene platelets (NGPs) were added in order to enhance heat transfer. The corresponding enhancement when 10% of NGPs was added to the form stable PCM was as follows: the poor thermal conductivity was increased by about 102.2% for solid phase and 97.7% for liquid phase, the specific heat capacity was increased by 52% for solid phase and 64% for liquid phase, the thermal diffusivity was increased by 47% for solid phase and 54% for liquid phase. The enhanced form stable PCM was found to have relatively higher latent heat (165.6 J/g for melting, and 164.1 J/g for freezing) compared to other enhanced form-stable PCM in literature. The MP-LA/HPEC/NGP10% was found to have excellent freezing behavior using both the DSC and the experimental apparatus, with less than 0.1°C different between melting and freezing temperature. The thermal reliability test indicated that the enhanced form-stable eutectic mixture had reliable thermal performance with no significant changes on phase transition temperatures and latent heat values over 30000 thermal cycles.

Simulation and modelling tools are usually used to predetermine the optimum distribution and loading of PCMs in real life based different climate regions, therefore the study provided a useful database for the thermo-physical properties such as specific heat, thermal diffusivity, thermal conductivity, enthalpy as function of temperature, and density. Despite the desirable thermal and physical properties of the enhanced form stable PCM, additional information on the compatibility of this PCM with the construction materials requires further investigations. It is concluded that the enhanced form-stable PCM is a promising material for thermal energy storage and thermal comfort.

5. DEVELOPMENT OF HIGH-TEMPERATURE PCMs FOR ENHANCING PASSIVE SAFETY AND HEAT REMOVAL CAPABILITIES IN NUCLEAR REACTOR SYSTEM

Researchers have identified several PCMs for nuclear reactor applications, such as lithium chloride, to enhance the load-following ability of advanced Generation IV nuclear power stations and improve their economic outlook [155]. A secondary outcome of this effort was improved inherent safety.

The objective of this study is to identify high-temperature PCMs as a potential passive safety mechanism to improve the safety and reliability of the reactor containment structure in the event of a loss of coolant accident (LOCA). During nuclear reactor accidents, such as LOCA, the steam vented from the RPV to the containment causes an increase in temperature and pressure in the containment structure. Ice condenser systems have been designed to condense steam in the containment and thus reducing pressure. Ice is stored in 1944 baskets (24 bays each consists of 81 basket) to condense and absorb energy from steam [156] as shown in Figure 5.1. These baskets hold 1.1 million kilograms of ice. Currently, there are 10 units of ice condensers located at 5 sites in the U.S. [157]. The current design of ice condensers has many advantages: 1. Ice is very effective because of the ability to absorb large amount of energy which aids the condensation of steam. 2. Reducing the size of containment because the pressure it needs to withstand is reduced. While ice condensers provide an effective safety mechanism, they require constant maintenance due ice sublimation, and require constant cooling between -18°C to -7°C. The primary concern is when ice leaves the baskets in the middle and moves to the edges of the condenser. If left unchecked, this sublimation could cause the system to fail in case of an

accident. Baskets that are too light are usually emptied and re-filled. This process needs continuous maintenance to insure balanced melting during accidents. These maintenance issues have led to long-term shutdowns. For instance, in 1992 the Sequoyah Nuclear Plant Unit #2 was promptly shut down due ice blockage in 27 of the 48 ice condenser doors [157, 158]. A similar problem was found in the nearby reactor unit #1. Ice condenser are also considered a high-risk foreign material zone [156]; Which means if anything is accidently dropped into the system it may be impossible to recover it. This can lead to major problem when the system needs to function. The foreign material in the system can be released when a flash of steam is run through it and therefore clog the outlet that allows water to exit. At this point condensation is less effective and can build up a steam pressure in the containment. In 1997, Donald C. Cook Nuclear Plant was shut down for 3 years and 3 months due to concerns about foreign materials in its ice condenser system [156].

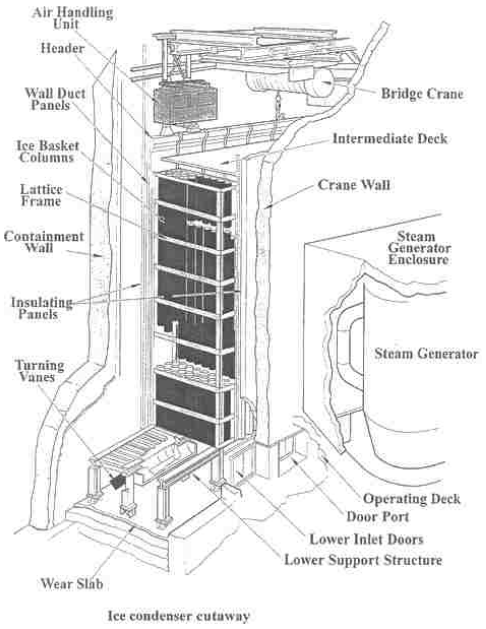

Figure 5.1. Sketch for ice condenser [156]

The use of PCMs of high phase transition temperatures represent a unique passive safety mechanism to avoid these issues by eliminating the need for constant cooling, reducing the need for constant maintenance and eliminating problems due to sublimation. In addition, such passive systems that does not require regular maintenance can reduce the risk due to entry of foreign materials.

The objective of this can be accomplished by developing PCMs with suitable phase transition behavior. The PCM should have a freezing temperature that is high enough (higher than normal operating temperature) and melting temperature that is as high as reasonably possible to condense steam by absorbing thermal energy during accidents (below 100ºC). PCMs with phase transition temperature in the range of 70 ºC to 90 ºC and latent heat of around 200 kJ/kg or higher, can help absorb energy to condense additional steam at lower temperatures and will remain solid (uncharged) when the reactor is in normal operation prior to any accident. The final PCM can then be incorporated into the system in a variety of ways from the addition of aluminum sheets/film of PCM pockets – a typical commercial PCM product – or by mixing the PCM with the structural concrete used in reactor systems.

5.1. PRELIMINARY SCREENING OF SUITABLE PCMs

Thermal energy storage applications using PCMs in the temperature range 0 ºC and 60 ºC are very popular, i.e. from low temperature thermal shipping systems for temperature sensitive products to the medium temperatures such as solar heating systems and industrial waste heat recovery. In contradiction, industrial applications of PCMs at elevated temperatures (70 ºC to 100 ºC) are nearly unknown. Therefore, previous research and

commercially available PCMs in that range are very limited. The first step of this project was a preliminary screening on PCMs at elevated temperature range. As a result of this step, an optimum PCM candidate was selected for the intended application and further research was extended to deep analysis on this PCM.

The research was restricted to organic based PCMs during the preliminary screening of potential PCM candidates. This is due to their defined and reproducible melting and freezing temperatures, larger energy storage capacity, small volume changes, chemical stability, availability, and economic viability. Preliminary screening of PCMs with suitable phase change behavior for the project have shown a trend given in Figure 5.1.

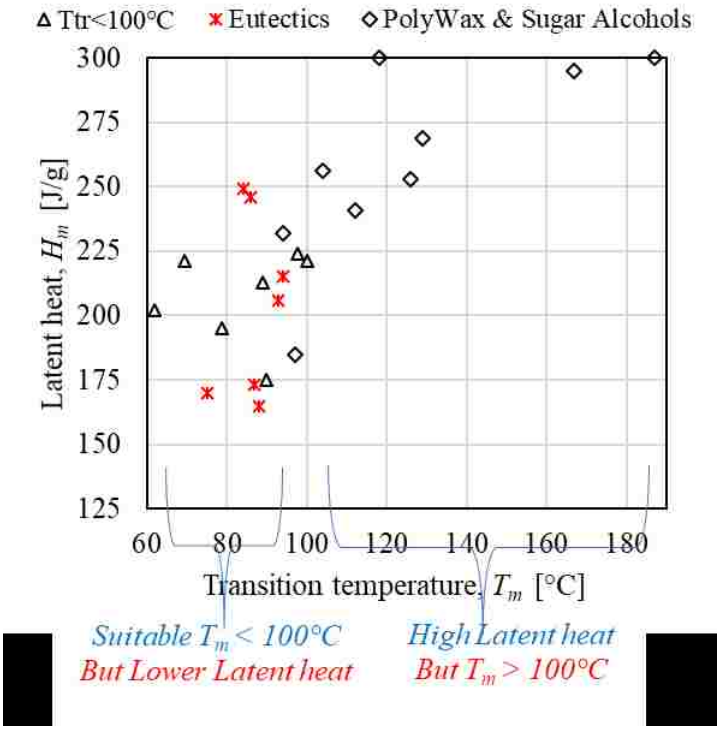

Figure 5.2. Preliminary screening of PCMs with suitable phase change temperature.

The phase transition properties of these PCMs are given in Table 5.1. The PCMs of high latent heat have phase transition temperatures higher than the suitable temperature range for the intended application of this study. PCMs of high latent heats and suitable phase change transition temperatures in the range of 70 ºC to 100 ºC are very limited compared to the available PCMs higher temperature ranges.

Table 5.1. List of high-temperature PCMs during the preliminary screening.

Group	PCM	T_m [ºC]	H_m [J/g]	Origin of data
$T_{tr} \leq 100$℃	Myristic Acid	54	199	Experimental
	Palmitic Acid	62	202	Experimental
	Octadecanoic acid	70	221	Experimental
	PolyWax 400	79	195	Experimental
	PolyWax 500	89	213	Experimental
	HCO	90	175	Experimental
	PolyWax 756	98	224	Experimental
	PolyWax 655	100	221	Experimental
Eutectics	Xylitol/Sorbitol	75	170	Theoretical and [159]
	Erythritol/Xylitol	84	249	Diarce et al. [159]
	Erythritol/TME	86	246	Hidaka et al. [160]
	Erythritol/Sorbitol	87	173	Diarce et al. [159]
	Wax400 + Wax500	88	165	Experimental
	Sorbitol/Manitol	93	206	Theoretical
	Wax655 + Wax756	94	215	Experimental
Polywaxes & Sugar alcohols	Xylitol	94	232	Experimental
	Sorbitol	97	185	Kakuichi Et Al. 1998 [161]
	Adonitol	104	256	Tong Et Al. 2010 [162]
	PolyWax 1000	112	241	Experimental
	Erythritol	118	319	Lopes Et Al 2005 [163]
	PolyWax 2000	126	253	Experimental
	PolyWax 3000	129	269	Experimental
	Mannitol	167	295	Kakuichi Et Al., 1998 [161]
	Dulcitol	187	300	Barone, 1998 [164]

The preliminary results showed promising candidates for the intended application. Figure 5.3 shows an example for several the ploywax PCMs with relatively high phase transition temperatures and high latent heat values in the range of 195-269 J/g. Polywax PCMs are fully saturated homopolymers of ethylene of various molecular weight distributions. Polywaxes are widely available materials commercially known as polyethylene with phase transition temperatures in the range of 105 ºC (low density, LDPE) to 138 ºC (ultra-high density, UHMWPE). Information regarding the exact chemical composition and detailed methods to produce the lower temperature polyethylene based PCMs with phase transition temperature lower than 105 ºC are still unknown or not well documented in literature. Manufacturers such Baker Hughes Inc. [165] offers some of these lower temperature PCMs under commercial names such as PolyWax 756, 655, 500, and 400.

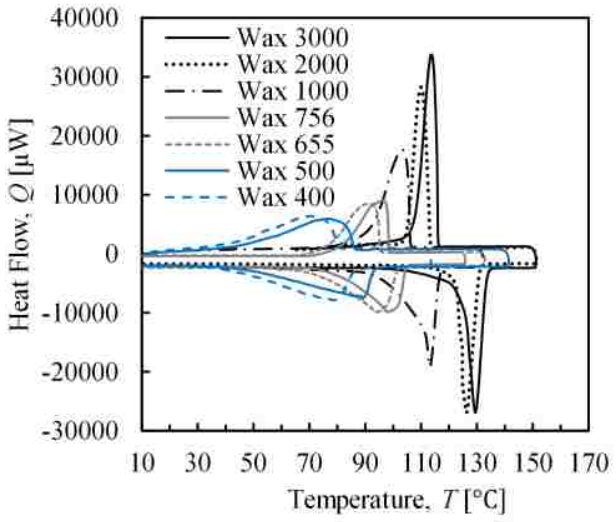

Figure 5.3. Experimental DSC spectrums for the polywax PCMs.

As seen in the figure, the higher temperature polywax PCMs are showing better phase transition behavior as they exhibit a sharper melting peak, however, their phase transition temperatures are higher than the suitable temperature for the intended application. On the contrary, lower temperature PCMs (<100ºC) showed suitable phase transition temperature for the intended application but their phase transition temperatures are relatively spread over wider temperature range. Therefore, eutectic mixture using the higher temperature polywaxes can be considered to develop PCM with lower melting temperature than 100°C, sharp melting peak, and high latent heat similar to that of higher temperature PCMs.

Unfortunately, at this point the chemical information and exact composition of the lower temperature poly-wax PCMs are unknown as they are trade secret materials developed by Baker Hughes Inc. [165]. The lack of information regarding the exact chemical compositions of these PCMs has limited the ability to predict eutectic mixture compositions as well as other challenges such as availability and economic viability. For instance, commercial polywax 756 is no longer available now from the manufacturer. The lower temperature polywax PCMs have shown a relatively undesirable wide phase change spectrum as the latent heat is spread over a wider temperature range compared to that of PCMs with higher transition temperatures. In addition, efforts on developing several eutectic mixtures of two polywax PCMs represented significant challenges and did not seem very promising. Figures 5.4 shows an example of some experimental efforts on two eutectic mixtures, Figure 5.4-a for polywax 756 and polywax 600 and Figure 5.4-b for polywax 400 and polywax 500.

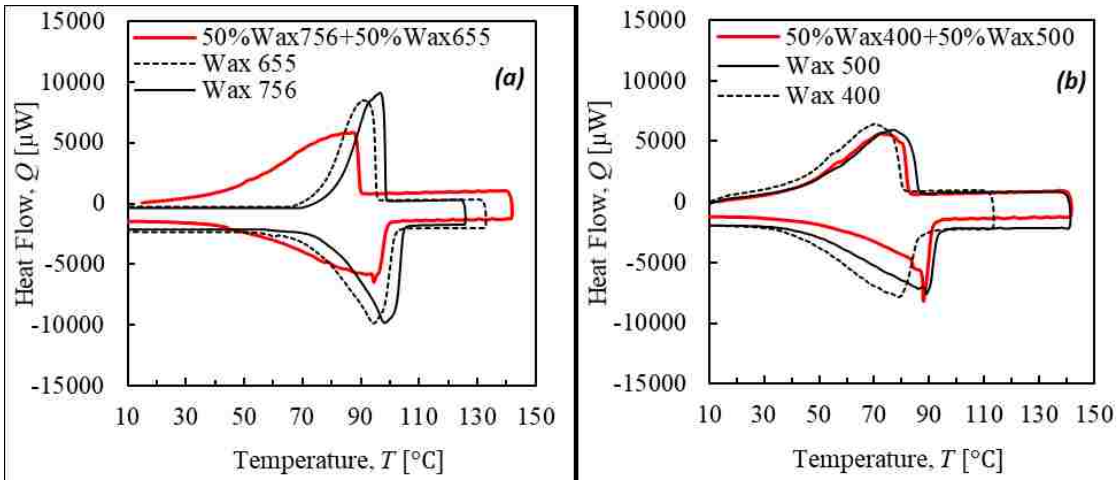

Figure 5.4. Eutectic mixtures of polywax 756 and 655 (a) and ploywax 500 and 400 (b).

Eutectic mixtures in general tend to form a new PCM at lower temperatures. It is suggested that polywaxes do not follow a phase diagram similar to that of organic PCMs as the polywax eutectic mixtures showed a melting peak that is in between the two individual components as well as reduced latent heat as given in Table 5.1. In future, it will be interesting to study how the temperature of polywaxes can be further depressed without affecting the narrow temperature range of phase transition and its original high latent heat. Kissin in his book [166] showed the experimental melting curve of ethylene/hexane copolymer containing 7% molar ratio of hexane with a reduced phase transition peak temperature of around 82 ºC (Section 3.3.3, Figure 3.7 in [166]). The melting curve however was too wide with an onset temperature of about 40 ºC, similar to the wide DSC melting spectrum of polywax 400 and polywax 500 as shown in the experimental data in Figure 5.3. This behavior is not desirable as part of the phase change latent heat takes place at very low temperatures. For all these reasons, the single or eutectic mixtures of Polywax PCMs have not been considered for further or deep analysis at this point for this project.

The high latent heat of sugar alcohol PCMs is promising. Sugar alcohols are sometimes referred to as polyols. In fact, there are over 900 polyols listed in the dictionary edited by Peter Collins [167]. However, only few sugar alcohols have known phase change properties. This has limited their availability and ability to choose suitable candidates during the preliminary screening. Despite the high transition temperature of sugar alcohols as given in Table 5.2, eutectic mixtures of sugar alcohols can provide a great solution. Unfortunately, the use of many sugar alcohols and their eutectics such as sorbitol, mannitol and xylitol is limited due their polymorphic transition, also called vitrification or decomposition, upon melting. This behavior can be seen in the experimental DSC results of xylitol in Figure 5.5.

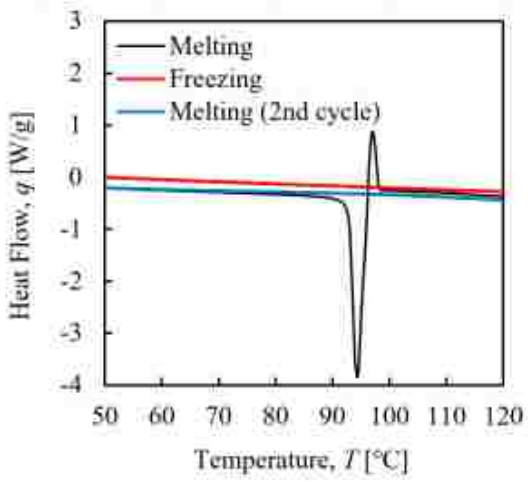

Figure 5.5. Experimental phase transition spectrum for xylitol

The polymorphic transition is observed by the DSC spectrum at 97.1 ºC during the first melting cycle. This is indicated by an exothermic decomposition signal observed at

the end of the endothermic melting peak. As a result, xylitol vitrified and formed a glass-like material due to the polymorphic transition. The modulated-DSC (Discovery MDSC, TA Instruments) provides a great benefit in these cases by detecting such non-transition thermal events. No solid to liquid phase transition was observed during the cooling cycle and no melting phase transition observed during the second DSC heating scan. Similar behavior was experimentally observed for Sorbitol and Adonitol. Similar behavior for mannitol was reported in the literature [168]. Gobas et al. [168] tried to eliminate the polymorphic transition of sorbitol mixtures and mannitol by mixing, pressing and crushing the two components in a controlled pressure environment. However, the vitrification of sorbitol component had not been avoided and crystallization had not been achieved.

Besides, it is worth noting that Barrio et al [159] have examined several eutectic mixtures of sugar alcohols, but a time consuming technique was used to avoid polymorphism and vitrification upon melting. First. the single sugar alcohol components were ground by mortar and pestle, and the resulting powder of the two PCMs was prepared for further analysis. The preparation of each mixture has been limited to preparing small samples of 6-30 μl of each mixture deposited on a thin aluminum plate. The authors however did not discuss how the process can prevent vitrification of some sugar alcohols in the mixture. In addition, DSC tests were carried out by heating fresh powders for one cycle only, and solidification cycle was not studied. Diarce et al. [159] also studied eutectic mixtures of sugar alcohols using a very similar preparation technique, and fresh samples were used for measurements. However, DSC solidification peaks have not been examined for any of the prepared mixtures. It was noted that the nucleation of xylitol for instance can be initiated by seeding the PCM with gamma crystals of the same PCMs, however, the

crystallization was only measured starting from a temperature of 80 ºC and lower. Therefore, it is believed that the PCM did not complete its initial melting phase transition as the end-set point of transition was not reached. Due to the challenges associated with preparing eutectic mixtures of sugar alcohols and their polymorphic transition detailed analysis on these PCMs has been disregarded.

Hidaka et al. [160] investigated a mixture containing erythritol and trimethylethane (TME) with suitable melting temperature range (86°C) and relatively high latent heat (246 J/g). However, the mixture showed non-congruent melting.

Further analysis on myristic acid and palmitic has also been disregarded because of their lower phase transition temperature for the intended application. In addition, their phase transition temperature can only be further depressed in case of eutectic mixtures with sugar alcohols or other PCMs. Similarly, hydrogenated castor oil (HCO) was not considered because of its low latent heat (175 J/g), wide phase transition temperature range, and large supercooling (30 ºC) as shown in Figure 5.6.

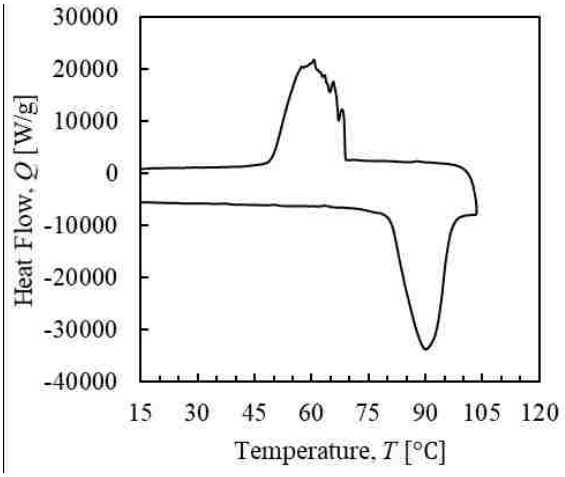

Figure 5.6. DSC spectrum of hydrogenated castor oil (HCO).

The suitable phase transition temperature and high latent heat of octadecanoic acid are not the only crucial factors to make this PCM a suitable candidate for the intended application. The non-toxicity to human when handling, biodegradability, availability, and economic viability of this PCM are undoubtedly of primary importance [169]. The next section provides a comprehensive study on this selected PCM.

5.2. OCTADECANOIC ACID AS A PROMISING PHASE CHANGE MATERIAL FOR ICE CONDENSORS

Requirements for a suitable PCM candidate include: appropriate phase transition temperature; high latent heat of fusion; good chemical and thermal stability; little supercooling; low cost. The preliminary screening revealed several potential candidates. Of those, octadecanoic acid ($CH_3(CH_2)_{16}COOH$, also known as stearic acid) is a saturated fatty acid obtained from fats and vegetable oil with concentrations of about 35% and 5%, respectively. In some cases, octadecanoic acid concertation can be as high as 45% such as in cocoa butter and shea butter [35].

The phase transition temperature of octadecanoic acid (~70 ^{o}C) is relatively high for the typical applications such as solar heat storage, water heating systems, or room temperature applications. Therefore, most previous research concerning octadecanoic acid was focused on analyzing eutectic mixtures of this PCM with other PCMs. For instance, several composites and eutectics utilizing this PCM have been proposed such as mixtures of octadecanoic acid with: palmitic acid and expanded graphite [170], myristic/lauric acid and expanded graphite [171], acetamide [172], and palmitic acid [170].

Despite the vast number of studied composites and applications utilizing octadecanoic acid, to date, only limited experimental work has been published describing in detail the temperature-dependent phase change behavior of octadecanoic acid. It has been found that there are significant deficiencies in the current experimental database for octadecanoic acid. To the best of our knowledge, yet there is no theoretical or experimental database/model to describe all the temperature-dependent thermophysical properties – specific heat in particular - of octadecanoic acid. In addition, no data is available for the specific heat in the overlap and phase transition regions due to measurement challenges. In summary, there are significant gaps in the knowledge of physical properties which is critical for pre-evaluation of octadecanoic acid as a candidate for enhanced passive safety features of nuclear reactors with ice condensers. Moreover, phase transition behavior and direct specific heat are yet to be measured using the new advanced modulated DSCs.

One more deficiency in current existing data is the inconsistent and huge discrepancy in phase transition data. For example, despite that most previous reports were limited only to the enthalpy, transition temperature and in some cases thermal conductivity, the melting temperature was inconsistent: 52.95 ºC [173], 53.12 ºC [174], 59.4 ºC [175], 65.1 ºC [176], 68.8 ºC [177], 71.45 ºC [178]. The latent heat also varied from 191.4 J/g to 240.6 J/g [174-180]. Reliable temperature-dependent thermal conductivity and specific heat in the phase transition region are not available. The thermal conductivity differed by a factor of 1.88 and mainly available for only the liquid state either at one single temperature or without stating the temperature [16, 45, 175, 177]. The uncertainty here is unusual. However, after a deep research on the available feedstocks and details of the PCM source used in several papers, It has concluded that unlike other PCMs the feedstock purity

of this PCM can significantly change the apparent or measured phase change behavior of octadecanoic acid. In other words, it is suggested that the discrepancy was due to PCM misrepresentation rather than measurement error. Octadecanoic acid is commercially offered under the name of stearic acid as emulsifier, chemical intermediaries, release agent, lubricant, rubber compound, or textile finishes [181, 182]. For that reason, the main purpose or use is not always a phase change heat storage medium. CHEMPOINT [181] for instance offers various grades of octadecanoic acid; As per the technical data sheets of each grade the reported melting points vary from 54 ºC to 67 ºC. The inconsistent commercial grades from various feedstocks has resulted in huge discrepancies in the published values causing a confusing and unreliable reported data for octadecanoic acid.

Sari et al. [183] for instance studied commercial grade octadecanoic acid (stearic acid) PCM. In his study he reported that the PCM contains traces of palmitic acid. In 2013 Board et al. [184] revealed that octadecanoic acid (stearic acid) from some commercial sources contains high concentrations of palmitic acid. It was also reported that in some cases based on the purification and stilling method, particularly for octadecanoic acid, the resulting PCM is by no means pure PCM or even pure compound. This indicates that in many cases the studied octadecanoic acid PCM was in fact a eutectic PCM mixture of octadecanoic acid and palmitic acid (or others) of different characteristic than octadecanoic acid only, thus causing material misrepresentation. This explains the discrepancies in literature. Another document that supports the hypothesis that some commercial grades of octadecanoic acid studied in previous literature are different than pure octadecanoic acid is the information disclosed in the patent US1659790 entitled (Methods of Producing Commercial Stearic Acid) [185]. The patent presented an invention on producing a

commercial octadecanoic acid by utilizing some impurities in the mixture that are mainly fat-based impurities. At the end of the process described in the invention the resulting octadecanoic acid is separated and distilled from the mixture and impurities. The hypothesis here is that palmitic acid or other fatty acids can be one of these impurities which has not been clearly identified in the process. If this hypothesis is true, this can also explain the discrepancies in melting point and other properties concerning research on octadecanoic acid in literature. This may be due to the fact that the resulting compound is a eutectic PCM mixture of octadecanoic acid and palmitic acid (or other fatty acids) involved in the process after an imperfect distilling and separation for lower commercial grade octadecanoic acid.

For these reasons mentioned above, only pure reliable octadecanoic acid should be considered when studying this PCM as a heat storage medium. Here, pure octadecanoic acid of >98% purity from a reliable source (Sigma Aldrich) processed using a very recent development processing method known as capillary gas chromatography (Capillary GC) implement by Sigma Aldrich which provides an ideal separation and purification.

In the near future thermal storage systems utilizing octadecanoic acid will need to be validated either experimentally using prototypes or using advanced simulation and modelling capabilities. The objective here is not only to provide an accurate and reliable database for phase transition behavior, but also to close the gaps in the existing experimental database and to measure the currently unknown temperature-dependent properties which will be required for ensuring reliable design and safe conditions during operation or accidents. Octadecanoic acid is known since 1889 [62], however much of the experimental data was not taken with sufficient resolution and accuracy within the standard

limits for the nuclear industry, and in some cases measured at only single temperature. No data currently exists for specific heat in the region of phase transition or overlap region between sensible and latent heat. Finally, data for thermo-physical properties at various temperatures (temperature-dependent) are very limited and in some cases not available for some properties.

The determination of temperature dependent thermo-physical properties is essential for the design of a passive safety mechanism that allows for an effective condensation of steam within the desired time under certain flow conditions for a given geometry. Due to the large discrepancy in current existing data and lack of some temperature-dependent properties, a new experimental database is required. This is particularly for specific heat within and beyond the phase change transition region which is a critical factor in determining the expected thermal response of the PCM during an accident. To refine these gaps in the experimental database, several measurements are performed to accurately determine all the temperature-dependent thermo-physical properties from 0 ºC to 110 ºC, and to measure the specific heat capacity in the phase transition range and overlap region between sensible and latent heat for the first time. An advanced modulated DSC implementing a modified heat transfer model will be used for phase transition analysis and direct specific heat measurement within and beyond the phase transition region with an accuracy of better than 2%. This will make significant contributions to rectifying the gaps in the existing experimental database and provide a valuable database to predict the transient response of energy storage systems utilizing octadecanoic acid in nuclear reactor.

5.2.1. Background on Modulated DSCs and Direct Specific Heat Capacity Measurements in the Overlap and Phase Transition Region. Recently in 2017, TA Instruments has presented a new generation of advanced modulated DSCs that measure direct specific heat capacity as disclosed in their patents US20080052032A1 granted in 2008 [186] and EP1139083B1granted in 2016 [187]. Using this technology, it becomes possible for the first time to measure the specific heat capacity in the overlap and phase transition regions. Historically, specific heat capacity for liquid or solid phase is usually measured using a three-run artifact method as described in the methods section of Sections 3 and 4. This kind of measurements were possible for the sensible (non-transition) region, however it was not possible to perform the same analysis for the overlap and phase transition region because of the baseline non-linearity and independency of the DSC signal on the original baseline during kinetic events or thermal phase transitions. In other words, it is not possible to predict the actual baseline during thermal events when the signal becomes larger. This is due to the large curvature, slope and offset of the baseline during such thermal event [188]. In conventional heat flux DSCs, the heat flow signal is based on over simplified one term heat flux model that is equal to the first term only of equation 13. Meaning that the conventional heat flux DSCs measure the differential heat flux through the experimental sample using the thermal equivalent ohm's law where the heat flow (q) equals the temperature difference between the sample and reference over the resistance of the thermoelectric heating disk. Upon calibration, the DSC signal (q) is converted to heat flow rate using a single proportionally factor.

As shown in Danley [189] and disclosed in U.S Pat. No. 6431747 to Danley [83], a more sophisticated model is required to account for many of the assumptions that are

used in such simple models. The simple one-term equation is adequate upon calibration to measure the area under the curve of thermal events and glass transition or peak temperatures within certain resolution. The model however does not account for quantitative and accurate heat flux absolute values which can be used for further analysis of specific heat capacity within adequate resolution and precision, particularly during thermal events such as phase transitions. In our previous work [2], we addressed and described several thermal events that can result in significant uncertainty sources, but at that time the imbalance of these conditions had not been incorporated into an available commercial DSC instrument. For instance, in Figure 5.7 we evaluated the dependency of maximum heat flow signal on the imbalance due to different sample masses and heating rates. Therefore, using a conventional DSC it was only possible to recommend certain measurement conditions to accurate measure enthalpy (area under the curve) and temperature (peak temperatures) of PCMs.

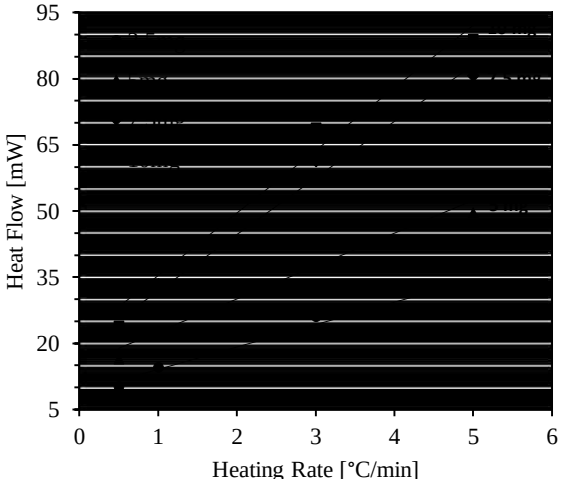

Figure 5.7. Dependency of the DSC maximum heat flow signal on the measurement conditions [2].

As claimed by TA Instrument, their patented “Tzero” DSC cell (Patent No. U.S. 20080052032A1 [186]) is currently the only commercially available DSC measuring tool -Discovery DSC; commercially available since 2017- that can account for the thermal contact resistance due to imperfections contact between interface of the sample container (pan) and calorimeter, account for thermal capacitance due to the heat capacity of the sample pan and refence pan, eliminate the dependency on fluctuating baseline, measure the imbalance due to sample mass and heating rate, and separate several types of kinetic and transition thermal events by utilizing a four-term heat flow equation given below:

$$q = -\frac{\Delta T}{R_r} + \Delta T_o\left(\frac{1}{R_s} - \frac{1}{R_r}\right) + (C_r - C_s)\frac{dT_s}{dt} - C_r\frac{d\Delta T}{dt} \qquad (13)$$

Where q is the heat flow rate, the first term alone is equivalent to the model used in conventional DSCs for heat flux which is over simplified compared to the actual thermal events in the DSC, (ΔT) is temperature difference ($\Delta T = T_s - T_r$) between the sample (T_s) and reference (T_r), (ΔT_o) is the second temperature difference ($\Delta T_o = T_o - T_s$) between the sample (T_s) and the furnace (T_o), (R) is the calorimeter resistance, (C) is the calorimetric heat capacity, and the subscripts “r” and “s” refer to the reference and sample.

To account for the imbalance due to heating rate and sample mass difference between the sample and reference pan, the equation becomes:

$$q = \frac{\Delta T_o}{R_s} - C_s\frac{dT_s}{dt} - \left[\frac{\Delta T_o + \Delta T}{R_r} - C_r\left(\frac{dT_s}{dt} - \frac{d\Delta T}{dt}\right)\right] * \frac{m_{ps}}{m_{pr}}\frac{dT_{ps}/dt}{dT_{pr}/dt} \qquad (14)$$

Where (m_p) is the mass of DSC pan, (T_p) is the measured temperature difference between the reference pan or sample pan ($T_{pr}\ or\ T_{ps}$) which can be calculated using the thermal contact resistance (R_p) between each calorimeter and its pan using the following equations:

$$T_{ps} = T_s - \left[\frac{T_o - T_s}{R_s} - C_s \frac{dT_s}{dt}\right] * R_{ps} \tag{15}$$

$$T_{pr} = T_r - \left[\frac{T_o - T_r}{R_r} - C_r \frac{dT_r}{dt}\right] * R_{pr} \tag{16}$$

Contrary to common DSC measurements, the precision of this heat flux model applied in this kind of new M-DSCs provides a useful tool to explore the temperature-dependent specific heat accurately, and more importantly to measure the direct specific heat capacity in the phase transition region and overlap region between sensible and latent heat for the first time. To use this model, one cannot simply apply it to a conventional DSC heat flow signal as the DSC must include two thermal independent calorimeters for the sample and reference position in the same furnace. The thermal parameters are determined following a calibration procedure. The instrument is normally calibrated using two steps calibration, first is an empty DSC cell experiment where the machine automatically calibrates for a consistence repeatable baseline, and sample/reference cell time constant as a function of temperature. The second calibration experiment uses a calibration sample of well-known specific heat capacity. Sapphire is recommended and provided by the manufacturer. The theoretical temperature-dependent specific heat capacities of the calibration sapphire sample can be substituted in equation 17 and 14 to obtain the thermal

constants $C_S, C_r, R_{ps}, R_{pr}, R_r$ and R_s. The theoretical work required for calibration is automatically performed by the instrument during a calibration-mode experiment.

$$q = m_s . C_{P\_sapphire} . \frac{dT_s}{dt} \tag{17}$$

Figure 5.8 shows the experimental measured specific heat capacity of sapphire sample and compares it to the theoretical values. The instrument uncertainty for specific heat measurements is 2% as per the manufacturer, which is consistent with the experimental maximum absolute error of 1.71%, and the mean absolute percentage error (MAPE) of 1.2%. The experimental repeatability was found to be better than 1%.

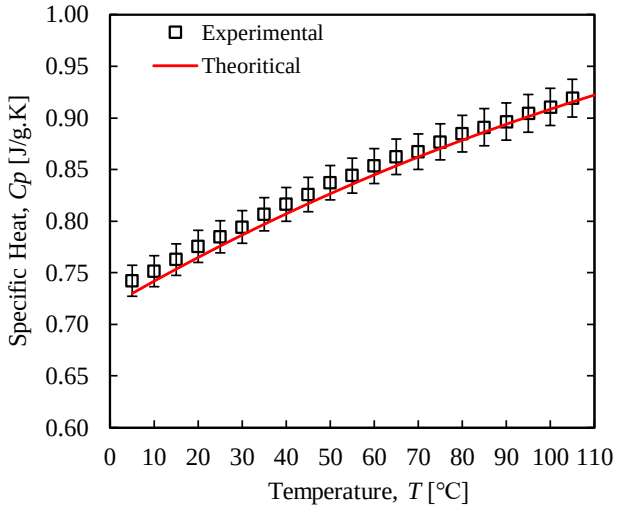

Figure 5.8. The measured experimental and theoretical specific heat capacity of Sapphire.

5.2.2. Temperature Dependent Phase Transition and Specific Heat Capacity.

Octadecanoic acid (98.5% pure, Signa Aldrich) has been used in these experiments. To insure optimum measurement accuracy, the PCM was melted first and then added to the DSC pan in liquid state to establish good thermal contact between the PCM and DSC pan. The DSC measurements were repeated three times using different samples to ensure that repeatability is within ±0.3 ºC for phase transition temperatures and 2% for enthalpy of fusion. For the temperature-dependent specific heat, the Discovery Modulated-DSC (TA Instrument) was used in direct specific heat measurement mode.

Figure 5.9 shows the experimental DSC results for the phase transition of octadecanoic acid. The average solid to liquid phase transition temperature is 69.4 ºC, which is suitable temperature range as a potential PCM candidate to enhance passive safety features of nuclear reactors compared to ice condensers. The liquid to solid phase transition temperature is 65.5 ºC which results in less than 3.9 ºC of supercooling. The latent heat of fusion is 221.2 J/g and 220.4 J/g for melting and solidification, respectively.

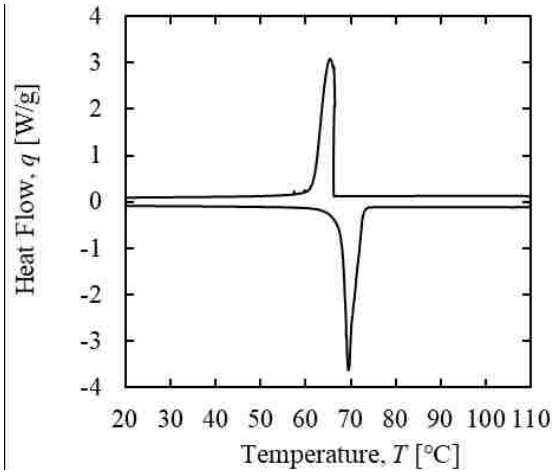

Figure 5.9. DSC results for phase transition of octadecanoic acid.

Figure 5.10 shows the specific heat capacity of octadecanoic acid measured in a crimped “Tzero” DSC pans. A temperature hold time for 10 minutes (equilibrium step) at -10 ºC was applied prior to starting the experiment. The octadecanoic acid was melted once in the DSC pan prior to starting measurements to insure full contact between the sample and bottom of the pan. The measurements were repeated three times using different samples to insure repeatability of the results by measuring the relative standard deviation (RSD) of sensible heat capacity $C_p(T)$ which was found to have a maximum RSD value of 2.6% and average RSD of 1.0%. The experiment with values closest to the mean is reported here. For clarity, the blue shaded area is plotted to separate the different regions for the solid phase, overlap and phase transition region, and liquid phase.

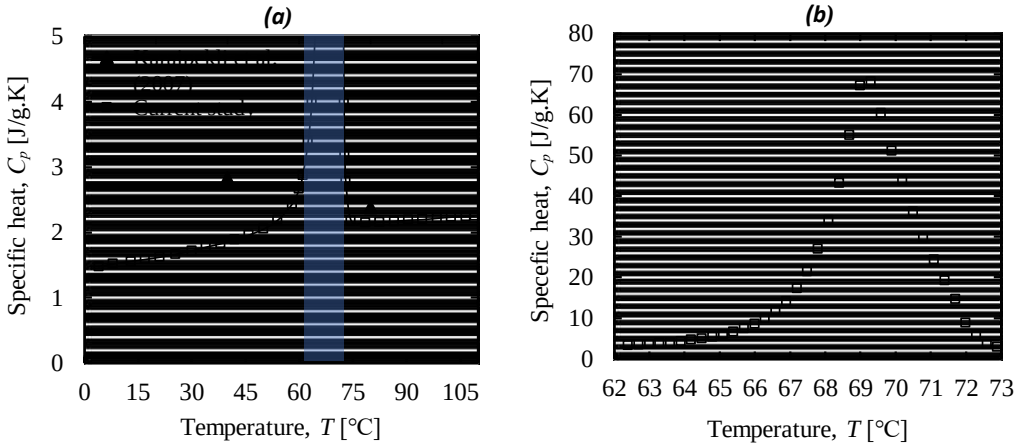

Figure 5.10. Temperature-dependent specific heat capacity for the solid phase and liquid phase regions (figure a, white region) and the overlap phase transition region (figure b).

As seen in Figures 5.10-a and 5.10-b, the specific heat capacity in the solid phase just before the melting in the blue shaded area starts to increase due to the latent heat

associated with the solid to liquid phase transition. This results in a sudden increase in specific heat capacity at nearly constant temperature. Similarly, specific heat capacity starts to decrease rapidly after the solid to liquid phase transition temperature due to the relaxation of latent heat. There is a trend of increase in specific heat as a function of temperature in both phases.

The temperature dependent specific heat $C_p(T)$ for solid phase and liquid phases in the temperature ranges 0 ºC < T < 62.5 ºC and 73.2 ºC < T < 110 ºC is given using the best fit model in equations 18 and 19, respectively. Several prediction formulas were compared, and the best fit equation was chosen on the bases of the lowest root mean square error.

$$C_p^{sol}(T) = -\frac{0.072\,T}{T - 65.521} + 0.0076\,T + 1.436 \tag{18}$$

$$C_p^{liq}(T) = -\frac{2.698\,T}{T + 21.981} + \frac{0.0019\,T}{T - 73.005} \tag{19}$$

For the overlap and phase transition region 62.5 ºC ≤ T < 73.2 ºC, because the specific heat capacity "peak" shown in figure 5.10-b is not a perfect symmetrical peak, it is generally best to describe the $C_p(T)$ in the phase transition region using two equations, one for the left side of the phase transition peak when 62.5 ºC ≤ T ≤ T_m given in equation 20, and one for the right side of the phase transition peak when T_m ≤ T ≤ 73.2 ºC given in equation 21.

$$C_p^{tr}(T) = \frac{67.361^3}{((60.48\,T - 4188.09)^2 + 67.361^2)} + 1.6191 \tag{20}$$

$$C_p^{tr}(T) = \frac{42.887}{(1 + \mathrm{e}^{539.9 - 7.45\,\mathrm{T}})^{-0.04053}} - 40.0459 \tag{21}$$

Equations 18 and 19 are valid to measure the sensible (non-transition) specific heat capacity for the solid and liquid phase, respectively. The mean absolute percentage error for $C_p(T)$ using this model for the sensible heat regions is 0.26% for 0 ºC ≤ T < 62.5 ºC, and 0.29% for 73.2 ≤ T < 110 ºC. The maximum relative error between the experimental values and predicted values using the given equations for $C_p(T)$ is 0.62% and 0.57% for equation 18 and 19 respectively. Equations 20 and 21 are valid for $C_p(T)$ in the overlap and phase transition region. The mean absolute percentage error for $C_p(T)$ is 2.15 % for 62.5 ºC < $T \leq T_m$ and 3.25% for $T_m < T \leq$ 73.2 ºC. The maximum relative error between the experimental values and predicted values using the given equation for $C_p(T)$ is 2.15% and 4.94% for equation 20 and 21 respectively. This uncertainty is too small to construct error bars in the figure.

5.2.3. Temperature Dependent Thermal Conductivity. Accurate determination of thermal conductivity is essential for the design of an optimum thermal energy storage system that allows for an effective condensation of steam within the desired time under certain flow conditions.

The thermal conductivity of the solid phase was measured by several researchers, however the magnitude of discrepancy in thermal conductivity of the solid phase is significant and ranges from 0.29 W/mK to 0.41 W/m.K [16, 45, 175, 177]. In addition, the temperature was not stated in many cases. Here, the temperature-dependent thermal conductivity was determined over a wide temperature range as given in Figure 5.11 for the solid and liquid phases.

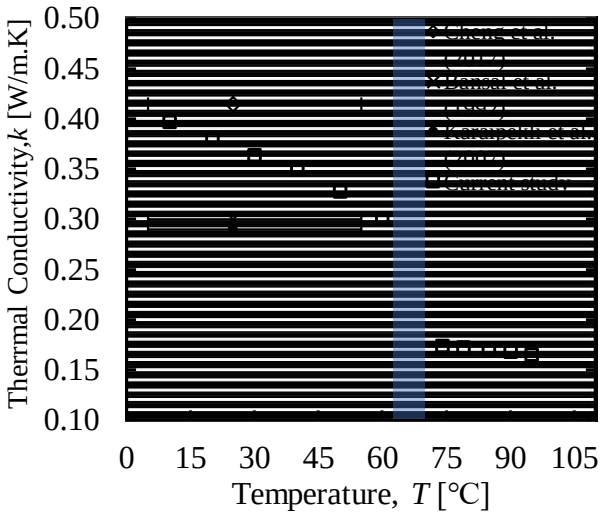

Figure 5.11. Temperature dependent thermal conductivity *k*(T) for solid and liquid phases.

The temperature dependent thermal conductivity for solid and liquid phase of octadecanoic acid in the temperature range 0 < T < 60 ºC and 72 < T < 98 ºC can be expressed using the empirical equations 22 and 23, respectively:

$$k(T) = -0.0019T + 0.4183 \text{ ; for } 0\,℃ < T < 60\,℃ \quad (22)$$

$$k(T) = -0.0004T + 0.2040 \text{ ; for } 74\,℃ < T < 95\,℃ \quad (23)$$

In general, the liquid and solid thermal conductivities are relatively low, however these values are typical for organic PCMs [18, 20, 21]. The coefficient of determination (R^2) for the linear fit equations is better than 98.6% and 98.2% for the solid phase and liquid phase, respectively. The thermal conductivity in general was found to be relatively higher for the solid phase compared to that of liquid phase. This may be due to the nature of heat transfer in solids compared to liquids [25, 190]. The 2% uncertainty for thermal conductivity measurements is too small to construct error bars in the figure.

5.2.4. Temperature Dependent Density. The density of octadecanoic acid was measured using the volume displacement method. The apparatus consists of a 100 ml glass graduated measuring cylinder with 1 ml graduation interval (31 mm in diameter and 240 mm in height). The material of the cylinder is made from polymethyl-pentene which provides a non-wetting interior surface to enhance reading accuracy and allows accurate measurements up to 125 ºC. The graduated measuring cylinder meets the international quality criteria according to ISO 6706 standards and tolerances according to DIN 12681.

For liquid phase density measurements, sufficient PCM of about 90 ml was added to the graduated cylinder and placed in an environmental temperature-controlled chamber. The density of liquid PCM was calculated as $\rho(T) = m \,/\, V(T)$. Measurements were taken at various set temperatures, and an equilibrium time of 30 minutes was allowed between the measurements to allow for thermal equilibrium and relaxation.

For solid phase density measurements, the same volume displacement apparatus was used but with slight changes in the experimental steps to enhance accuracy. First, sufficient water of about 50 ml was added to the 100 ml graduated measuring cylinder and exact volume was recorded (V_i). Second, the PCM was melted and allowed to re-solidify in a flat laboratory aluminum weighing dish/pan that is less than 15 mm in height to ensure no air is trapped in the core of the PCM during solidification. Third, a small cut of PCM was taken with width and depth that is 15 mm or less (smaller than the inner diameter of the cylinder) and shorter than the height of water in the graduated cylinder. Forth, the mass of the PCM cut was recorded using an analytical balance with uncertainty of 0.01 mg. Finally, the PCM cut was immersed in the water in the graduated measuring cylinder and the final volume (V_f) was recorded. Octadecanoic acid is naturally insoluble in water. Also,

octadecanoic acid density is less than water, therefore extra precautions were taken to ensure the PCM is fully immersed in water before recording the volume change ($V_f - V_i$) readings by using a needle to push the PCM down. The volume change due to the presence of the needle in water was accounted for by taking the initial volume while the needle is immersed prior to adding the PCM; However, the volume change due to the presence of needle was found to be negligible. The volume change was used to calculate the density of solid PCM using the equation $\rho_{pcm}(T) = m_{pcm} / [V_f(T) - V_i(T)]$. The measurements uncertainty (1.5%) using this method was too small to construct error bars in a figure.

Figure 5.12 shows the density of octadecanoic acid at various temperatures for the solid and liquid state. The density for solid phase was limited to two data points only at two distinct temperatures due to the negligible volume expansion over small temperature increments, one measurement at relatively low temperature (20 ºC) and another at higher temperature (50 ºC).

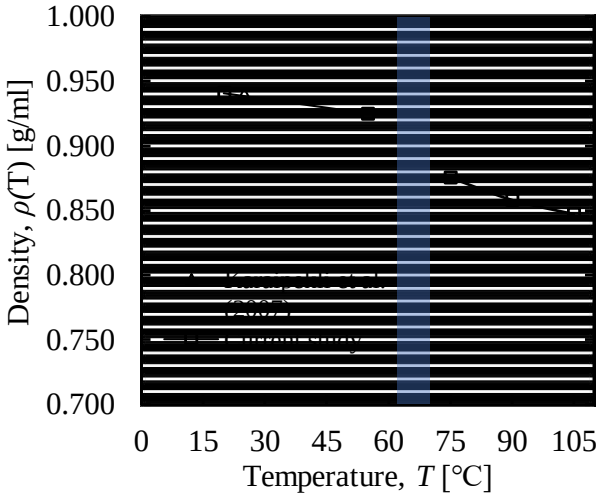

Figure 5.12. Temperature dependent density ρ(T) for solid and liquid phases.

Equations 24 and 25 give the octadecanoic acid temperature-dependent density ρ(T) for the solid and liquid phases in the range 0 ºC < T < 65 ºC and 75 ºC < T < 85 ºC, respectively.

$$\rho(T) = -0.0005T + 0.9501 \text{ ; for } 15\,℃ < T < 60\,℃ \quad (24)$$

$$\rho(T) = -0.0009T + 0.9445 \text{ ; for } 75\,℃ < T < 105\,℃ \quad (25)$$

Unlike water, the density of the liquid phase PCM is lower than that of the solid phase. Therefore, this PCM expands during phase transition from solid to liquid phase and the design must account for the potential volume expansion. This behavior is generally desirable as the expansion takes place when the material is in its liquid form but not solid, thus eliminating any potential stresses during solidification. The PCM volume change $\Delta V = (V_{solid-}V_{liquid})/V_{solid}$ between the solid and solid phase transition from 55 ℃ to 75 ℃, respectively, is 5.3% only which is acceptable when compared to the ice to water volume expansion (-9%). The volume change for liquid phase as the temperature changes is relative larger when compared to that of the solid phase. The temperature dependent density is not only useful for the design of the system to account for PCM expansion or contraction, but also important to measure the temperature-dependent thermal diffusivity.

5.2.5. Temperature Dependent Thermal Diffusivity. For PCMs in general, only few existing studies examined the additional thermo-physical properties such as thermal diffusivity in a detailed manner. Such information is required for simulation, modelling and theoretical models to predetermine the optimum design before integrated PCM into a thermal storage system.

The thermal diffusivity was measured using the procedure outlined in Section 2.4. As the specific heat capacity, thermal conductivity and physical density are measured as a function of temperature, the temperature-dependent thermal diffusivity (α) is calculated using equation (26):

$$\alpha(T) = \frac{k(T)}{\rho(T).\, C_p(T)} \tag{26}$$

Figure 5.13 shows the thermal diffusivity of octadecanoic acid at various temperatures, whereas equation 27 and 28 give an empirical equation for the temperature-dependent thermal diffusivity for the solid phase and liquid phase, respectively.

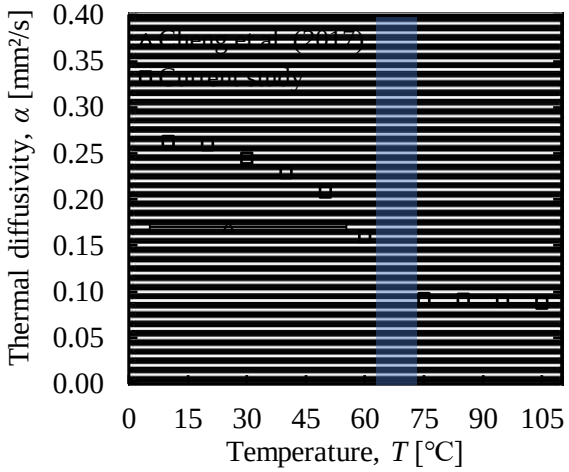

Figure 5.13. Temperature dependent thermal diffusivity α(T) for solid and liquid phases.

$$\alpha(T) = -0.0002\,T + 0.1071\ ;\ \text{for } 15\,℃ < T < 60\,℃ \tag{27}$$

$$\alpha(T) = -8.055 \times 10^{-7}\,T^3 + 4.012 \times 10^{-5}\,T^2 - 1.403 \times 10^{-3}\,T + 0.2751;\ \text{for } 75\,℃ < T < 105\,℃ \tag{28}$$

The thermal diffusivity is nearly constant for the liquid phase PCM. However, it tends to gradually decrease with the increase in temperature. Cheng et al. [178] reported the solid state thermal diffusivity, however the temperature was not stated. Aggressive reduction in thermal diffusivity for solid state was detected near the phase transition region. This may be due to the increased specific heat in the overlap and transition regions where the PCM tends to store heat rather than diffusion. The experimental error associated in the temperature-dependent thermal diffusivity calculations is ±3.2%. This value is slightly higher compared to other measurements mainly due to the contribution of the uncertainty of all other parameters in the determination of thermal diffusivity (2% for thermal conductivity, 2% for specific heat and 1.5% for density), thus $\alpha_{error} = \sqrt{0.02^2 + 0.02^2 + 0.015^2} = 3.2\%$ which is too small to construct error bars in the figure.

5.3. OUTCOMES AND DISCOVERIES

The concept of thermal energy storage using PCMs to reduce temperature and pressure in the reactor containment during accidents has been presented. Several high-temperature PCMs are evaluated as potential candidates. The temperature-dependent thermo-physical properties and phase change behavior of octadecanoic acid were studied in detail. Octadecanoic acid was found to be a promising PCM for nuclear reactor safety applications in the containment structure in the event of LOCA accidents, due to its suitable phase change behavior and high latent heat. The temperature-dependent thermo-physical properties provide a valuable database for future design concepts, experiments and predictions models using modelling and simulation efforts. The study closed the gaps in the existing experimental database and measured the currently unknown temperature-

dependent properties for octadecanoic acid. This information is required for ensuring reliable design and safe conditions during operation or accidents. In near future, design concepts utilizing octadecanoic acid will have to be validated using experimental prototypes or advanced simulation and modelling tools.

6. LOAD SHIFTING OF NUCLEAR POWER PLANTS USING THERMAL ENERGY STORAGE: A REVIEW

6.1. LOAD SHIFTING

Nuclear power plants are load-based source of electricity production, and therefore the plant may be subject to variable electricity demand in an energy grid. A balance must exist between the supply and demand. In order to meet this balance, the power of nuclear reactors will have to be down-regulated regularly during off-peaks demands. In these circumstances the capacity factor can be negatively affected due the variable power demands, causing economic penalties [191]. In other words, the cost of electricity generation becomes higher when operating at partial capacity. For economic and reliable operation of nuclear power plants, it is best to operate at the base-load condition or at constant power level as frequent changes in power level affect the aging of equipment and performance of fuel [192]. In recent decades, considerable efforts have been focused on developing approaches for maintaining the nuclear power plant at nearly constant power level [191, 193-195]. Several possibilities including steam accumulator storage, hydrogen production, and pumped hydro storage have been proposed, but these methods have materials or location limitations [196].

Load-following by coupling the nuclear reactor to a large-scale thermal energy storage system allows the power plant to meet the variation in power demand profiles. During low electricity demand, the heat can be stored in a thermal energy storage system equipped with PCMs of suitable phase transition temperature and thermal storage capacity. The heat can be extracted later during the peak demand hours and converted to electricity using a standard thermal plant. This approach has been studies in the past with salts such

as lithium chloride as a PCM in an effort to enhance the load-following ability of advanced Generation IV nuclear power stations and to improve their economic outlook [155]. A secondary outcome of this effort was improved inherent safety. Lee et al. [194] proposed a similar idea but with the use of underground rock instead of PCM as a storage medium. Among various technical options for thermal energy storage, PCMs are very attractive because of their high latent heat storage capacity and the flexibility of its phase transition temperature.

Alameri et al. [155] stimulated high temperature reactor coupled to a thermal energy storage vessel. Lithium chloride PCM was used as the thermal storage material. In their simulation, the thermal power of the nuclear reactor was kept at constant level as the demand is met using the energy stored in the TES vessel. Figure 6.1 shows a block diagram for the proposed TES system.

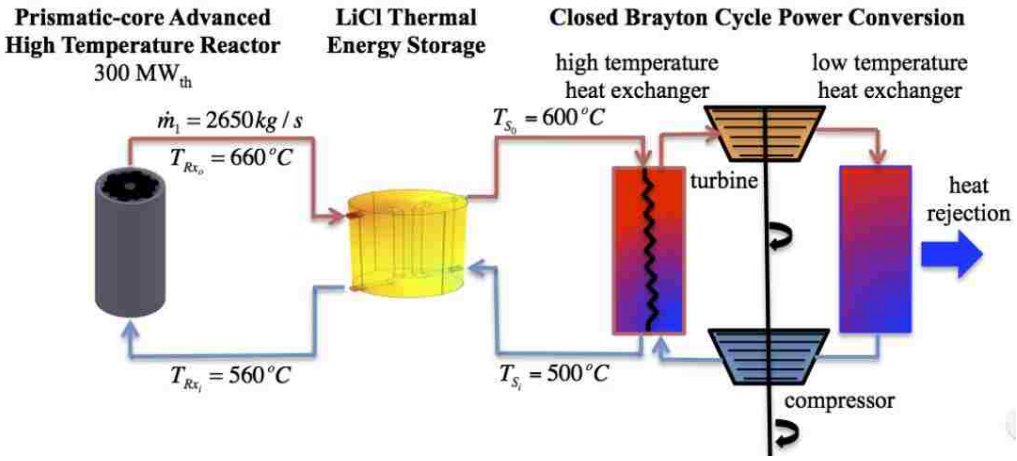

Figure 6.1. System block diagram for a nuclear reactor coupled with TES system taken from [155].

The study also demonstrated the inherent safety of such system during unplanned shutdown. The decay heat can be removed to the TES vessel by natural circulation during loss of forced circulation. The reactor reached a shutdown state in less than half an hour, and the average temperature of the fuel and coolant were kept within safety limits during the transient.

Section 6.2 of this study provides a review on technical aspects of coupled nuclear reactor thermal energy storage units and reviews suitable PCMs based on several reactor types. The next section (Section 7) represents a first step on experimentally studying the design aspects of a real system based on PCMs for load shifting purposes. The effort in this step will be focused on experimentally demonstrating the potential benefits and behavior of PCMs in a thermal energy storage system.

6.2. DESIGN ASPECTS

When coupling a nuclear reactor with a TES unit, the power production is assumed to remain constant while the energy storage unit acts as a buffer by storing excess energy during periods when demand is low and supplying heat when the demand exceeds the supply of the power plant. The expected variations of the electricity demand profile are critical to understand before determining the relative size of the required TES unit. It is important to note that such systems are yet to be implemented or experientially evaluated. A key area of future research would be studying the impact of such thermal storage units on the safety aspects and emergency shutdown scenarios of nuclear reactors. The concept is still in its early development stages and extensive research work will be needed in future

before developing a final design. The area of research in this field can be divided into four main categories: materials, design, safety, and licensing regulations.

Designing such TES system requires the use of high-temperature PCMs. One challenge will be developing PCMs with suitable melting temperatures that corresponds to the exact operating conditions of the system, and latent heats high enough to be useful and effective. Currently, there are several potential high-temperature PCM candidates that could be considered for this concept. However, different types of reactors would require different designs and energy storage characteristics.

Table 6.1 provides the thermal characteristics such as the coolant outlet flow conditions and thermal power for several types of pressurized water reactors (PWRs). Only PWRs are considered here as their design already features an intermediate heat exchanger to transfer the heat from the reactor to a secondary side. The considered reactors are the light water small modular reactors (LW-SMR), Pebble bed-fluoride salt cooled high-temperature reactors (PB-FHR), and Modular high-temperature gas cooled reactors (MHTGR).

Table 6.1. Thermal characteristics for several types of nuclear reactors.

	LW-SMR [197]	PB-FHR [198]	MHTGR [199]
Coolant	Water	FLiBe	Helium
Thermal power	500 MWth	236 MWth	600 MWth
Outlet Temperature	325 ºC	700 ºC	850 ºC

The design storage temperature will depend on the flow conditions, particularly temperature, whereas the size of the thermal energy storage system can be significantly reduced by utilizing a PCM with higher latent heat enthalpy. Edwards et al. [200] presented a conceptual design and theoretical exergy analysis for a coupled thermal energy storage unit with the three nuclear reactors listed in Table 6.1. Figure 6.2 shows a proposed design for LW-SMR coupled with thermal energy storage units.

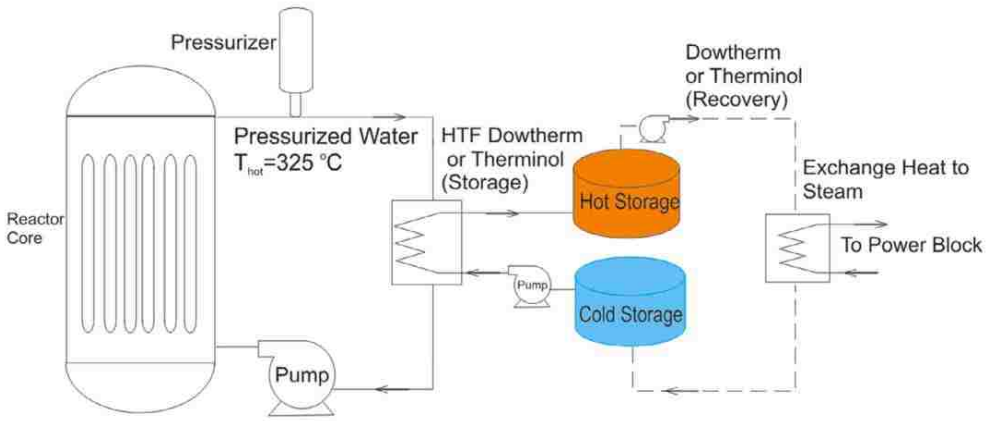

Figure 6.2. LW-SMR coupled with thermal energy storage [200].

The proposed design shown in Figure 6.2 will require an intermediate heat exchanger between the reactor coolant and heat transfer fluid housed inside the reactor containment. This is due to the radioactivity containment of the reactor coolant which is not allowed to leave the containment. Therefore, two synthetic heat transfer fluids, dowtherm or therminol, can be used as a heat transfer fluid and sensible storage medium

in an insulated thermal energy storage vessel located outside the containment. The two fluids are stable at the operating reactor temperature, remain liquid near the reactor coolant temperature at atmospheric pressure, and have a melting temperature lower than room temperature. Dowtherm is a mixture of alkyl benzenes and therminol is a modified terphenyl [201, 202], and they are both commercially available. It is assumed that the storage vessels will have enough sensible heat storage due to the specific heat of the synthetic heat transfer fluid. However, latent heat storage can provide much larger storage capacity by utilizing phase change materials with melting temperature close to the vessel inlet temperature.

A proposed design for a PB-FHR coupled with thermal energy storage is given in Figure 6.3 [200]. The reactor coolant (FLiBe, fluoride molten salt) of the pebble bed core can reach an outlet temperature of 700 ºC. Due to its low vapor pressure at elevated temperatures, the molten salt remains in liquid state at atmospheric pressure. The study compared Therminol and nitrate molten salt as a heat transfer fluid [200]. Therminol was found to be more economical, however nitrate molten salt results in higher energy efficiency due to it higher outlet temperatures. The proposed heat transfer fluid and storage medium is solar salt, also known as nitrate molten salt ($40\%KNO_3+60\%NaNO_3$), which has a melting point of 141.9 ºC [203]. This molten salt has been previously used as a high temperature storage medium in a solar power station in Spain [204, 205]. The design assumed that the sensible heat of the molten salt is sufficient for thermal storage capacity. Again, latent heat storage using PCMs can significantly increase the storage capacity by an order of magnitude compared to sensible heat mediums.

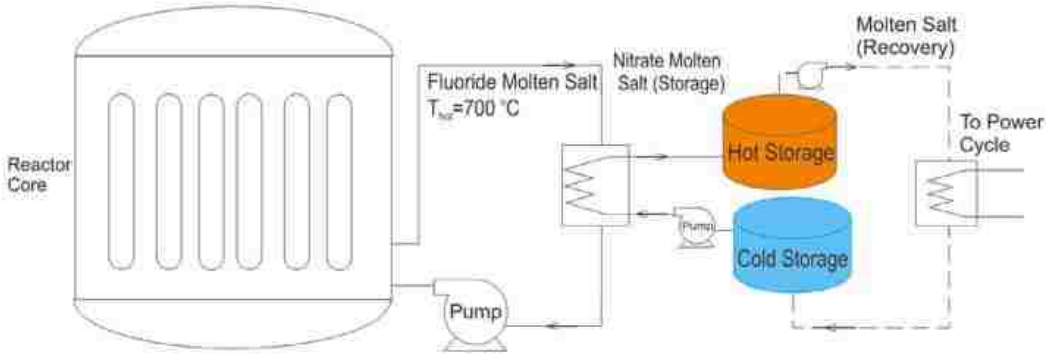

Figure 6.3. PB-FHR coupled with thermal energy storage [200].

Figure 6.4 shows a proposed design for a MHTGR coupled with thermal energy storage [200]. In this design, helium is utilized as a reactor coolant through the graphite moderated core. The helium outlet temperature can reach up to 850 ºC or higher which gives the advantages of higher thermal to electrical efficiency, and no film boiling or two phase flow risk [199]. Similar to LW-SMR, a heat transfer fluid is required to transfer heat from the reactor coolant to a thermal energy storage unit. The effectiveness of the intermediate heat exchanger needs to be carefully investigated in order to reduce the differences between the outlet temperature of the reactor coolant and the inlet of the thermal energy storage unit. High effectiveness will allow the system to utilize a heat storage temperature that is closer to the reactor coolant temperature. A packed bed of alumina was proposed as a storage medium with air as the heat transfer fluid [200]. Anderson et al. [206] studied a thermal energy storage vessel of alumina in a cylindrical packed bed at elevated temperature (700 ºC) utilizing air as the heat transfer fluid. Their results showed that the temperature-dependent thermophysical properties of the storage medium are critical for

accuracy of the model. Alumina is expected to store sensible heat which is limited its specific heat. In contrary, PCMs with suitable phase transition behavior can store larger amounts of energy in a smaller volume.

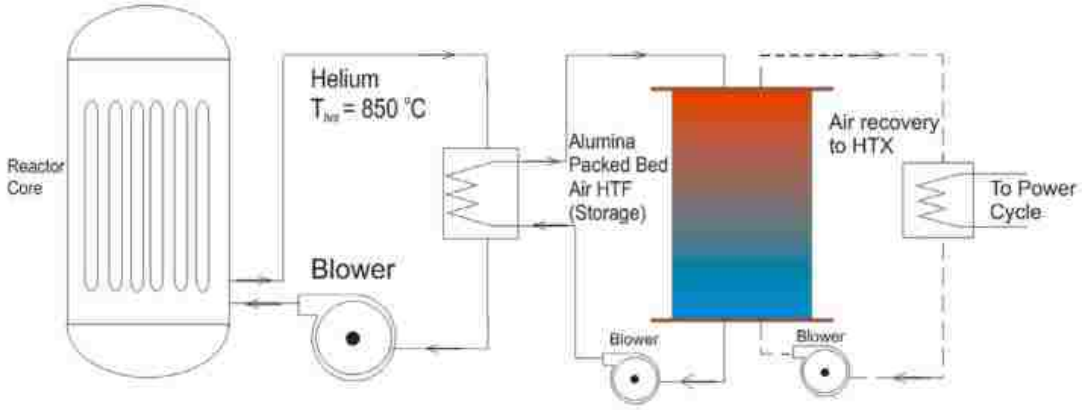

Figure 6.4. MHTGR coupled with thermal energy storage [200].

Current research shows several options of high-temperature PCMs. The suitable PCM candidates must have chemical and thermal stability, suitable phase change temperature, high storage capacity, relatively high thermal conductivity, compatibility with heat exchanger components and economic viability. A list of potential high-temperature PCMs is given in Table 6.2 summarizing their available properties such as melting temperature (T_m), latent heat of fusion (ΔH), density (ρ), and thermal conductivity (K). In future, further effort will be required to study other binary or ternary mixtures of high-temperature PCMs, particularly molten salts and alloys.

Table 6.2. High-temperature PCMs and their available thermo-physical properties.

PCM	T_m [ºC]	ΔH [J/g]	ρ [kg/m^3]	K [W/mK]	Ref
$NaNO_3$	308	200	2257 (solid)		[207]
NaOH	318	165	2100 (solid)		[208]
KNO_3	333	267	2110 (solid)		[207]
Mg-Zn (46.3/53.7 wt%)	340	185			[209]
KOH	360	134	2040 (solid)	0.5	[210]
$MgCl_2$-KCl-NaCl (60/20/20 wt%)	380	400	1800 (solid)		[210]
$MgCl_2$/KCl (39/61 wt$)	435	351	2110 (solid)	0.81	[211]
Al-Mg-Zn (59/33/6 wt%)	443	310	2380 (solid)		[212]
Mg-Al (24.7/65.4 wt%)	497	285	2155 (solid)		[209]
$Mg(NO_3)_2$	526				[211]
$Ca(NO_3)_2$	560	145			[211]
Al-Si (12/86 wt%)	576	560	2700 (solid)	160	[213]
Al-Si (20/80 wt%)	585	460			[213]
$MgCl_2$	714	452	2140 (solid)		[214]
LiF/CaF_2 (80.5/19.5 nol%)	767	790			[215]
KCl	771	353			[211]
NaCL	802	420	2160 (solid)	0.5	[216]
Na_2CO_3	854	276	2533 (solid)	0.2	[207]
Na_2SO_4	884	165			[211]
K_2CO_3	897	236	2290 (solid)	0.2	[207]

It was found that all previous research with respect to high-temperature PCMs was focused on molten salts, eutectics of molten salts, and alloys as primary candidates. Research on high-temperature PCMs remains insufficient and limited to melting and latent heat values only. This may be because no high-temperature application has been

commercialized yet. A comprehensive database of high-temperature PCMs will be required, focusing on the compatibility of these PCMs with other materials, temperature dependent thermo-physical properties, and physical aspects such as vapor pressure, flammability, and density changes. In addition. It is also critical to evaluate the environmental impact, costs, and availability.

7. DESIGN AND EXPERIMENTAL INVESTIGATION ON THE THERMAL PERFORMANCE OF PCM ENERGY STORAGE HEAT EXCHANGER

7.1. THERMAL ENERGY STORAGE FOR LOAD SHIFTING

Whereas the objective of the previous section was reviewing the applications of PCMs for thermal energy storage and load shifting in nuclear reactors, this section presents experimental investigation on a thermal energy storage design utilizing PCMs in the form of a heat exchanger storage vessel for load shifting purposes. The experimental setup is a parallel-plate heat exchanger design utilizing PCMs as latent heat storage medium. This proposed phase change energy storage system can deliver substantial benefits not only as thermal energy storage medium but provide savings in infrastructure, equipment and operational maintenance costs compared to conventional systems.

After decades of research, phase change materials are now finding their way into many applications, in thermal protection of flight data, hot and cold medical therapy, transportation of temperature sensitive products, solar power plants, photovoltaic cells, solar-activated heat pumps, waste heat recovery, building envelopes, and many others [217-220]. The experimental investigation of heat exchangers utilizing PCMs in the form of a storage vessel for electrical load shifting is a pressing topic. One example is the thermal energy storage technology of ice storage that has been used extensively for industrial applications and load shifting in data centers and server control rooms. The system comprises of an atmospherically vented tank in which heat exchangers are fully immersed in water. For load shifting, the ice storage system can be charged – by freezing the water- during off-peak electric hours and utilized when the demand charges during peak hours are high. Figure 7.1 shows an example of a typical load profile. The peak loading of any

industrial system usually occurs during the day at noon time when the internal thermal load, temperatures and solar gain are higher. Instead of running mechanical chillers during peak hours as a heat sink, if a thermal energy storage system is utilized to supply "cold" thermal energy during the peak hours, the on-peak load can be shifted to off-peak periods, thus, avoiding the high demand charged as shown in Figure 7.1. In our research, the aim is to validate the effectiveness of PCM-based systems to store and release energy in an efficient way and to expand the limited range of traditional sensible/latent thermal storage of ice/chilled water installation strategies. The proposed design technology uses the well-established principal of the latent heat of fusion at the desired design temperature when PCM changing its phase from liquid to solid, or vice versa.

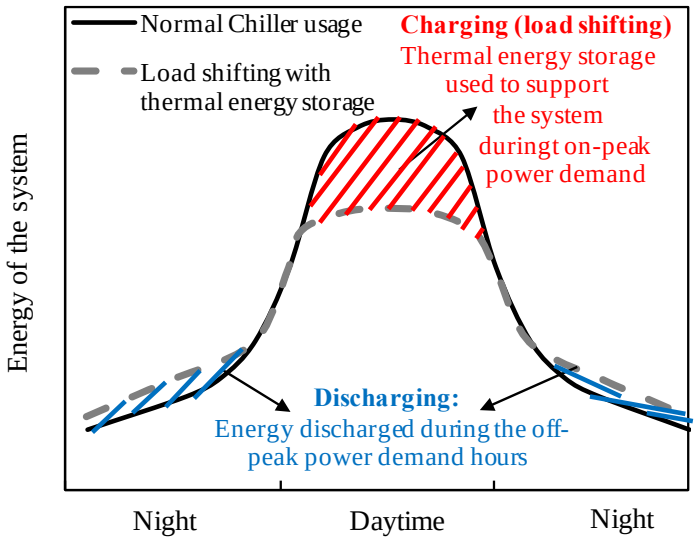

Figure 7.1. A typical load profile of an industrial thermal system.

The current existing conventional storage systems run chilled antifreeze –glycol- through a heat storage vessel at night -when power costs less- to freeze the water in a storage tank or vessel; In other words, it stores “cold” energy in ice by running the chillers during off-peak hours. Figure 7.2 shows an example for such systems. The ice is used the next day by extracting the stored “cold” energy during the day time - when electricity costs more during peak hours - by simply chilling a heat transfer fluid (water/glycol loop coming for the heat source) running through tubes in the ice storage vessel before it absorbs heat from a secondary (heat source) system, i.e. air handling units. This process eliminates the need to run chillers during that time. In other words, heat is extracted from the secondary system and stored in the cold thermal energy storage unit (Ice). The advantages can be summarized as follows: (a) Chillers are used during off-peak hours at night – at low cost of electricity – to extract energy from water and form ice, (b) The ice acts as a heat sink to store energy the next day without the need to run chillers by simply running water/glycol loop through the ice in the storage vessel, (c) the chiller energy consumption is shifted to off-peak hours.

Figure 7.2. A typical commercial ice/water thermal storage system by CALMAC [221]

Sensible heat storage systems such as chilled water vessels for cooling systems have also been used for various applications. For instance, Castano et al. [223] studied a sensible heat storage system utilizing chilled water/glycol to support the reactor cooling system of Missouri S&T pool-type nuclear reactor. The limited energy storage capacity of sensible heat systems, however, is the main reason for the limited use of these systems for practical applications. Additionally, a gradual temperature increase often occurs when using a sensible heat storage system. In contrary, latent heat storage systems provides constant supply temperature as the phase change process occurs at constant temperature.

Despite that ice thermal energy storage systems have been proven to be a cost-effective latent heat energy storage method, some design limitations and challenges need to be solved. The disadvantages can be summarized as follows: (a) An increased system complexity due to the need for two separate loops - glycol primary loop to freeze/discharge water at 20-25 ºF during off-peak hours (night) and a secondary water-only loop used during the day or peak hours to transfer heat from the heat source to the ice storage system. (b) Fixed transition temperature of water/ice in the vessel at 0°C. (c) Negative set point temperatures (-7°C to -4°C) are required for chillers to be able to cool the glycol loop and freeze the water in the heat storage vessel, meaning that chillers will be less efficient due to the very low set temperature, hence, running at a higher power level.

The current study presents an alternative storage medium so simplify the design and enhance the efficiency of energy storage systems. PCMs can be utilized as a thermal energy storage medium to replace water/ice in the storage vessel. The magnitude of energy involved in each system can be demonstrated by comparing the latent heat capacity. For instance, the latent capacity of water/ice is (334 J/g), whereas excellent PCMs are in the

range (200-240 J/g). Although ice has a higher latent heat storage capacity, it is limited to a fixed storage temperature at (0°C/32°F), unlike PCMs which can be developed for wide range of storage temperatures between (-50°C to +800°C) either by using naturally occurring PCMs or developing new eutectic mixtures.

The use of PCMs has the following advantages: (a) PCMs can be utilized to be charged and discharged at various temperatures with high latent heat storage capacity (b) PCMs can be developed to store energy at higher temperatures than 0°C, Hence the secondary loop of glycol can be eliminated since the PCM system can be discharged at a relatively higher temperature using water-only loop instead of anti-freeze/glycol. This way the system is simplified by using a single loop to store heat during the day and discharge the energy during off-peak hours at night. (c) Running expenditures are minimized when PCMs are used, as the use of PCMs makes chillers more efficient due to the ability to work at higher set-point temperatures that corresponds to the PCM phase transition temperature. Moreover, service life would be extended, and less maintenance is required. This is because PCMs usually do not expand when they freeze but instead they slightly shrink; In the contrary, water expands when solid ice is formed causing design stresses (d) Capital expenditures are minimized since smaller size chillers can be used. (e) PCM based storage systems can be directly integrated into existing utilities without the need to increase existing chillers capacity or installation of new inefficient glycol-based systems. In conclusion, PCMs based storage systems not only can deliver energy cost savings, but also provide savings in infrastructure, equipment and therefore operational maintenance costs. A comparison between the proposed PCM energy storage systems and the conventional storage systems is given in Figure 7.3 and Table 7.1.

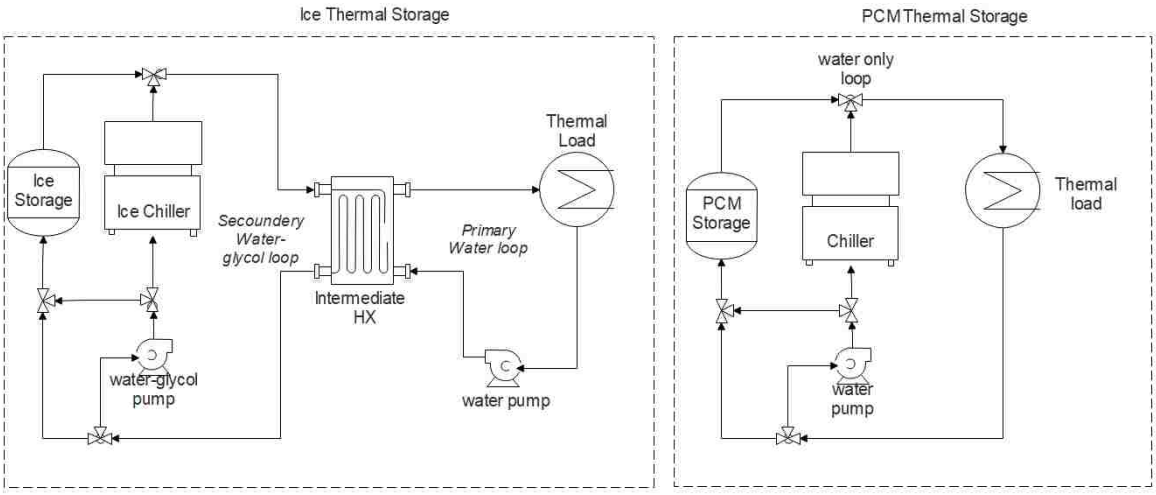

Figure 7.3. A comparison between the proposed PCM energy storage system and ice energy storage system.

Table 7.1 A comparison between the PCM and ice energy storage system.

	conventional Storage Systems	The proposed energy Storage System
Storage medium:	Water (ice)	Phase change material (PCM)
Type of energy:	Sensible or Latent heat	Latent heat mainly + sensible
Operation temperature:	Sub-zero for latent >0°C for sensible	Varies – PCMs can be developed to be as close as reasonably possible to the load temperature
Additional Equipment:	Valves and controls	Valves and controls
Secondary loop:	Yes	No (directly to water primary loop)
Glycol management:	Yes	No (water from primary loop)
Secondary pump:	Yes	No (No secondary loop)
Chiller size required:	Larger (Lower set-point)	Smaller (Higher set-point)
Chiller consumption:	Higher (lower set-point)	Lower (Higher set-point)
Foot print:	Small compared to sensible/chilled systems	Smaller

The proposed design has the benefits of being flexible in terms of scalability to fit various applications for load shifting purposes and thermal energy storage using systems in the form of a heat exchanger design utilizing PCMs. For this reason, the design was characterized as a function of absolute temperature differences relative to the PCM transition temperature at various inlet conductions. This provides insights into the scalability and performance of the system at differing design temperatures by only varying the phase transition of PCM to account for different applications at higher or lower temperatures. Table 7.2 shows the operating temperature and recommended PCM thermal storage temperature of various applications that require utilization of PCMs in the form of a heat exchanger vessel.

Table 7.2. Potential applications of PCM energy storage heat exchanger system.

Application / example	Allowable Operating/storage temperature	Recommended PCM storage and transition temperature
Coupled nuclear reactors	300-550 °C	300-550 °C
Nuclear Ice condensers	70-90 °C	60-80 °C
Industrial waste heat recovery	80-110 °C	70-100 °C
Solar power plants	500-700 °C	450-550 °C
Solar heating systems	50-60 °C	40-50 °C
HVAC energy storage support	8-10 °C	6-8 °C
Independent residential cooling	15-20 °C	16-18 °C
Data centers and servers	25-32 °C	16-23 °C
Nuclear pool reactor heat removal system (i.e.: Missouri (MST-R))	18-24	Chilled water was proposed; 18 °C PCMs have potential.
Subzero / Ice storage	0°C	0°C
Space applications	(-40) to (-10) °C	(-40) to (-10) °C

Despite challenges such as working pressure and extreme flow rate for certain application, the proposed design can be appropriate and scalable to lower or higher temperature applications (-40) to 80 °C. In the current study, a PCM with phase change transition temperature of around 18 °C was chosen to for the energy storage system, which makes the system in its current design temperature and geometry an ideal solution for data centers, such as those used by Apple, Google, Verizon, AT&T, Facebook, Dell, Cisco, etc. Temperatures in data centers and servers normally rises because of the generated heat of electronics and servers. In 2008, ASHRAE's standards and thermal guidelines [95, 222] increased the maximum allowable operating temperature range of data centers and servers to 32°C for class A1 of server equipment, and recommended a 27°C as the average high-end temperature for all classes. This means that the data center thermal load can be met by the HVAC with a chiller water supply at a temperature of 22-24 ºC. Perhaps more importantly, the higher supply temperatures open new possibilities for the use of new smart strategies in data centers for load shifting purposes, such as utilizing the latent heat of PCMs with phase transition temperature of 18-19 ºC. For data centers, it becomes also possible to utilize 16-17 ºC or lower water temperature from cooling towers to store "cold" energy in PCM during off-peak hours – at night – without mechanical chiller systems. The PCM storage vessel can be cooled during night hours using only advanced/efficient polymer fluid cooler (PFC) or cooling towers when the wet bulb temperatures are lower. In this case, PFC/cooling towers could produce water at 15-16 ºC, which is lower than the phase transition temperature of PCM, thus freezing the PCM that can be utilized later during the day. In other scenarios, assuming the leaving water temperature from the PFC or the cooling tower at night is not cold enough, the chilled water from the PFC/cooling

tower would also pass to a small chiller as a secondary cooling stage to further reduce the water temperature before being utilized to freeze the PCM in the heat exchanger vessel. This process should occur at night when the electric rates and wet bulb temperature are low. During the day, the designed PCM storage heat exchanger should be able to meet the data center load without the need to run mechanical chillers. To the best of our knowledge, utilities and data centers have yet to implement such passive PCM latent heat storage systems that can be discharged at reduced demand charges without the need for mechanical systems, or at least, using much smaller chillers. This demonstration will be the first of its kind for a modern data center.

As previously discussed, ice storage systems offer many of the same benefits that PCM storage provides while using a small foot-print. However, many existing chillers cannot make ice, and for those that can, the loss of chiller efficiency and chiller capacity at the low temperature required to make ice (-8 °C to -5 °C), along with higher pumping costs, and the need for glycol secondary loop and increased system complexity off-sets the benefit of using ice as the thermal energy storage medium.

A thermal energy storage design equipped with PCM of phase transition temperature at around 18 °C can help to avoid the huge on-peak demand charges of existing chillers during the day, save energy, and keep the server components within the ASHRAE's and manufacturer's specified temperature level. As previously mentioned, the proposed experimental design can be scaled up/down to lower/higher temperatures by only choosing different PCM of higher/lower phase transition temperature to meet the desired operating storage temperature of the application.

Another opportunity for thermal energy storage in example is the sensible heat cooling system used for Missouri S&T nuclear pool reactor heat removal system. Castano et al. [223] studied a sensible heat removal system utilizing chilled water/glycol tank to maintain the reactor water pool between 65-75°F (18-24 °C) and to increase the rate at which heat is removed from the system during shutdown. The main challenge was that the pool water temperature increases by 2 °F per 1 hour during operation, However, the cooling rate after shutdown is less than 2 °F per 48 hours. To remedy this, their study proposed a chilled water-glycol tank and an intermediate plate-type heat exchanger for the reactor cooling system to exchange the heat between the pool water and chilled water loop. The analysis of the reactor cooling system showed that 30,000 gallon of pool water can be cooled from 88 °F to 68 °F in 1.5 hr. These sensible heat storage systems in the form of chilled water storage tanks are a relatively inexpensive and well-established technology but are often limited by the specific heat of the medium – water in this case with specific heat of ~4.18 J/g.K. Additionally, temperature variability and gradual increase often occurs through the process of sensible heat storage. In order to extend the continuous operation of the facility for even longer periods at full power, and to enable a reactor power upgrade in the future with a more reliable system design, it is required to have a higher cooling capacity than the proposed sensible heat system. The use of PCM based thermal energy storage systems can overcome these limitations. A PCM system enables higher storage capacities and capable of targeting defined and constant discharge/charge temperatures. By utilizing the latent heat of PCMs, the passive energy capacity of the system can be increased by an order of magnitude. Moreover, latent heat storage systems provide higher cooling capacity for an extended period in case of accidents, yet with smaller foot print.

7.2. EXPERIMENTAL FACILITY

The construction of the heat exchanger unit consists of an insulated vessel of aluminum to hold the PCMs and the heat exchanger plates of the heat transfer fluid. Figure 7.4 shows an image for one unit of the heat exchanger and schematic of its components. The specifications of the heat exchanger are given in Table 7.3.

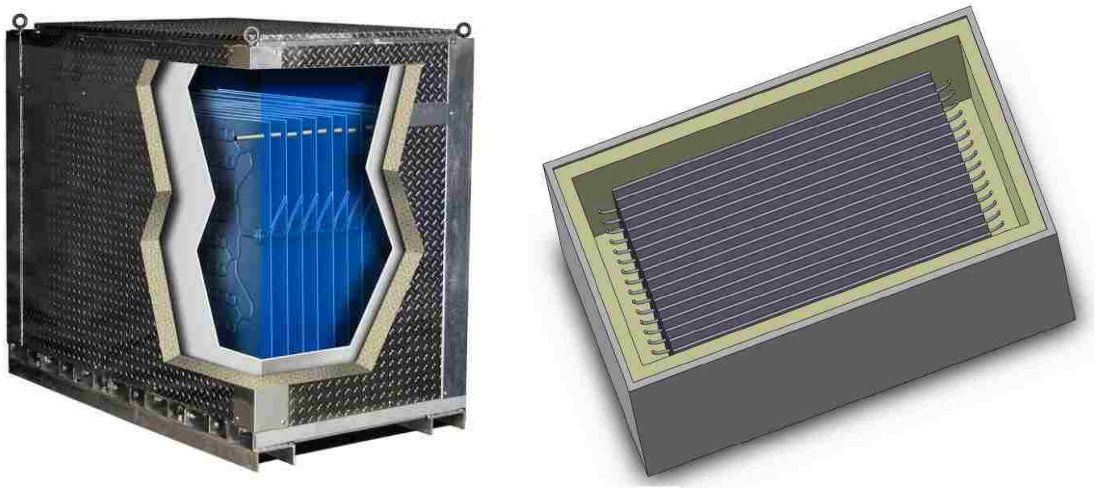

Figure 7.4. Image and schematic for the experimental storage heat exchanger unit

Table 7.3. Specifications of the energy storage heat exchanger

Net thermal capacity (latent) per unit	Dimensions of one unit (outer) LxWxH [m]	PCM weight per unit	Number of plates	Heat exchange surface area per one plate
114,432.0 kJ =108,460.6 Btu	1.22x0.81x1.52	480 kg	20 Aluminum plates (2.7 kg each)	0.67 m^2

The PCM chosen for the heat exchanger has latent heat of 238.4 J/g as shown in Section 7.5, this equates to a total latent heat thermal capacity of 114,432.0 kJ or 108,460.6 Btu for a single heat exchanger unit. Due to the high latent heat capacity, small footprint for the entire system was possible. The heat exchange plates are made from two overlaid sheet layers of aluminum giving a heat exchange surface of high thermal conductivity. The two overlaid sheet layers are housing channels where the heat exchange fluid is circulated. The design of the channel is optimized to ensure an extremely uniform surface temperature, and to maximize the heat transfer between the heat transfer fluid and PCM. The designed flexibility of the aluminum plates allows to withstand the expansion and contraction of the PCM during solid-liquid phase transition. Figure 7.5 shows a schematic of the heat exchange plates. A leak (burst) and pressure drop tests were carried out using water as the heat exchange fluid at various mass flow rates. The operating pressures for all experiments were lower than the burst pressure. The plates were connected to each other in parallel to achieve lower overall pressure drop and better heat transfer.

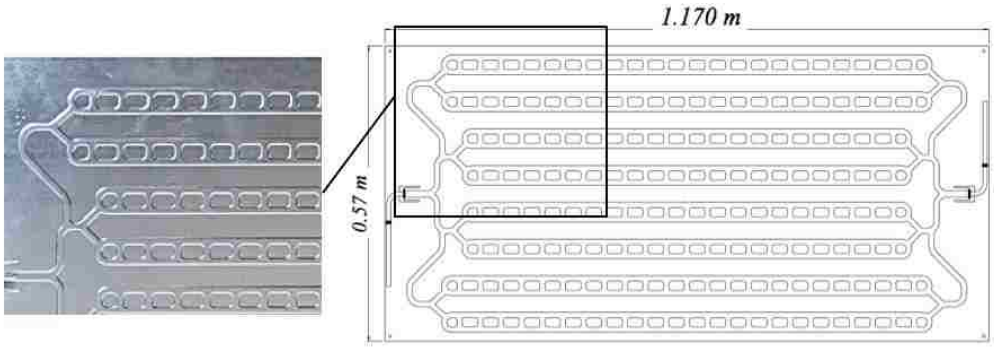

Figure 7.5. Picture and schematic for the heat exchange plates.

The impact of the plate-plate spacing and heat transfer surface area were investigated by experiments. The plate-plate spacing was tested for optimization at 1 inch (25.4mm) and 2 in (50.8 mm), and the impact of spacing distance on the phase transition progress was carried out visually and experimentally. Figure 7.6 shows the experimental setup for different plate-plate spacings.

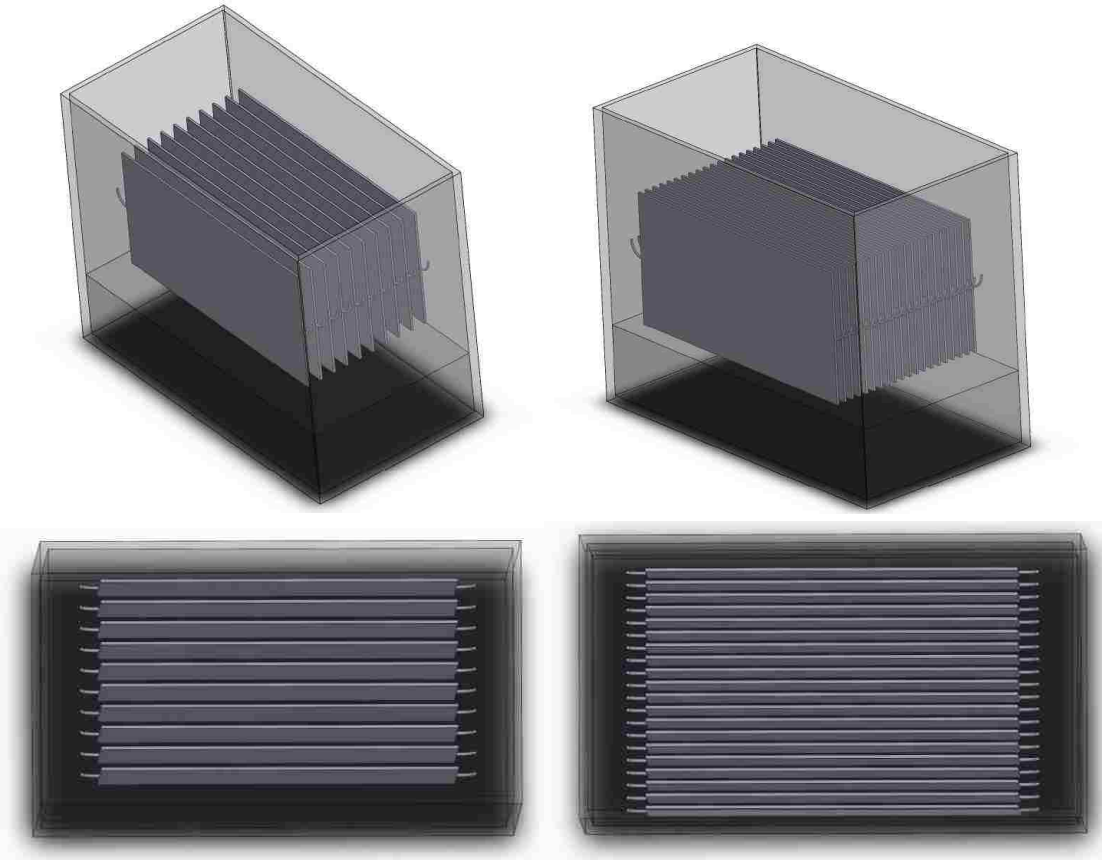

Figure 7.6. The experimental setup for optimization of various plate-plate spacing, 1 inch (25.4mm) left figures, and 2 in (50.8 mm) for right figures.

The heat exchanger vessel was made from aluminum sheets of 1/8 inch thick forming the outside walls of the vessel with 1-inch thick aluminum supporting rods. An insulation of 2-inch thick polyisocyanurate foam was used on the interior walls of the heat exchanger vessel. A liner of vinyl was then applied as a barrier between the insulation walls and the filled PCM to avoid any leakage. The polyisocyanurate insulation is in compliance with ASTM C1289-17 standards for Faced Rigid Cellular Polyisocyanurate, and ASTM E2357 as a component of an air barrier assembly. The insulation is capable to handle temperatures between -40 to 93°C. The R-value of the Polyisocyanurate insulation was measured using the FOX314 TA instrument as a heat flow apparatus by establishing a steady state 1-D heat flux through a 12x12 inch insulation sample between two parallel plates. Four optical encoders were used to control the position of plates and to establish a full contact with the sample. Figures 7.7 gives the measured thermal conductivities and R-values at (10, 20, 30, 40, 50, and 60 °C).

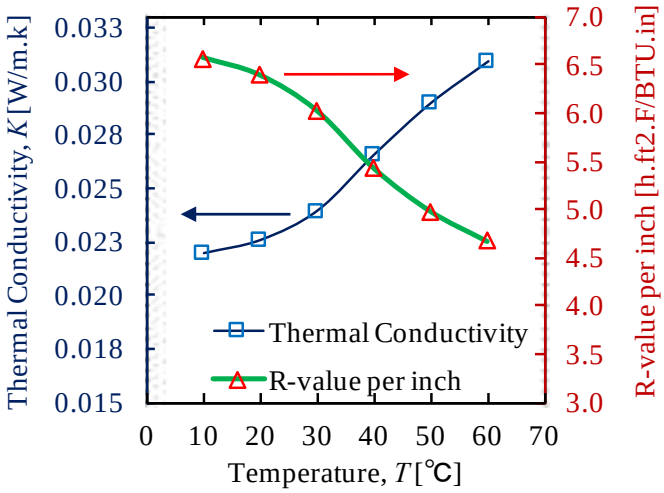

Figure 7.7. The measured thermal conductivities and R-values of the vessel insulation

The temperature of the inlet and exit fluid were measured using a S-TMB-M002 smart temperature sensors to an accuracy of ±0.2°C. The locations of the sensors were fixed at the plates just before the inlet/exit of the plates and above the PCM level. The fluid flow velocity was measured by Dynasonics DXNP-ABS-NN ultrasonic flow meter with an accuracy of 0.03 m/s. In addition to this, GPI TM series water flow meters with a measurement accuracy of ±3% were installed on the inlet and outlet pipes of the PCM heat exchanger for redundancy. The experimental facility is shown in Figure 7.8. Water is held in two tanks with combined volume of 2000 gallon, one tank as a source for chilled water and one for hot water. Two pumps of 2 horsepower were used to circulate water from the hot and cold loops to the PCM heat exchanger.

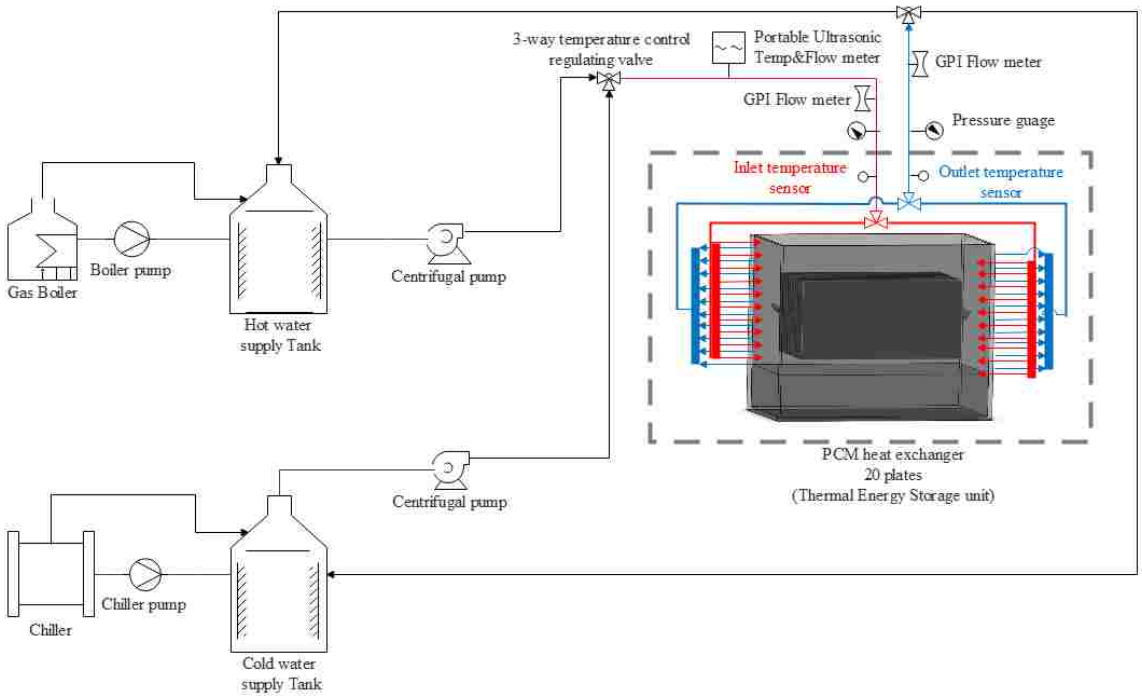

Figure 7.8. Schematic of the experimental facility

A 1.5” Belimo G340+SVB24-SR mixing valve coupled to Honeywell T775M2006 controller with proportional 4-20mA output was used to provide temperature feedback. This temperature feedback was used to control the valve position and achieve sufficiently uniform flow by mixing two water inlets, one from the hot source tank and one from cold source tank to, at the desired temperature set point. In other cases, based on the required inlet temperature only one loop was utilized. The cold loop utilizes a 120,000 Btu refrigeration chiller (Temptek CFD-10A) connected to a chilled water storage tank. Hot water loop includes a hot water storage tank attached to a 400,000 Btu capacity Hayward H400FDN boiler.

Pressure gauge with an accuracy of ±1 kPa were used to measure the pressure drop across the plates assembly. All the supply and return pipes, including the chiller and boiler side pipes were 1.5” PVC pipes. Check valves were used to prevent the back flow of water into the storage tanks. The pipes between the heat exchanger and the mixing valve were insulated to minimize heat loss/gain from the environment. The set temperature of the Honeywell temperature controller was manually calibrated to supply water at the desired temperature at the inlet of the heat exchanger.

As described by Belusko et. al. [224], the Number of Transfer Units (NTU) decreases with time for plate heat exchanger, assuming that phase change process takes place in the direction of flow. Therefore, the inlet design was optimized to accommodate a counter flow condition in adjacent plates, thus enhancing the effectiveness of heat exchanger. The PCM heat exchanger was designed such that the trend of the experimental work was toward experiments at various inlet temperatures and mass flow rates. Such trends are necessary to evaluate the energy storage performance of the PCM heat exchanger

and to provide insights on the behavior of system under different conditions as well as for scalable sizes and applications. The experimental conditions were chosen very carefully to be within the design limits of the heat exchanger plates and components.

7.3. EXPERIMENTAL PROCEDURE AND METHODS

During charging (melting) tests, water at intel temperatures of (75, 85, and 95 °F) was circulated through the channels of the heat exchange plates at various mass flow rates (0.126, 0.252, 0.378 kg/s) for each inlet temperature. Prior to each charging experiment, the PCMs were pre-conditioned (frozen) at around 55-60 °F.

During discharging (cooling) experiment, water inlet temperatures of (55, 50, and 45 °F) was circulated for discharging. For discharging, it is important to discharge at an inlet temperature that is as high as reasonably possible as the chiller is more efficient at higher temperatures. Ideally, the discharge of the vessel needs to be as short as possible during off-peak hours. Therefore, only the highest mass flow rate of 0.378 kg/s was used for energy discharge at various inlet temperatures. Prior to each discharging experiment the PCMs were melted at around 75 °F.

The tests conditions for the experiments are illustrated in Table 7.4, where the various inlet temperatures (T_i) and mass flow rates (m^o) are given for several charging and discharging tests.

Table 7.4. Inlet conditions for the experiments

Mode	Inlet temperature, T_i	Flow rate, m^o
Charging	75 °F (23.9 °C)	6 GPM (0.378 kg/s)
Charging	85 °F (29.5 °C)	6 GPM (0.378 kg/s)
Charging	95 °F (35.0 °C)	6 GPM (0.378 kg/s)
Charging	75 °F (23.9 °C)	4 GPM (0.252 kg/s)
Charging	85 °F (29.5 °C)	4 GPM (0.252 kg/s)
Charging	95 °F (35.0 °C)	4 GPM (0.252 kg/s)
Charging	75 °F (23.9 °C)	2 GPM (0.126 kg/s)
Charging	85 °F (29.5 °C)	2 GPM (0.126 kg/s)
Charging	95 °F (35.0 °C)	2 GPM (0.126 kg/s)
Discharging	55 °F (12.8 °C)	6 GPM (0.378 kg/s)
Discharging	50 °F (10.0 °C)	6 GPM (0.378 kg/s)
Discharging	45 °F (7.2 °C)	6 GPM (0.378 kg/s)

7.4. ENERGY ANALYSIS

The total energy stored by the heat transfer fluid can be obtained by considering the temperature variation across the heat exchanger vessel as given in equation 29 for the rate of energy storage (Q^o), and equation 30 for cumulative energy storage (Q).

$$Q^o(t) = m^o * C_p * [T_i - T_o(t)] \tag{29}$$

$$\mathrm{Q} = \int_0^t Q^o(t).dt = m^o * C_p \int_0^t \big(T_i - T_o(t)\big).dt \tag{30}$$

Where m^o is the mass flow rate of water, T_i is the temperature inlet, T_o is the temperature outlet, C_p is the specific heat of the heat transfer fluid, and t is the time

In physical terms, the heat exchanger effectiveness can be defined as the ratio of actual heat transferred to the theoretically maximum possible heat transfer between the two sides of heat exchanger. Effectiveness - number of transfer units NTU (ε-NTU) technique

is a well-documented method of characterizing the performance of a heat exchanger. Tay et al. [225] developed a simplified mathematical model based on the ε-NTU technique. Equations 31, 32, 33 summarize the effectiveness model considered for the analysis of the heat exchanger. Equation 31 gives the instantaneous effectiveness (ε) at any time during the experiment at a given T_o and T_i, whereas equation 32 gives the averaged effectiveness ($\bar{\varepsilon}$) of the heat exchanger during the PCM phase transition time ($t_2 - t_1$) during which the latent heat shoulder is observed in the leaving water temperature-time curve. Similarly to the method shown in [225, 226] , Equation 33 accounts for NTU between the PCM and the heat transfer fluid.

$$\varepsilon = \frac{m_w^o C_{p,w}(T_o - T_i)}{(m^o C_p)_{min}\,(T_{tr} - T_i)} = \frac{(T_o - T_i)}{(T_{tr} - T_i)} \tag{31}$$

$$\bar{\varepsilon} = \frac{\int_{t_1}^{t_2} \varepsilon . dt}{t_2 - t_1} \tag{32}$$

$$\varepsilon = 1 - \exp(-NTU) \tag{33}$$

The NTU is a dimensionless parameter that is defined by the ratio of the product of overall heat transfer coefficient (U) and the contact surface area to the heat capacity rate of the transfer fluid (water) as given in equation 34.

$$NTU = \frac{U * A}{\dot{m} * c_p} \tag{34}$$

It is to be noted that a more general definition of NTU can be given by equation 35 [227], where C_{min} is the minimum heat capacity rate of the two fluids.

$$NTU = \frac{U * A}{C_{min}} \tag{35}$$

As in the design relevant to this study, the flow rate of PCM is always zero, which if used in equation 35 and 33 will always lead to an effectiveness of 1. Therefore, Tay et al. [225] suggested the use of the specific heat of heat transfer fluid to get an estimate of effectiveness of a thermal energy storage heat exchanger. In this study however, equation 31 were used to calculate the instantaneous effectiveness. The integration was performed as given in equation 32 using the trapezoidal rule and averaged over the period of a complete phase transition.

Despite that energy storage vessel is well insulated, some energy loss or gain from/to the environment may exist due to the thermal bridges and design deficiencies. The physical significance of energy efficiency given in equation 36 is to compare the total amount of available energy storage in the PCM to the amount of energy stored in the PCM.

$$\eta = \frac{Energy\ stored}{Energy\ availabe\ in\ PCM} = \frac{Q_{Charged\ experimentally}}{Q_{total\ in\ PCM}} = \frac{\int_0^t Q^o(t).dt}{Q_{latent} + Q_{sensible}}$$
$$= \frac{m^o * C_p(T) \int_0^t \left(T_i - T_o(t)\right).dt}{\mathrm{M_{PCM}} \left[\Delta H_{DSC} + C_p^{solid} * [T_{tr} - T_{initial}] + C_p^{liquid} * [T_i - T_{tr}]\right]} \quad (36)$$

Where M_{PCM} is the mass of PCM in the heat exchanger, ΔH_{DSC} is the enthalpy of the PCM as experimentally measured using the DSC method in J/g, T_{tr} is the phase transition temperature of the PCM, $T_{initial}$ is the initial temperature of the PCM in the heat exchanger when the experiment starts.

7.5. ANALYSIS OF THE PHASE CHANGE MATERIAL

Phase Change Materials other than ice have been extensively studied in many applications. Because of their attractive features, organic PCMs such as fatty acids and

paraffin have received a special attention [30, 140, 141, 228]. The long-term thermal stability, high latent heat, non-corrosiveness and ability to make new eutectic mixtures are the major advantages of organic PCMs. For an efficient thermal energy storage system and to maximize the effective transient thermal management time, the phase transition temperature needs to be as close as reasonably possible to the temperature range at which the system needs to be maintained at. Several PCMs have been screened as candidates for the proposed heat exchanger design. The criteria of selection are given below:

1. Higher latent heat capacity, to increase the amount of energy storage for a given volume.
2. Long-term thermal stability.
3. Small volume changes during solid-liquid transition, to reduce pressure and stresses on the heat exchanger components during contraction and expansion. While Ice expands during solidification, PCMs tend to shrink during solidification and expands only during melting which results in much less stresses because of the mobility of liquid PCM during expansion compared to solid ice during expansion.
4. Non-corrosiveness and non-toxicity.
5. Availability and cost of the PCM.

A paraffin PCM, namely Hexadecane ($C_{16}H_{34}$), with phase change transition temperature of around 18°C was chosen to analyze the energy storage heat exchanger. Hexadecane is a linear n-alkanes hydrocarbon paraffin consists of a chain of 16 carbon atoms and 34 hydrogen atoms. The PCM is supplied by Sigma-Aldrich with 99% purity. This section is intended to experimentally study thermal characteristics of the PCM used for the design of the heat exchanger thermal energy storage system. The chemical and physical data are given in Table 7.5.

Table 7.5. The chemical and physical data of the PCM

PCM	Scientific name	Purity	Molecular weight [g/mol]	CAS Number	Molecular Formula
Hexadecane	n-Cetane	99%	226.44	544-76-3	$C_{16}H_{34}$

Differential scanning calorimetry measurements were carried out to study the phase transition characteristics of the PCM using Modulated-DSC (Discovery MDSC, TA instruments). Five measurements performed, and the averages are reported here. Figure 7.9 shows the melting and freezing phase transition. The phase transition temperature is one of the most important properties to consider as it determines the temperature at which the energy can be charged or discharged. A summary for thermal characteristics of hexadecane is given in Table 7.6.

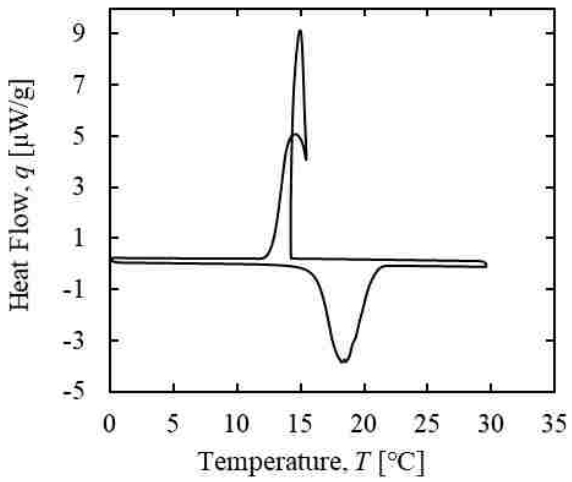

Figure 7.9. DSC results for the phase change transition of hexadecane ($C_{16}H_{34}$).

Table 7.6 Results for the thermal characteristics of hexadecane ($C_{16}H_{34}$).

Melting		Freezing		Specific heat		Density	
T_m	ΔH_m	T_f	ΔH_f	Solid	Liquid	Solid	Liquid
°C	J/g	°C	J/g	J/g.K	J/g.K	g/ml	g/ml
18.3	238.4	15.5	234.5	1.925	2.350	0.775	0.828

The behavior of the freezing phase transition is of interest. The DSC profiles in Figure 7.9 reveal a great deal of information regarding the crystallization of the PCM. For other PCMs, in most cases the exothermic peak continues to raise with somewhat decrease in temperature responding to the cooling rate demand of the DSC cell. The crystallization rate for the measured PCM however was too fast that the DSC scanning rate was relatively too slow to cool the PCM temperature further to lower temperature. This is indicated by the increase in temperature from 15.06°C peak temperature to 15.45°C before it continues to decrease to lower temperature. There is some time required for the crystallization of PCM to develop, in this case the rate of crystallization was relatively fast compared to other PCMs. The hexadecane PCM exhibited a satisfying latent heat capacity of 238.4 J/g for melting and 234.5 J/g for freezing. The specific heat and density for the solid (10 ℃) and liquid (28 ℃) phases of PCM are given in Table 7.6. The experimental DSC results were found to be in a good agreement with the reported values in other studies [229, 230], except for the freezing phase transition data. This may be attributed to the higher resolution (0.005 ℃) of the advanced M-DSC used in this study which revealed more detailed information on the liquid to solid crystallization rate and behavior.

The thermal conductivity (*k*) was measured using the heat flux meter (Fox314, TA instrument) as described in Section 2.2. The measurements were conducted in accordance with ASTM 1784 (Standard Test Method for Steady-State Thermal Transmission Properties by Means of the Heat Flow Meter Apparatus). The thermal conductivity was found to be 0.152 W/mK for the solid state at 10ºC and 0.295 W/m.K for the liquid state. These values are in good agreement with the values in [231] as shown in the comparison given in Table 7.7.

Table 7.7. Results for the thermal conductivity of hexadecane ($C_{16}H_{34}$).

Thermal conductivity @10°C		Thermal conductivity @28°C	
k^{solid} W/mK	k^{solid} W/mK	k^{liquid} W/mK	k^{liquid} W/mK
0.295	0.280 [231]	0.152	0.145 [231]

7.6. EXPERIMENTAL ANALYSIS OF THE PCM HEAT EXCHANGER

Phase Change Materials are characterized by their low thermal conductivity which may diminish the rate of heat exchange during energy storage process. Heat exchangers of coil-in-PCM arrangement have been extensively studied in literature [225, 226, 232]. In order to compensate for the low thermal conductivities and to insure efficient charging/discharging of thermal energy, an improved design has to be adopted such as dispersing high thermal conductivity particles, embedding metallic matrix structures, or design different geometries with enhanced heat exchange surface between the PCM and heat transfer fluid other than the coil-in-PCM arrangement. The current research studied

the performance of PCMs for thermal energy storage using a plate-type heat exchanger arrangement at various inlet conditions.

7.6.1. Effect of Plate-Plate Spacing. With the low thermal conductivity of the PCM medium, the plate-plate spacing is a critical parameter that must be carefully chosen and optimized. Figure 7.10 shows the temperature-time curve for two experiments of different plate-plate spacings, 1 inch and 2 inches. During these experiments, the inlet temperature was fixed at 23.9 ºC. As shown in Figure 7.10, T_r represents the transition temperature of the PCM (18.3 ºC) while the two solid lines show the outlet water temperature for two different plate-plate spacing. For the 2-inch plate-plate spacing a bundle of 10 plates was loaded in the heat exchanger, whereas a bundle of 20 plates was used for the 1-inch plate-plate spacing. The total flow rate across the heat exchanger was kept equal for both arrangements. The experiment performed with 1-inch plate-plate spacing showed a higher temperature difference between inlet and outlet, lower exit water temperature and a more pronounced transition shoulder meaning that effectiveness is higher. In addition, the latent heat energy storage was completed in shorter time meaning that the rate of energy storage is higher. Despite that the total mass flow rate across the whole bundle is the same for both arrangements, the mass flow rate per plate however is less for the bundle of 1-inch plate-plate spacing when compared to that of 2-inch plate-plate spacing this is because the total mass flow rate is divided over larger number of plates. Therefore, the heat transfer fluid takes longer time of heat exchange with the PCM. It can be concluded that the 1-inch plate-plate spacing arrangement showed better performance, hence this optimum arrangement was considered for further analysis in this study.

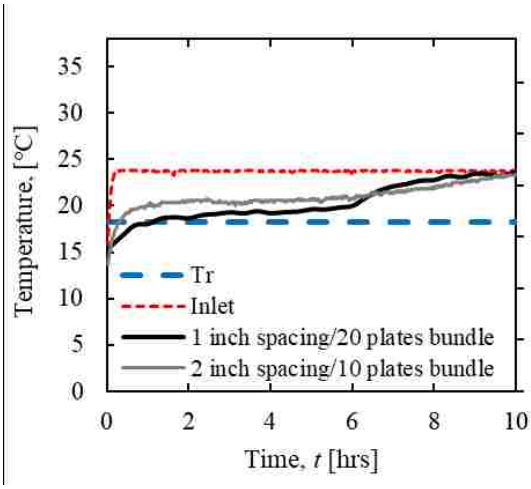

Figure 7.10. Outlet temperature profiles of different plate-plate spacing arrangement.

Figure 7.11 shows another important observation. During the pre-discharge (freezing) phase, the PCM close to the surface of plates experienced an increased freezing rate compared to the PCM in between the plates, therefore, forming a thin film of frozen PCM layer at the surface of plates. This was remedied upon decreasing the plate-plate spacing to 1-inch which resulted in a lower temperature gradient between the plates.

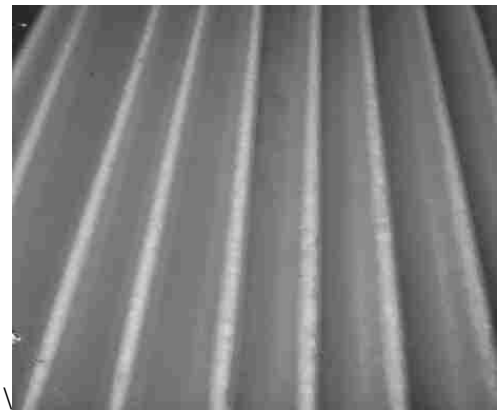

Figure 7.11. Thin film of PCM layer at the surface of plates during a discharge cycle.

7.6.2. Thermal Energy Storage Performance. Figure 7.12 compares various outlet water temperature profiles with respect to time during the melting tests at various flow rates and inlet water temperatures. The general behavior of the outlet temperature profiles asymptotes to the inlet temperature marking the steady state achieved after end of melting process and sensible heat region. At higher flow rates or higher inlet temperatures this steady state is achieved more quickly, representing a higher charging rate.

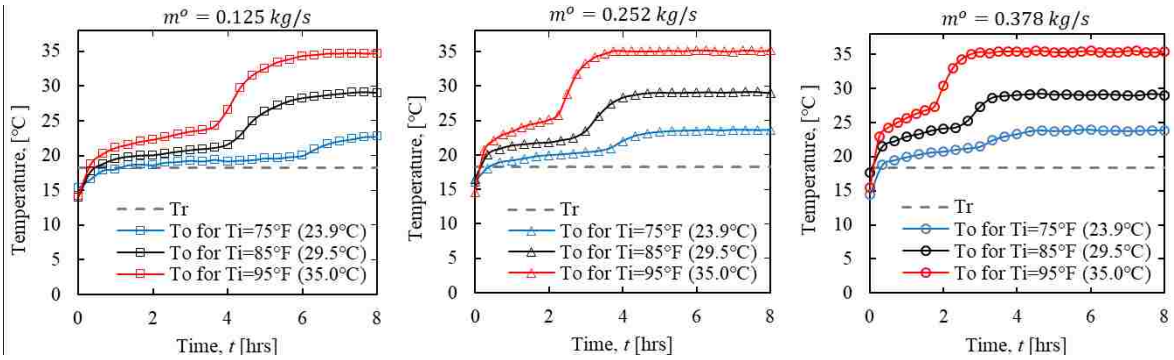

Figure 7.12. A comparison of various outlet water temperature profiles with respect to time during the melting cycle at various flow rates and inlet water temperatures.

The profiles for the cumulative energy stored in the PCM heat exchanger at various inlet temperatures and mass flow rates are given in Figure 7.13. As the time increases, rate of heat transfer to PCM decreases and the cumulative energy value saturates with the maximum amount of energy that the system can store.

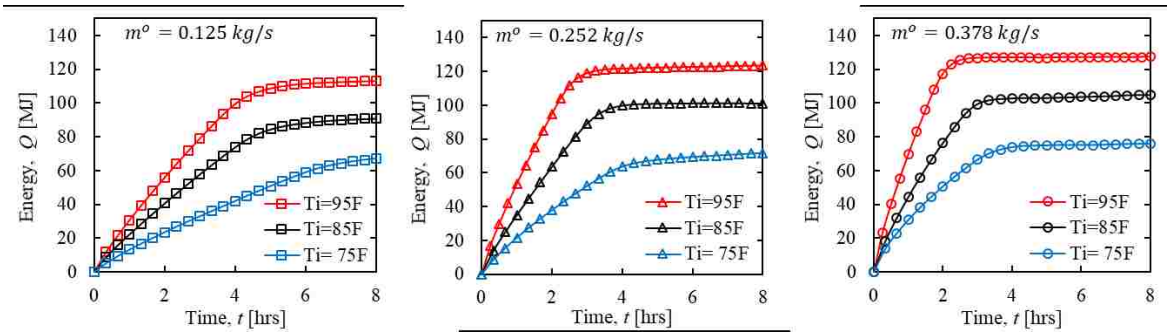

Figure 7.13. The cumulative energy storage profiles at various inlet conditions

The energy storage profiles of various flow parameters provide a great deal of insight into the behavior of the heat exchanger under various conditions. However, to discuss these results, Figures 7.14-7.15 show several important trends. For the experiments at higher inlet temperatures at the same flow rate, the overall heat transfer coefficient (U) tends to slightly decrease. This may be due to localized phase change conditions around the plates. The PCM layer next to the heat exchanger plates – the phase change front – melts sooner than the PCM further away from the plates, and a thin film of PCM layer forms at the surface of the plates. This results in a fully-charged melted PCM film that acts as an insulation layer of low thermal conductivity (0.152 W/m.K) which is 48% lower than the uncharged solid PCM (0.295 W/mK). This layer is known as the phase change front whereas the phenomenon is known as self-shielding of PCMs. This is similar in concept to the formation of solid/frozen layer of PCM during the discharge/freeze cycle that is most obvious at larger plate-plate spacing's as previously shown in Figure 7.11. However, the decrease in the overall heat transfer coefficient in Figure 7.14 is not supported by the trends seen in Figure 7.13. Figure 7.13 indicates that as the inlet temperature increases, the total energy stored tend to increase. At first glance, it might appear that the decrease of energy

storage in Figure 7.13 as the inlet temperature decreases is counter-intuitive because the values of overall heat transfer coefficient tends to increase for lower inlet temperatures. However, this can be explained in a way that the energy storage gain from sensible heat for the higher inlet temperature overweight the effect of lower heat transfer coefficient. Additionally, for lower inlet temperatures the charging period becomes longer as seen in Figure 7.12, which may result in a higher heat leakage between the PCM in the heat exchanger and the environment due to the longer experimental time, thus reducing the available storage energy for the fluid for the experiments of lower inlet temperatures. Rosen et al [233] described that as "cold" energy loss in a study he carried out on the energy balance of latent heat storage systems. Additionally, This trend in energy storage appears to be consistent with the results of relevant research on an ice storage heat exchanger [232].

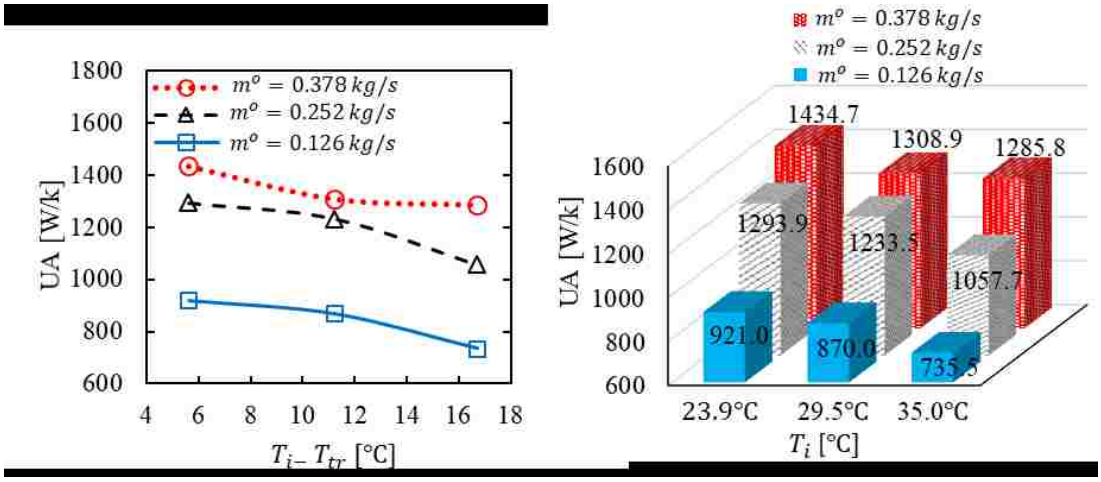

Figure 7.14. Heat transfer coefficient of the PCM heat exchanger at conditions.

Figure 7.15 presents the effectiveness profiles of the PCM heat exchanger at various inlet conditions. For lower inlet temperatures, the effectiveness of the heat exchanger is higher, meaning that the leaving water temperature (T_o) is relatively closer the phase transition temperature (T_{tr}). However, the cumulative energy storage is less for lower inlet temperatures as implied by the energy storage data discussed above. Similarly, the effectiveness of the heat exchanger is higher for lower flow rates. This trend is also carried through the average leaving water temperature in Figure 7.12, where the difference between T_o and T_r is lowest for lower mass flow rates due to the higher effectiveness. It can be said that the measured effectiveness is within an excellent range for a heat exchanger when the secondary side – PCM in this case – is stationary. At a mass flow rate of 0.126 kg/s per one heat exchanger unit and T_i-T_r<*10*°C, the optimum effectiveness is better than 82%. The optimum effectiveness compares well when compared with conventional heat exchangers utilizing PCM for thermal energy storage which have an optimum effectiveness of 0.68-0.75 for a tube in PCM arrangement [49], less than 0.67 for PCM encapsulated in plates arrangement [234], and 0.5-0.7 for PCM and gas direct contact arrangement [235].

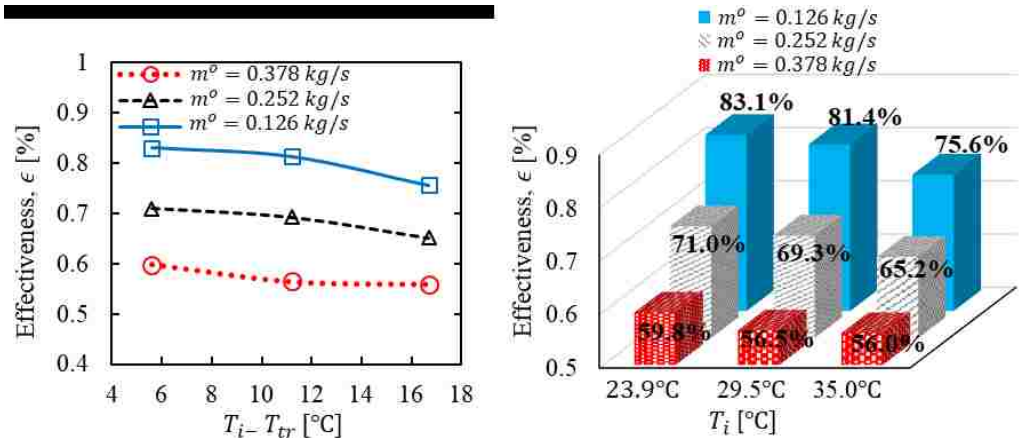

Figure 7.15. Effectiveness of the PCM heat exchanger at various inlet conditions.

It can be concluded that an effectiveness of more than 80% was possible even when the fluid inlet temperature was 10 °C higher than the phase transition temperature of PCM. As the effectiveness somewhat decreases with increasing mass flow rate, the effectiveness can still be maintained at >80% by fixing the mass flow rate per unit and increasing the number of heat exchanger units by installing them in parallel. This way each unit can run at the optimum effectiveness for the required total mass flow rate and design inlet temperature. For instance, 20 heat exchanger units can be connected in parallel each at 0.252 kg/s per unit giving a total mass flow rate of 5.04 Kg/s for the entire system at any inlet temperature of T_i-T_r<*10* °C to maintain an effectiveness of 70% or higher.

It was noted that the effect of varying the mass flow rate on the cumulative energy storage is very less determinative when compared to that of the inlet fluid temperature as shown in Figure 7.13. Theoretically, for the same inlet temperature the cumulative energy storage of various mass flow rates should be the same in an ideal case. A trend of very slight increase in the cumulative energy storage was observed for the experiments of higher mass flow rates for the same inlet temperatures. This may be due to the higher overall heat transfer coefficients and shorter experimental time during which the charging process was completed for the higher mass flow rates at the same inlet temperature. As previously discussed, The shorter experimental time for heat leakage resulted in less “cold energy loss [233], whereas the higher overall heat transfer coefficient helps in utilizing more PCMs far away from the plates. For these reasons, a trend of somewhat higher cumulative energy storage is observed for the experiments at higher flow rates and same inlet. Whereas the lower effectiveness at higher flow rates as shown in Figure 7.15 may results in larger deviations between leaving water temperature and the phase transition temperature, a

different PCM with lower phase change temperature can be utilized to achieve the same high cumulative energy storage at high flow rates as well as relatively lower leaving water temperature as required by the end user's or the thermal load system. For that reason, the performance of a PCM heat exchanger can be described with respect to the difference between T_o and T_r (T_o-T_{tr}) as a function of (T_i-T_{tr}) and mass flow rate (m^o). This trend is shown in Figure 7.16. The leaving water temperature follows a linear trend with increase in inlet water temperature. This can be extrapolated to suit the actual operating conditions and predict the average outlet temperature with respect to the inlet conditions.

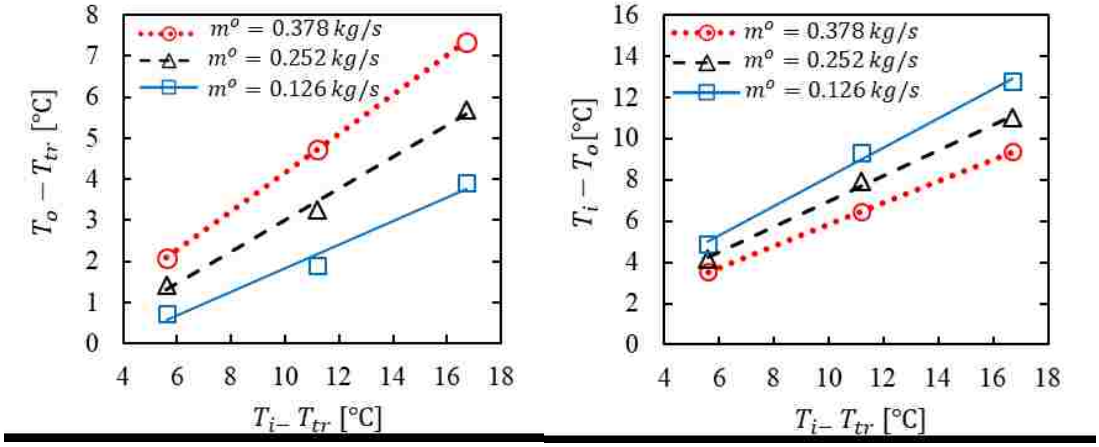

Figure 7.16. Outlet temperature as a function of PCM transition temperature, inlet temperature and mass flow rate.

Figure 7.17 provides the discharge (freezing) profiles for various inlet conditions. The discharge time is one of the most parameters to consider along with the discharging inlet temperature as it is important in determining the rate at which energy can be extracted.

In general, the discharge time needs to be as short as possible to reduce that time at which the chiller will be running during the off-peak hours. In addition, the inlet temperature during the discharge (freezing the PCM during off-peak hours) needs to be as high as reasonably possible because chillers are more efficient at higher temperatures, thus reducing cost and energy consumption. For that reason, only a high mass flow rate (0.378 kg/s) was used for all the discharging experiments at various discharge inlet temperatures of (12.8 ℃, 10 ℃ and 7.2 ℃).

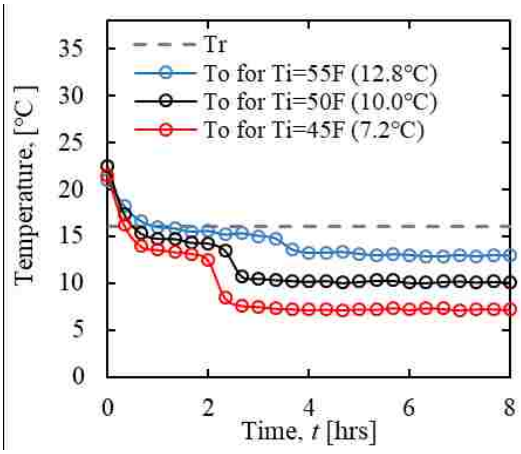

Figure 7.17. Discharge profiles for various inlet condition.

The freezing temperature-time curves show some important trends: First, the discharge profiles showed a reasonably shorter latent heat period when compared to the charging profiles of the same mass flow rate (0.3785 kg/s) and (T_i-T_r) temperature differences (i.e. T_{tr}-T_i=5.5 ºC for discharge, and T_i-T_{tr}=5.6 ºC for charge). As previously discussed, during a discharge process the PCM next to the heat exchanger plates will solidify, forming a thin film of PCM layer that is 94% higher in thermal conductivity. This

in contrast to the self-shielding effect during the charging process. Second, The temperature-time curves in Figure 7.17 for all the discharge process are somewhat more pronounced in the region of phase transition latent heat when compared to that for the charging curves in Figure 7.12, in part due to the narrower liquid to solid phase transition peak as supported by the differential calorimetric measurements (Figure 7.9), and in part due to the higher thermal conductivity and thermal diffusivity [231] for the solid PCM during liquid to solid phase transition which results in lower temperature gradient.

7.6.3. Parametric Analysis. A summary of the thermal characteristics of the heat exchanger is presented in Table 7.8. The energy efficiency was calculated based on the thermodynamic calculations given in Section 7.4. The physical significance of energy efficiency is to compare the total amount of available energy storage in the PCM to the amount of energy stored in the PCM. Higher mass flow rates and higher inlet temperatures showed higher efficiencies. This was attributed to the fact that higher inlet temperatures or flow rates achieve a smaller experimental time which reduces the time for heat leakage, thus increasing the efficiency as opposed to lower inlet flow rates and temperatures. The experimental times for various inlet conditions are given in Table 7.8. It is also suggested that for higher flow rates (higher UA values) there will be higher chances to utilize the PCMs next to the vessel walls at the peripheries, hence increasing the amount of PCM that can be utilized for energy storage and enhancing the stored energy to available energy ratio (efficiency). Higher inlet temperatures also include higher available sensible heat capacity in the vessel structure and aluminum plates; This amount however is relatively very small compared to the latent heat capacity of PCM.

Table 7.8. Summary for thermal characteristics of the heat exchanger at various operating conditions.

m^o kg/s	$T_i - T_{tr}$ [℃]	$T_i - T_o$ [℃]	$\mathcal{E}_{effectivene}$	Energy Efficiency η	UA [W/K]	Storage time [hr]	Total energy storage [kJ]
0.126	5.6	4.9	0.831	0.533	921.0	8.6	=N*67,069
	11.2	9.3	0.814	0.688	870.0	5.1	=N*90,850
	16.7	12.8	0.756	0.817	735.5	4.2	=N*113,309
0.252	5.6	4.2	0.710	0.570	1293.9	7.1	=N*71,693
	11.2	7.9	0.693	0.766	1233.5	4.1	=N*101,173
	16.7	11.0	0.652	0.886	1057.7	3.5	=N*122,621
0.378	5.6	3.5	0.598	0.603	1434.7	5.9	=N*75,850
	11.2	6.5	0.565	0.793	13089	3.5	=N*104,743
	16.7	9.4	0.560	0.919	1285.8	2.7	=N*127,299

Table 7.8 also presented the cumulative energy storage that can be stored where *N* is the number of heat exchanger units. Parametric analysis was conducted to predict the number of heat exchanger units as a function of the thermal load demand of the end user or heat load of the system. As given in equation 37, Figure 7.18 presented the required number of heat exchanger units (*N*) required to supply a certain thermal load in kWh. Here, the necessary number of heat exchanger units was evaluated on the bases of monthly kWh requirements of the facility/thermal load using the thermal energy storage heat exchanger at a particular inlet conditions. For the monthly kWh requirements, it was assumed that each thermal energy storage unit will be charged and discharged once per day, for a total of 30 thermal cycles per month as given in equation 37. For *N* number of heat exchanger units installed in parallel, the thermal characteristics and operating conditions of each heat exchanger unit is supposed to remain the same and within the experimental conditions with a total mass flow rate for the entire system equals to $N * m^o$ and total energy storage of

$N * Q(kWh)$. The experimental conditions in the legend of Figure 7.18 represents the inlet conditions of each heat exchanger unit, hence for N heat exchanger units the inlet temperature for each unit will be the same as those T_i values in the legend for a given T_r, whereas the mass flow rate of the entire system will be the product of N and the m^o value in the legend to meet the required thermal load (Q_{load}) value. T_o is a function of T_i, T_r and m^o per unit as given in Figure 7.16.

$$N[\#] = \frac{thermal\ load}{\int_0^t Q_{exp}^o\, dt} = \frac{thermal\ load\ \left[\frac{kWh}{month}\right]}{Q_{exp}\left[\frac{MJ}{thermal\ cycle}\right] * \frac{1}{3.6}\left[\frac{kWh}{MJ}\right] * 30\left[\frac{thermal\ cycle}{month}\right]} \tag{37}$$

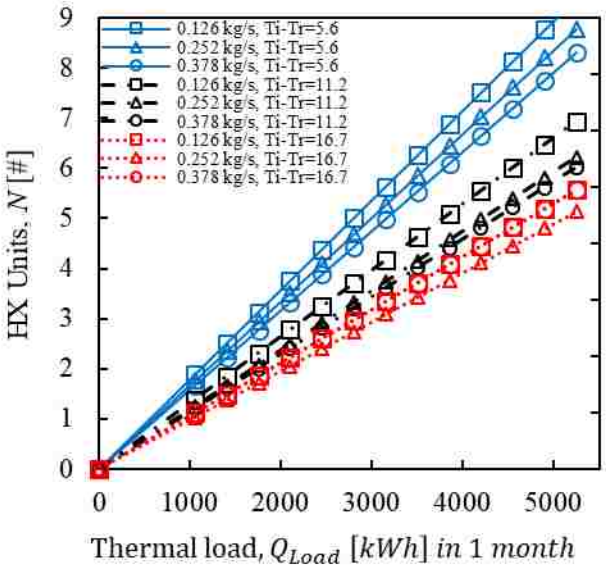

Figure 7.18. The required number of heat exchanger units as a function of monthly thermal load at various operating/inlet conditions.

7.7. FINDINGS AND PERFORMANCE REMARKS

Energy analysis was carried out for a PCM thermal energy storage unit in the form of parallel-plate heat exchanger. The following remarks can be concluded from the current study:

- Compared to sensible heat systems, the latent heat storage of PCM in the current design can provide larger energy storage capacity using smaller foot-print and constant supply temperature during the phase transition.
- Compared to ice storage latent heat systems, the PCM system can deliver substantial benefits not only as thermal energy but provide savings in infrastructure, equipment and operational maintenance costs.
- The PCM design storage temperature (18.3 ºC) in this study provides a unique opportunity for energy storage and load shifting in data centers.
- This demonstration will be the first of its kind for modern data centers by implementing such passive PCM latent heat storage system that can be discharged at reduced demand charges without the need for mechanical systems or in other cases using much smaller chillers, and help to avoid the huge on-peak demand charges of existing chillers.
- The leaving water temperatures, energy storage profiles, effectiveness and efficiency were studied at various inlet conditions.
- Parametric analysis was carried out to predict the number of heat exchanger units required to meet a certain thermal load.

Because of the narrow design of the channels in the plates where the heat exchange fluid is circulated, the heat exchanger plates may be subject to fouling. Therefore, pre-filtration or cooling water debris filters need to be installed and regularly checked for maintenance in case of any precipitation.

In future research efforts, different type of immersion plates such as those in Figure 7.19 will be considered. With this design, it will also be interesting to test a reversed arrangement where the PCMs are encapsulated in the plates and the heat transfer fluid (water) flows through the shell side.

Figure 7.19. Immersion plates manufactured by Omega Thermo Products

8. CONCLUSION

Thermal energy storage using Phase Change Materials (PCMs) presents a unique solution to reduce energy consumption, greenhouse gases emission and dependency on fossil fuels. While PCMs are being introduced into many applications for thermal energy storage, continuous refinements and improvements are needed to match the requirements of the vast number of their applications of PCMs. The accomplishments resulting from this effort include:

- Verified and improved a number of key factors affecting the performance of PCMs which resulted in a more scientific design approach for developing eutectic PCMs.
- Presented techniques to develop PCMs characterized by an enhanced thermal performance, as well as novel (Solid to Gel) shape-stable eutectic PCM and reduced supercooling.
- Studied PCMs with phase transition temperature in the range 70 ºC to 90 ºC and proposed a new system to solve many of the design issues of the nuclear ice condenser system in Small Modular Reactors (SMRs).
- Discussed the technical and design aspects of a coupled nuclear reactor thermal energy storage system utilizing high-temperature PCMs for load shifting, and identified wide range of binary and ternary mixtures of high-temperature eutectic PCMs as potential candidates.
- Characterized a parallel-plate heat exchanger utilizing PCMs which was built and experimentally studied for thermal energy storage applications and load shifting purposes.

REFERENCES

1. EIA, *International energy outlook*, in *U.S. Energy Information Administration*. 2017.

2. Saeed, R.M., et al., *Uncertainty of Thermal Characterization of Phase Change Material by Differential Scanning Calorimetry Analysis.* International Journal of Engineering Research & Technology, 2016. **5**(1): p. 405-412.

3. Saeed, R.M., et al., *Preparation and thermal performance of methyl palmitate and lauric acid eutectic mixture as phase change material (PCM).* Journal of Energy Storage, 2017. **13**: p. 418-424.

4. Saeed, R.M., et al., *Preparation and enhanced thermal performance of novel (solid to gel) form-stable eutectic PCM modified by nano-graphene platelets.* Journal of Energy Storage, 2018. **15**: p. 91-102.

5. Saeed, R.M.R., *Thermal characterization of phase change materials for thermal energy storage*. 2016: Missouri University of Science and Technology.

6. Ercan, A.O., *Storage of thermal energy*. Energy Storage Systems, Eolss Publishers, 2006.

7. Paksoy, H.Ö., *Thermal energy storage for sustainable energy consumption: fundamentals, case studies and design*. Vol. 234. 2007: Springer Science & Business Media.

8. Teng, T.-P. and C.-C. Yu, *The Effect on Heating Rate for Phase Change Materials Containing MWCNTs.* International Journal of Chemical Engineering and Applications, 2012. **3**(5): p. 340-342.

9. Mehrali, et al., *Shape-stabilized phase change materials with high thermal conductivity based on paraffin/graphene oxide composite.* Energy Conversion and Management, 2013. **67**: p. 275-282.

10. Alkan, C. and A. Sari, *Fatty acid/poly (methyl methacrylate)(PMMA) blends as form-stable phase change materials for latent heat thermal energy storage.* Solar Energy, 2008. **82**(2): p. 118-124.

11. Lazaro, A., et al., *Intercomparative tests on phase change materials characterisation with differential scanning calorimeter.* Applied Energy, 2013. **109**: p. 415-420.

12. Sharma, S.D., H. Kitano, and K. Sagara, *Phase change materials for low temperature solar thermal applications.* Res. Rep. Fac. Eng. Mie Univ, 2004. **29**(1).

13. Lane, G.A., et al. *Heat of fusion systems for solar energy storage*. in *Proc. Workshop on Solar Energy Storage Subsystems for the Heating and Cooling of Buildings*. 1975.

14. Herrick, C. and D. Golibersuch, *Qualitative behavior of a new latent heat storage device for solar heating/cooling systems*. 1977: General Electric Company Corporate Research and Development.

15. Lane, G., *Macro-encapsulation of PCM.* Report No. oro/5117-8, Dow Chemical Company, Midland, Michigan, 1978. **152**.

16. Abhat, A., *Low temperature latent heat thermal energy storage: heat storage materials.* Solar energy, 1983. **30**(4): p. 313-332.

17. Khudhair, A.M. and M.M. Farid, *A review on energy conservation in building applications with thermal storage by latent heat using phase change materials.* Energy conversion and management, 2004. **45**(2): p. 263-275.

18. Oró, E., et al., *Review on phase change materials (PCMs) for cold thermal energy storage applications.* Applied Energy, 2012. **99**: p. 513-533.

19. Safari, A., et al., *A review on supercooling of Phase Change Materials in thermal energy storage systems.* Renewable and Sustainable Energy Reviews, 2017. **70**: p. 905-919.

20. Sharma, A., et al., *Review on thermal energy storage with phase change materials and applications.* Renewable and Sustainable Energy Reviews, 2007. **13**(2): p. 318-345.

21. Zalba, B., et al., *Review on thermal energy storage with phase change: materials, heat transfer analysis and applications.* Applied thermal engineering, 2003. **23**(3): p. 251-283.

22. Mehling, H. and L.F. Cabeza, *Heat and cold storage with PCM*. 2008: Springer.

23. Baran, G. and A. Sari, *Phase change and heat transfer characteristics of a eutectic mixture of palmitic and stearic acids as PCM in a latent heat storage system.* Energy Conversion and Management, 2003. **44**(20): p. 3227-3246.

24. Soares, N.M.L., *Thermal energy storage with phase change materials (PCMs) for the improvement of the energy performance of buildings*. 2016.

25. Mehling, H. and L. Cabeza, *Heat and cold storage with PCM: An up to date introduction into basics and applications 2008.* Berlin: Springer. **16**(308): p. 4.

26. Castellón, C., et al., *Determination of the enthalpy of PCM as a function of temperature using a heat-flux DSC—A study of different measurement procedures and their accuracy.* Int J Energy Res, 2008. **32**(13): p. 1258–1265.

27. Kumar, R.S. and D.J. Krishna. *Differential Scanning Calorimetry (DSC) Analysis Of Latent Heat Storage Materials For Low Temperature (40-80oC) Solar Heating Applications*. in *International Journal of Engineering Research and Technology*. 2013. ESRSA Publications.

28. Braga, C.I., M.C. Rezende, and M.L. Costa, *Methodology for DSC calibration in high heating rates.* Journal of Aerospace Technology and Management, 2011. **3(**2): p. 179-192.

29. Mehling, H., et al. *A new measurement and evaluation method for DSC of PCM samples*. in *Proceedings of Effstock-11th International Conference on Energy Storage, Stockholm, Sweden*. 2009.

30. Li, X., J.G. Sanjayan, and J.L. Wilson, *Fabrication and stability of form-stable diatomite/paraffin phase change material composites.* Energy and Buildings, 2014. **76**: p. 284-294.

31. Tyagi, V.V. and D. Buddhi, *PCM thermal storage in buildings: a state of art.* Renewable and Sustainable Energy Reviews, 2007. **11**(6): p. 1146-1166.

32. Ryu, H.W., et al., *Prevention of supercooling and stabilization of inorganic salt hydrates as latent heat storage materials.* Solar energy materials and solar cells, 1992. **27**(2): p. 161-172.

33. Qian, T., et al., *The preparation of a green shape-stabilized composite phase change material of polyethylene glycol/SiO 2 with enhanced thermal performance based on oil shale ash via temperature-assisted sol–gel method.* Solar Energy Materials and Solar Cells, 2015. **132**: p. 29-39.

34. Lane, G., *Solar heat storage: Latent heat materials. Volume II. Technology*. 1986, Dow Chemical Co., Midland, MI.

35. Beare-Rogers, J., A. Dieffenbacher, and J. Holm, *Lexicon of lipid nutrition (IUPAC Technical Report).* Pure and Applied Chemistry, 2001. **73**(4): p. 685-744.

36. Khoo, I.-C. and S.-T. Wu, *Optics and nonlinear optics of liquid crystals*. Vol. 1. 1993: World Scientific.

37. Zhang, Y., Y. Su, and X. Ge, *Prediction of the melting temperature and the fusion heat of (quasi-) eutectic PCM.* Journal of China University of Science and Technology, 1994. **25**(4): p. 474-478.

38. Zhao, P., et al., *Study on phase diagram of fatty acids mixtures to determine eutectic temperatures and the corresponding mixing proportions.* Applied Energy, 2014. **115**: p. 483-490.

39. Buckley, T.M., *Phase change material thermal capacitor clothing*. 2005, Google Patents.

40. Gendreau, K.C., et al. *The neutron star interior composition explorer (NICER): design and development*. in *SPIE Astronomical Telescopes+ Instrumentation*. 2016. International Society for Optics and Photonics.

41. Barlev, D., R. Vidu, and P. Stroeve, *Innovation in concentrated solar power.* Solar Energy Materials and Solar Cells, 2011. **95**(10): p. 2703-2725.

42. Fleischer, A.S., *Thermal energy storage using phase change materials: Fundamentals and applications*. 2015: Springer.

43. Guillot, S., et al., *Corrosion effects between molten salts and thermal storage material for concentrated solar power plants.* Applied Energy, 2012. **94**: p. 174-181.

44. Ghoneim, A., *Comparison of theoretical models of phase-change and sensible heat storage for air and water-based solar heating systems.* Solar Energy, 1989. **42**(3): p. 209-220.

45. Bansal, N. and D. Buddhi, *An analytical study of a latent heat storage system in a cylinder.* Energy conversion and management, 1992. **33**(4): p. 235-242.

46. Chaurasia, P. *Phase change material in solar water heater storage system*. in *Proceedings of the 8th international conference on thermal energy storage*. 2000.

47. Bajnóczy, G., et al., *Heat storage by two-grade phase change material.* Chemical Engineering, 1999. **43**(2): p. 137-147.

48. Kaygusuz, K., *Experimental and theoretical investigation of latent heat storage for water based solar heating systems.* Energy conversion and management, 1995. **36**(5): p. 315-323.

49. Tay, N., M. Belusko, and F. Bruno, *Designing a PCM storage system using the effectiveness-number of transfer units method in low energy cooling of buildings.* Energy and Buildings, 2012. **50**: p. 234-242.

50. Zhang, M., M.A. Medina, and J.B. King, *Development of a thermally enhanced frame wall with phase-change materials for on-peak air conditioning demand reduction and energy savings in residential buildings.* International Journal of Energy Research, 2005. **29**(9): p. 795-809.

51. Shilei, L., Z. Neng, and F. Guohui, *Eutectic mixtures of capric acid and lauric acid applied in building wallboards for heat energy storage.* Energy and Buildings, 2006. **38**(6): p. 708-711.

52. Fang, G., S. Wu, and X. Liu, *Experimental study on cool storage air-conditioning system with spherical capsules packed bed.* Energy and Buildings, 2010. **42**(7): p. 1056-1062.

53. Dolado, P., et al., *Experimental validation of a theoretical model: uncertainty propagation analysis to a PCM-air thermal energy storage unit.* Energy and Buildings, 2012. **45**: p. 124-131.

54. Biwole, P.H., P. Eclache, and F. Kuznik, *Phase-change materials to improve solar panel's performance.* Energy and Buildings, 2013. **62**: p. 59-67.

55. Zuo, J., W. Li, and L. Weng, *Thermal performance of caprylic acid/1-dodecanol eutectic mixture as phase change material (PCM).* Energy and Buildings, 2011. **43**(1): p. 207-210.

56. de Gracia, A. and L.F. Cabeza, *Phase change materials and thermal energy storage for buildings.* Energy and Buildings, 2015. **103**: p. 414-419.

57. Zhou, G., et al., *An assessment of mixed type PCM-gypsum and shape-stabilized PCM plates in a building for passive solar heating.* Solar energy, 2007. **81**(11): p. 1351-1360.

58. Biwole, P., P. Eclache, and F. Kuznik. *Improving the performance of solar panels by the use of phase-change materials*. in *World Renewable Energy Congress*. 2011.

59. Hendricks, J. and W. Sark, *Annual performance enhancement of building integrated photovoltaic modules by applying phase change materials.* Progress in Photovoltaics: Research and Applications, 2013. **21**(4): p. 620-630.

60. Baetens, R., B.P. Jelle, and A. Gustavsen, *Phase change materials for building applications: a state-of-the-art review.* Energy and Buildings, 2010. **42**(9): p. 1361-1368.

61. Emery, K., et al. *Temperature dependence of photovoltaic cells, modules and systems*. in *Photovoltaic Specialists Conference, 1996., Conference Record of the Twenty Fifth IEEE*. 1996. IEEE.

62. Radziemska, E. and E. Klugmann, *Thermally affected parameters of the current–voltage characteristics of silicon photocell.* Energy Conversion and Management, 2002. **43**(14): p. 1889-1900.

63. Hasan, A., et al., *Increased photovoltaic performance through temperature regulation by phase change materials: Materials comparison in different climates.* Solar Energy, 2015. **115**: p. 264-276.

64. Atkin, P. and M.M. Farid, *Improving the efficiency of photovoltaic cells using PCM infused graphite and aluminium fins.* Solar Energy, 2015. **114**: p. 217-228.

65. Ma, T., et al., *Using phase change materials in photovoltaic systems for thermal regulation and electrical efficiency improvement: A review and outlook.* Renewable and Sustainable Energy Reviews, 2015. **43**: p. 1273-1284.

66. Kandasamy, R., X.-Q. Wang, and A.S. Mujumdar, *Transient cooling of electronics using phase change material (PCM)-based heat sinks.* Applied Thermal Engineering, 2008. **28**(8): p. 1047-1057.

67. Alrashdan, A., A.T. Mayyas, and S. Al-Hallaj, *Thermo-mechanical behaviors of the expanded graphite-phase change material matrix used for thermal management of Li-ion battery packs.* Journal of Materials Processing Technology, 2010. **210**(1): p. 174-179.

68. Yin, H., et al., *Experimental research on heat transfer mechanism of heat sink with composite phase change materials.* Energy Conversion and Management, 2008. **49**(6): p. 1740-1746.

69. Tan, F. and C. Tso, *Cooling of mobile electronic devices using phase change materials.* Applied thermal engineering, 2004. **24**(2): p. 159-169.

70. Zhang, X., *Heat-storage and thermo-regulated textiles and clothing.* Smart fibres, fabrics and clothing, Woodhead Publishing, UK, 2001: p. 34-57.

71. Lv, Y., Y. Zou, and L. Yang, *Feasibility study for thermal protection by microencapsulated phase change micro/nanoparticles during cryosurgery.* Chemical Engineering Science, 2011. **66**(17): p. 3941-3953.

72. Wang, C., et al., *Highly sensitive thermal detection of thrombin using aptamer-functionalized phase change nanoparticles.* Biosensors and Bioelectronics, 2010. **26**(2): p. 437-443.

73. Hauer, A., et al., *Advanced Thermal Energy Storage through Phase Change Materials and Chemical Reactions–Feasibility Studies and Demonstration Projects.* IEA, Final Report, 2001.

74. Ismail, K. and J. Henríquez, *Thermally effective windows with moving phase change material curtains.* Applied Thermal Engineering, 2001. **21**(18): p. 1909-1923.

75. Ling, Z., et al., *Experimental and numerical investigation of the application of phase change materials in a simulative power batteries thermal management system.* Applied Energy, 2014. **121**: p. 104-113.

76. Vasiliev, L., et al., *Latent heat storage modules for preheating internal combustion engines: application to a bus petrol engine.* Applied thermal engineering, 2000. **20**(10): p. 913-923.

77. Blüher, P., *Latentwärmespeicher erhöht den Fahrkomfort und die Fahrsicherheit.* Automobiltechnische Zeitschrift, 1991. **93**(10).

78. Gin, B., M. Farid, and P. Bansal, *Effect of door opening and defrost cycle on a freezer with phase change panels.* Energy Conversion and Management, 2010. **51**(12): p. 2698-2706.

79. Ahmed, M., O. Meade, and M.A. Medina, *Reducing heat transfer across the insulated walls of refrigerated truck trailers by the application of phase change materials.* Energy Conversion and Management, 2010. **51**(3): p. 383-392.

80. Buddhi, D., et al., *A simplification of the differential thermal analysis method to determine the latent heat of fusion of phase change materials.* Journal of Physics D: Applied Physics, 1987. **20**(12): p. 1601.

81. Hasan, A., et al., *Characterization of phase change materials for thermal control of photovoltaics using Differential Scanning Calorimetry and Temperature History Method.* Energy Conversion and Management, 2014. **81**: p. 322-329.

82. He, B., V. Martin, and F. Setterwall, *Phase transition temperature ranges and storage density of paraffin wax phase change materials.* Energy, 2004. **29**(11): p. 1785-1804.

83. Danley, R.L., *Heat flux differential scanning calorimeter sensor*. 2002, Google Patents.

84. Riesen, R., *Simple determination of the thermal conductivity of polymers by DSC.* UserCom, 2005. **22**(2): p. 2005.

85. Merzlyakov, M. and C. Schick, *Thermal conductivity from dynamic response of DSC.* Thermochimica acta, 2001. **377**(1): p. 183-191.

86. TA-Instruments. *FOX 314*. 2017 12/24/2017]; Available from: http://www.tainstruments.com/fox-314/.

87. *National Institute of Standards and Technology*. 2015; Available from: http://www.nist.gov/index.cfm.

88. Linseis. *User's Manual of Transient Hot Bridge Analyzer THB*. 2013; Available from: http://www.linseis.com/.

89. EIA, *Monthly Energy Review*. 2016, U.S Energy Information Administration: Washington, DC.

90. *Annual Energy Outlook, Energy information administration.* Department of Energy, 2016.

91. Kośny, J., D. Yarbrough, and W. Miller, *Use of PCM-enhanced insulations in the building envelope.* Journal of Building Enclosure Design, 2008: p. 55-59.

92. Zhang, Z., et al., *Thermal energy storage cement mortar containing n-octadecane/expanded graphite composite phase change material.* Renewable energy, 2013. **50**: p. 670-675.

93. Li, M., Z. Wu, and J. Tan, *Heat storage properties of the cement mortar incorporated with composite phase change material.* Applied Energy, 2013. **103**: p. 393-399.

94. Barreneche, C., et al., *Improvement of the thermal inertia of building materials incorporating PCM. Evaluation in the macroscale.* Applied Energy, 2013. **109**: p. 428-432.

95. The American Society of Heating, R.a.A.-C.E.A.S., *Thermal environmental conditions for human occupancy.* 2013.

96. Karkri, M., et al., *Thermal properties of smart microencapsulated paraffin/plaster composites for the thermal regulation of buildings.* Energy and Buildings, 2015. **88**: p. 183-192.

97. Cao, L., F. Tang, and G. Fang, *Synthesis and characterization of microencapsulated paraffin with titanium dioxide shell as shape-stabilized thermal energy storage materials in buildings.* Energy and Buildings, 2014. **72**: p. 31-37.

98. Cabeza, L.F., et al., *Materials used as PCM in thermal energy storage in buildings: a review.* Renewable and Sustainable Energy Reviews, 2011. **15**(3): p. 1675-1695.

99. Luo, Z., et al., *Fabrication and characterization of form-stable capric-palmitic-stearic acid ternary eutectic mixture/nano-SiO2 composite phase change material.* Energy and Buildings, 2017. **147**: p. 41-46.

100. Han, L., et al., *Thermal properties and stabilities of the eutectic mixture: 1, 6-hexanediol/lauric acid as a phase change material for thermal energy storage.* Applied Thermal Engineering, 2017. **116**: p. 153-159.

101. Pielichowska, K. and K. Pielichowski, *Phase change materials for thermal energy storage.* Progress in Materials Science, 2014. **65**: p. 67-123.

102. Liston, L.C., *Using mixtures of fatty acid methyl esters as phase change materials for concrete*. 2015, Purdue University.

103. Sarı, A., *Thermal characteristics of a eutectic mixture of myristic and palmitic acids as phase change material for heating applications.* Applied Thermal Engineering, 2003. **23**(8): p. 1005-1017.

104. Sarı, A., C. Alkan, and A.N. Özcan, *Synthesis and characterization of micro/nano capsules of PMMA/capric–stearic acid eutectic mixture for low temperature-thermal energy storage in buildings.* Energy and Buildings, 2015. **90**: p. 106-113.

105. Karaipekli, A. and A. Sarı, *Preparation, thermal properties and thermal reliability of eutectic mixtures of fatty acids/expanded vermiculite as novel form-stable composites for energy storage.* Journal of Industrial and Engineering Chemistry, 2010. **16**(5): p. 767-773.

106. Kahwaji, S., et al., *Stable, low-cost phase change material for building applications: the eutectic mixture of decanoic acid and tetradecanoic acid.* Applied Energy, 2016. **168**: p. 457-464.

107. Thambidurai, M., K. Panchabikesan, and V. Ramalingam, *Review on phase change material based free cooling of buildings—the way toward sustainability.* Journal of Energy Storage, 2015. **4**: p. 74-88.

108. Tian, H., et al., *Preparation of binary eutectic chloride/expanded graphite as high-temperature thermal energy storage materials.* Solar Energy Materials and Solar Cells, 2016. **149**: p. 187-194.

109. Yanping, Y., et al., *Theoretic prediction of melting temperature and latent heat for a fatty acid eutectic mixture.* Journal of Chemical & Engineering Data, 2011. **56**(6): p. 2889-2891.

110. Nikolić, R., et al., *New materials for solar thermal storage—solid/liquid transitions in fatty acid esters.* Solar energy materials and solar cells, 2003. **79**(3): p. 285-292.

111. Brown, M.E. and P.K. Gallagher, *Handbook of thermal analysis and calorimetry: recent advances, techniques and applications*. Vol. 5. 2011: Elsevier.

112. Marriott, R.A., et al., *Technique for determination of accurate heat capacities of volatile, powdered, or air-sensitive samples using relaxation calorimetry.* Review of Scientific Instruments, 2006. **77**(9): p. 096108.

113. Fan, L. and J.M. Khodadadi, *Thermal conductivity enhancement of phase change materials for thermal energy storage: a review.* Renewable and Sustainable Energy Reviews, 2011. **15**(1): p. 24-46.

114. Mills, A., et al., *Thermal conductivity enhancement of phase change materials using a graphite matrix.* Applied Thermal Engineering, 2006. **26**(14-15): p. 1652-1661.

115. Kutz, M., *Mechanical Engineers' Handbook, Volume 1: Materials and Engineering Mechanics*. 2015: John Wiley & Sons.

116. Liston, L.C., et al., *Binary mixtures of fatty acid methyl esters as phase change materials for low temperature applications.* Applied Thermal Engineering, 2016. **96**: p. 501-507.

117. Kosny, J., N. Shukla, and A. Fallahi, *Cost analysis of simple phase change material-enhanced building envelopes in southern US climates.* US Department of Energy, 2013.

118. Cheng, R., et al., *A new method to determine thermophysical properties of PCM-concrete brick.* Applied Energy, 2013. **112**: p. 988-998.

119. Socaciu, L.G., *Thermal energy storage with phase change material.* Leonardo Electronic Journal of Practices and Technologies, 2012(20): p. 75-98.

120. Félix, M. and J. Aguiar, *Study of a cement mortar with incorporation of PCM microcapsules.* 2009.

121. Zhang, L. and G. Shi, *Preparation of highly conductive graphene hydrogels for fabricating supercapacitors with high rate capability.* The Journal of Physical Chemistry C, 2011. **115**(34): p. 17206-17212.

122. Li, H., et al., *Development of thermal energy storage composites and prevention of PCM leakage.* Applied Energy, 2014. **135**: p. 225-233.

123. Lee, T., et al., *Control aspects of latent heat storage and recovery in concrete.* Solar energy materials and solar cells, 2000. **62**(3): p. 217-237.

124. Hadjieva, M., R. Stoykov, and T. Filipova, *Composite salt-hydrate concrete system for building energy storage.* Renewable Energy, 2000. **19**(1): p. 111-115.

125. Sarı, A., *Form-stable paraffin/high density polyethylene composites as solid–liquid phase change material for thermal energy storage: preparation and thermal properties.* Energy Conversion and Management, 2004. **45**(13): p. 2033-2042.

126. Nasef, M.M. and E.-S.A. Hegazy, *Preparation and applications of ion exchange membranes by radiation-induced graft copolymerization of polar monomers onto non-polar films.* Progress in Polymer Science, 2004. **29**(6): p. 499-561.

127. Sarı, A., et al., *Synthesis and thermal energy storage characteristics of polystyrene-graft-palmitic acid copolymers as solid–solid phase change materials.* Solar Energy Materials and Solar Cells, 2011. **95**(12): p. 3195-3201.

128. Pielichowska, K. and K. Pielichowski, *Biodegradable PEO/cellulose-based solid–solid phase change materials.* Polymers for Advanced Technologies, 2011. **22**(12): p. 1633-1641.

129. Fang, X., Z. Zhang, and Z. Chen, *Study on preparation of montmorillonite-based composite phase change materials and their applications in thermal storage building materials.* Energy conversion and management, 2008. **49**(4): p. 718-723.

130. Zheng, S., S. Wu, and G. Xu, *Melting intercalation method to prepare lauric acid/organophilic montmorillonite shape-stabilized phase change material.* Journal of Wuhan University of Technology-Mater. Sci. Ed., 2010. **25**(4): p. 674-677.

131. Sarier, N. and E. Onder, *The manufacture of microencapsulated phase change materials suitable for the design of thermally enhanced fabrics.* Thermochimica Acta, 2007. **452**(2): p. 149-160.

132. ZHANG, R., X. KE, and A. LI, *Preparation and Performance of Salt/ceramic Composite Energy Storage Materials [J]*. Chinese Journal of Material Research, 2000. **6**: p. 018.

133. Shin, D. and D. Banerjee, *Enhancement of specific heat capacity of high-temperature silica-nanofluids synthesized in alkali chloride salt eutectics for solar thermal-energy storage applications.* International journal of heat and mass transfer, 2011. **54**(5): p. 1064-1070.

134. Shin, D. and D. Banerjee, *Effects of silica nanoparticles on enhancing the specific heat capacity of carbonate salt eutectic (work in progress).* The International Journal of Structural Changes in Solids, 2010. **2**(2): p. 25-31.

135. Shin, D. and D. Banerjee, *Enhanced specific heat capacity of nanomaterials synthesized by dispersing silica nanoparticles in eutectic mixtures.* Journal of Heat Transfer, 2013. **135**(3): p. 032801.

136. Ran, S., et al., *Char barrier effect of graphene nanoplatelets on the flame retardancy and thermal stability of high-density polyethylene flame-retarded by brominated polystyrene.* Journal of Applied Polymer Science, 2014. **131**(15).

137. Johnson, M.B. and M.A. White, *Thermal methods.* Multi Length-Scale Characterisation, 2014: p. 63-119.

138. Teng, T.-P. and C.-C. Yu, *Characteristics of phase-change materials containing oxide nano-additives for thermal storage.* Nanoscale research letters, 2012. **7**(1): p. 1-10.

139. Tao, Y., C. Lin, and Y. He, *Preparation and thermal properties characterization of carbonate salt/carbon nanomaterial composite phase change material.* Energy Conversion and Management, 2015. **97**: p. 103-110.

140. Warzoha, R.J., et al. *Experimental characterization of the thermal diffusivity of paraffin phase change material embedded with herringbone style graphite nanofibers*. in *ASME 2012 Heat Transfer Summer Conference collocated with the ASME 2012 Fluids Engineering Division Summer Meeting and the ASME 2012 10th International Conference on Nanochannels, Microchannels, and Minichannels*. 2012. American Society of Mechanical Engineers.

141. Warzoha, R.J., R.M. Weigand, and A.S. Fleischer, *Temperature-dependent thermal properties of a paraffin phase change material embedded with herringbone style graphite nanofibers.* Applied Energy, 2015. **137**: p. 716-725.

142. Yuan, Y., et al., *Preparation and thermal characterization of capric–myristic–palmitic acid/expanded graphite composite as phase change material for energy storage.* Materials Letters, 2014. **125**: p. 154-157.

143. Tang, F., et al., *Synthesis and thermal properties of fatty acid eutectics and diatomite composites as shape-stabilized phase change materials with enhanced thermal conductivity.* Solar Energy Materials and Solar Cells, 2015. **141**: p. 218-224.

144. Li, M., et al., *Study on preparation and thermal property of binary fatty acid and the binary fatty acids/diatomite composite phase change materials.* Applied energy, 2011. **88**(5): p. 1606-1612.

145. Song, S., et al., *Stearic–capric acid eutectic/activated-attapulgiate composite as form-stable phase change material for thermal energy storage.* Energy Conversion and Management, 2014. **81**: p. 306-311.

146. Karaipekli, A. and A. Sarı, *Capric–myristic acid/expanded perlite composite as form-stable phase change material for latent heat thermal energy storage.* Renewable Energy, 2008. **33**(12): p. 2599-2605.

147. Cai, Y., et al., *Influences of expanded graphite on structural morphology and thermal performance of composite phase change materials consisting of fatty acid eutectics and electrospun PA6 nanofibrous mats.* Renewable energy, 2013. **57**: p. 163-170.

148. Zong, X., et al., *Fabrication and characterization of electrospun SiO 2 nanofibers absorbed with fatty acid eutectics for thermal energy storage/retrieval.* Solar Energy Materials and Solar Cells, 2015. **132**: p. 183-190.

149. Cai, Y., et al., *Effects of SiO 2 nanoparticles on structure and property of form-stable phase change materials made of cellulose acetate phase inversion membrane absorbed with capric-myristic-stearic acid ternary eutectic mixture.* Thermochimica Acta, 2017.

150. Zhang, X., et al., *Analysis of the nucleation of nanofluids in the ice formation process.* Energy Conversion and Management, 2010. **51**(1): p. 130-134.

151. Frank, F., *Supercooling of liquids.* Proceedings of the Royal Society of London. Series A, Mathematical and Physical Sciences, 1952: p. 43-46.

152. Sandnes, B. and J. Rekstad, *Supercooling salt hydrates: stored enthalpy as a function of temperature.* Solar Energy, 2006. **80**(5): p. 616-625.

153. Song, Q.-W., et al., *Supercooling of silver nano composite PCM microcapsules.* Journal of fiber bioengineering and informatics, 2008.

154. Lane, G., *Solar Heat Storage: Latent Heat Materials Volume I: Background and Scientific Principles. Vol. I. 1983, Florida*. CRC Press, Inc.

155. Alameri, S.A., *A coupled nuclear reactor thermal energy storage system for enhanced load following operation*. 2015: Colorado School of Mines.

156. C., J., *Returning To The Ice Condenser*, in *Action Economics*. 2014.

157. Pilch, M., K. Bergeron, and J. Gregory, *Assessment of the DCH Issue for Plants with Ice Condenser Containments*. 2000: The Office.

158. LOCHBAUM, D. *Nuclear Plant Containment Failure: Pre-Existing Damage*. Union of Concerned Scientists, 2016.

159. Diarce, G., et al., *Eutectic mixtures of sugar alcohols for thermal energy storage in the 50–90 C temperature range.* Solar Energy Materials and Solar Cells, 2015. **134**: p. 215-226.

160. Hidaka, H., et al., *New PCMs prepared from erythritol-polyalcohols mixtures for latent heat storage between 80 and 100 C.* Journal of chemical engineering of Japan, 2004. **37**(9): p. 1155-1162.

161. Kakiuchi, H. *A study of erythritol as phase change material*. in *IEA Annex 10, Phase Change Materials and Chemical Reactions for Thermal Energy Storage Second Workshop, Bulgaria, 1998*. 1998.

162. Tong, B., et al., *Thermodynamic investigation of several natural polyols (IV): heat capacities and thermodynamic properties of adonitol.* Thermochimica Acta, 2010. **499**(1): p. 117-122.

163. Lopes Jesus, A., et al., *Enthalpy of sublimation in the study of the solid state of organic compounds. Application to erythritol and threitol.* The Journal of Physical Chemistry B, 2005. **109**(38): p. 18055-18060.

164. Barone, G., et al., *Enthalpies and entropies of sublimation, vaporization and fusion of nine polyhydric alcohols.* Journal of the Chemical Society, Faraday Transactions, 1990. **86**(1): p. 75-79.

165. *BAKER HUGHES*. 12/28/2017]; Available from: https://www.bakerhughes.com/.

166. Kissin, Y.V., *Polyethylene: end-use properties and their physical meaning*. 2012: Carl Hanser Verlag GmbH Co KG.

167. Collins, P.M., *Dictionary of carbohydrates*. 1997: CRC Press.

168. Gombás, Á., et al., *Study of thermal behaviour of sugar alcohols.* Journal of thermal analysis and calorimetry, 2003. **73**(2): p. 615-621.

169. Bhadani, A., et al., *Sustainable oleic and stearic acid based biodegradable surfactants.* RSC Advances, 2017. **7**(17): p. 10433-10442.

170. Zhang, N., et al., *Preparation and properties of palmitic-stearic acid eutectic mixture/expanded graphite composite as phase change material for energy storage.* Energy, 2014. **78**: p. 950-956.

171. Liu, C., et al., *A novel PCM of lauric–myristic–stearic acid/expanded graphite composite for thermal energy storage.* Materials Letters, 2014. **120**: p. 43-46.

172. Zhang, S., W. Wu, and S. Wang, *Preparation, thermal properties and thermal reliability of a novel mid-temperature composite phase change material for energy conservation.* Energy, 2017.

173. Schaake, R., J. Van Miltenburg, and C. De Kruif, *Thermodynamic properties of the normal alkanoic acids II. Molar heat capacities of seven even-numbered normal alkanoic acids.* The Journal of Chemical Thermodynamics, 1982. **14**(8): p. 771-778.

174. Li, C., et al., *Enhanced performance and interfacial investigation of mineral-based composite phase change materials for thermal energy storage.* Scientific reports, 2013. **3**.

175. Latibari, S.T., et al., *Facile synthesis and thermal performances of stearic acid/titania core/shell nanocapsules by sol–gel method.* Energy, 2015. **85**: p. 635-644.

176. Moore, D.J., et al., *Infrared spectroscopy and differential scanning calorimetry studies of binary combinations of cis-6-octadecenoic acid and octadecanoic acid.* Chemistry and physics of lipids, 2007. **150**(1): p. 109-115.

177. Karaipekli, A., A. Sarı, and K. Kaygusuz, *Thermal conductivity improvement of stearic acid using expanded graphite and carbon fiber for energy storage applications.* Renewable Energy, 2007. **32**(13): p. 2201-2210.

178. Cheng, X., et al., *Effect of expanded graphite and carbon nanotubes on the thermal performance of stearic acid phase change materials.* Journal of Materials Science, 2017. **52**(20): p. 12370-12379.

179. Moreno, E., et al., *Polymorphism of even saturated carboxylic acids from n-decanoic to n-eicosanoic acid.* New Journal of Chemistry, 2007. **31**(6): p. 947-957.

180. Singleton, W., T. Ward, and F. Dollear, *Physical properties of fatty acids. I. Some dilatometric and thermal properties of stearic acid in two polymorphic forms.* Journal of the American Oil Chemists' Society, 1950. **27**(4): p. 143-146.

181. CHEMPOINT. *GRADES OF STEARIC ACID*. 2018 [cited 2018 January 2018]; Available from: https://www.chempoint.com/products/catalog/pmc-biogenix/pmc-fatty-acids/pmc-stearic-acid.

182. Univar-USA-Inc. *DP Double Pressed Stearic Acid*. 2018 [cited 2018 January 2018]; Available from: http://www.chemicalassociates.com/products/stearic-acid/rubber-grade-stearic-acid-detail.html.

183. Sarı, A. and K. Kaygusuz, *Some fatty acids used for latent heat storage: thermal stability and corrosion of metals with respect to thermal cycling.* Renewable Energy, 2003. **28**(6): p. 939-948.

184. Board, N., *Modern technology of oils, fats & its derivatives*. 2013: ASIA PACIFIC BUSINESS PRESS Inc.

185. Starrels, J., *Method of producing commercial stearic acid*. 1928, Google Patents.

186. Danley, R., *Differential scanning calorimeter sensor and method*. 2007, Google Patents.

187. Danley, R.L., *Differential scanning calorimeter*. 2003, Google Patents.

188. Danley, R.L., *New heat flux DSC measurement technique.* Thermochimica acta, 2002. **395**(1): p. 201-208.

189. Danley, R., T. Kelly, and J. Groh, *Improved DSC performance using Tzero technology.* International laboratory, 2001: p. 30-31.

190. Zhao, C.-Y., D. Zhou, and Z. Wu, *Heat transfer of phase change materials (PCMs) in porous materials.* Frontiers in Energy, 2011. **5**(2): p. 174-180.

191. Alameri, S.A., *A coupled nuclear reactor thermal energy storage system for enhanced load following operation.* 2007.

192. Li, Y., et al., *Load shifting of nuclear power plants using cryogenic energy storage technology.* Applied Energy, 2014. **113**: p. 1710-1716.

193. Zamengo, M., J. Ryu, and Y. Kato, *Chemical Heat Storage of Thermal Energy from a Nuclear Reactor by Using a Magnesium Hydroxide/Expanded Graphite Composite Material.* Energy Procedia, 2015. **71**: p. 293-305.

194. Lee, Y. and C.W. Forsberg, *Conceptual design of nuclear-geothermal energy storage systems for variable electricity production*. 2011, Massachusetts Institute of Technology. Center for Advanced Nuclear Energy Systems. Nuclear Energy and Sustainability Program.

195. Gomez, J., *High-temperature phase change materials (PCM) candidates for thermal energy storage (TES) applications*. 2011, NREL/TP-5500-51446: National Renewable Energy Laboratory.

196. Denholm, P., et al., *Decarbonizing the electric sector: Combining renewable and nuclear energy using thermal storage.* Energy Policy, 2012. **44**: p. 301-311.

197. Doster, M., A. Rominger, and S. Bragg-Sitton, *Reactor Subsystem Simulation for Nuclear Hybrid Energy Systems.* Idaho National Laboratory, 2012.

198. Ball, S., *Sensitivity studies of modular high-temperature gas-cooled reactor postulated accidents.* Nuclear engineering and design, 2006. **236**(5-6): p. 454-462.

199. Andreades, C., et al., *Technical description of the 'Mark 1'pebble-bed fluoride-salt-cooled high-temperature reactor (PB-FHR) power plant.* Department of Nuclear Engineering, UC Berkeley, Report UCBTH-14-002, 2014.

200. Edwards, J., H. Bindra, and P. Sabharwall, *Exergy analysis of thermal energy storage options with nuclear power plants.* Annals of Nuclear Energy, 2016. **96**: p. 104-111.

201. Dowtherm, A., *Heat transfer fluid.* Product Technical Data, 1997.

202. by Solutia, T.H.T.F., *Inc. Therminol VP 1*. 2012.

203. Sohal, M.S., et al., *Engineering database of liquid salt thermophysical and thermochemical properties*. 2010, Idaho National Laboratory (INL).

204. Yin, H., J. Ding, and X. Yang, *Heat Accumulation Technologies and System for Use in Concentration Type Solar Energy Thermal Power Generation.* Journal of Engineering for Thermal Energy and Power, 2013. **28**(1): p. 1-6.

205. Zuo, Y., J. Ding, and X. Yang, *Current status of thermal energy storage technologies used for concentrating solar power systems.* Chemical Industry and Engineering Progress, 2006. **25**(9): p. 995.

206. Anderson, R., et al., *Packed bed thermal energy storage: A simplified experimentally validated model.* Journal of Energy Storage, 2015. **4**: p. 14-23.

207. Herrmann, U. and D.W. Kearney, *Survey of thermal energy storage for parabolic trough power plants.* Journal of solar energy engineering, 2002. **124**(2): p. 145-152.

208. Steinmann, W.-D. and R. Tamme, *Latent heat storage for solar steam systems.* Journal of Solar Energy Engineering, 2008. **130**(1): p. 011004.

209. Akiyama, T., *Storage and Release of Heat in a Single Sphereical Capsule Containing Phase Change Material of High Melting Point.* Heat Transfer Japanese Research, 1992. **21**: p. 199-217.

210. Michels, H. and R. Pitz-Paal, *Cascaded latent heat storage for parabolic trough solar power plants.* Solar Energy, 2007. **81**(6): p. 829-837.

211. Kenisarin, M.M., *High-temperature phase change materials for thermal energy storage.* Renewable and Sustainable Energy Reviews, 2010. **14**(3): p. 955-970.

212. Gasanaliev, A.M. and B.Y. Gamataeva, *Heat-accumulating properties of melts.* Russian Chemical Reviews, 2000. **69**(2): p. 179-186.

213. Sun, J., et al., *Thermal reliability test of Al–34% Mg–6% Zn alloy as latent heat storage material and corrosion of metal with respect to thermal cycling.* Energy conversion and management, 2007. **48**(2): p. 619-624.

214. Zarza, E., et al., *Direct steam generation in parabolic troughs: Final results and conclusions of the DISS project.* Energy, 2004. **29**(5-6): p. 635-644.

215. Xing, Y.M., et al., *Numerical simulation of high-temperature phase change heat storage system.* Heat Transfer—Asian Research, 2004. **33**(1): p. 32-41.

216. Adinberg, R., A. Yogev, and D. Kaftori, *High temperature thermal energy storage an experimental study.* Le Journal de Physique IV, 1999. **9**(PR3): p. Pr3-89-Pr3-94.

217. Mondieig, D., et al., *Protection of temperature sensitive biomedical products using molecular alloys as phase change material.* Transfusion and apheresis science, 2003. **28**(2): p. 143-148.

218. Park, J., T. Kim, and S.-B. Leigh, *Application of a phase-change material to improve the electrical performance of vertical-building-added photovoltaics considering the annual weather conditions.* Solar Energy, 2014. **105**: p. 561-574.

219. Bhargava, A.K., *A solar water heater based on phase-changing material.* Applied Energy, 1983. **14**(3): p. 197-209.

220. Prakash, J., H. Garg, and G. Datta, *A solar water heater with a built-in latent heat storage.* Energy conversion and management, 1985. **25**(1): p. 51-56.

221. *CALMAC ICE STORAGE SYSTEM*. 2018 [cited 2017 12/28/2017]; Available from: http://www.calmac.com/.

222. Committee, A.T., *Thermal guidelines for data processing environments-expanded data center classes and usage guidance.* Atlanta, 2011.

223. Castano, C., et al., *Active heat removal system for continuous operation of the Missouri S&T Reactor.* Trans. Am. Nucl. Soc., American Nuclear Society, 2013: p. 1055-1057.

224. Belusko, M. and F. Bruno. *Design methodology of PCM thermal storage systems with parallel plates*. 2008. EUROSUN.

225. Tay, N., M. Belusko, and F. Bruno, *An effectiveness-NTU technique for characterising tube-in-tank phase change thermal energy storage systems.* Applied Energy, 2012. **91**(1): p. 309-319.

226. Liu, M., et al., *Investigation of cascaded shell and tube latent heat storage systems for solar tower power plants.* Energy Procedia, 2015. **69**: p. 913-924.

227. Bergman, T.L. and F.P. Incropera, *Fundamentals of heat and mass transfer*. 2011: John Wiley & Sons.

228. Akgün, M., O. Aydın, and K. Kaygusuz, *Experimental study on melting/solidification characteristics of a paraffin as PCM.* Energy Conversion and Management, 2007. **48**(2): p. 669-678.

229. Himran, S., A. Suwono, and G.A. Mansoori, *Characterization of alkanes and paraffin waxes for application as phase change energy storage medium.* Energy Sources, 1994. **16**(1): p. 117-128.

230. Zhang, P., Z. Ma, and R. Wang, *An overview of phase change material slurries: MPCS and CHS.* Renewable and Sustainable Energy Reviews, 2010. **14**(2): p. 598-614.

231. Vélez, C., M. Khayet, and J.O. De Zárate, *Temperature-dependent thermal properties of solid/liquid phase change even-numbered n-alkanes: n-Hexadecane, n-octadecane and n-eicosane.* Applied Energy, 2015. **143**: p. 383-394.

232. Ezan, M.A., A. Erek, and I. Dincer, *Energy and exergy analyses of an ice-on-coil thermal energy storage system.* Energy, 2011. **36**(11): p. 6375-6386.

233. Rosen, M.A., N. Pedinelli, and I. Dincer, *Energy and exergy analyses of cold thermal storage systems.* International Journal of Energy Research, 1999. **23**(12): p. 1029-1038.

234. Amin, N.A.M., et al., *Optimising PCM thermal storage systems for maximum energy storage effectiveness.* Solar Energy, 2012. **86**(9): p. 2263-2272.

235. Belusko, M., S. Sheoran, and F. Bruno, *Effectiveness of direct contact PCM thermal storage with a gas as the heat transfer fluid.* Applied Energy, 2015. **137**: p. 748-757.

VITA

Rami M. Saeed was born in Irbid, Jordan, on June 1991. He received his B.S. in Nuclear Engineering from Jordan University of Science and Technology, Ramtha, Jordan in July 2014. He did his summer training at the Jordan Atomic Energy Commission (JAEC) during the summer of 2013. In August of 2014, he attended Missouri University of Science and Technology, Rolla, USA in pursuit of a graduate studies in Nuclear Engineering. In May 2016, he received his M.S. degree in Nuclear Engineering in the field of phase change materials for thermal energy storage under the guidance of Dr. Joshua P. Schlegel.

Rami continued his PhD research in the field of thermal energy storage focusing on developing energy solutions using phase change materials under guidance of Dr. Joshua P. Schlegel. His PhD research was conducted at the R&D innovation center of Phase Change Energy Solutions (PCES) where he worked as a Research Scientist. As a result of these efforts, he was awarded a Ph.D. in Nuclear Engineering from Missouri University of Science and Technology, Rolla, USA in March of 2018.